NAIST-IS-DT0161037

Doctoral Thesis

Studies on Multipath Interference Canceller for Orthogonal Code-Multiplexed Channels in W-CDMA Forward Link

Akhmad Unggul Priantoro

February 6, 2004

Department of Information Science
Graduate School of Information Science
Nara Institute of Science and Technology

Doctoral Thesis
Submitted to Graduate School of Information Science
Nara Institute of Science and Technology
In partial fulfillment of the requirements for the degree of
Doctor of Engineering

Akhmad Unggul Priantoro

Thesis Committee

Heiichi Yamamoto, Professor
Mamoru Sawahashi, Visiting Professor
Masaki Koyama, Professor
Minoru Okada, Associate Professor

Studies on Multipath Interference Canceller for Orthogonal Code-Multiplexed Channels in W-CDMA Forward Link*

Akhmad Unggul Priantoro

Abstract

Tremendous growth of the cellular business during the last decade marked the success of Second Generation (2G) systems throughout the world. Thanks to the high spectrum efficiency of 2G systems and evolution of data communication services which turned mobile phone from a mere voice communication device into an interactive infotainment terminal.

The further evolutions to mobile multimedia communications and emerging mobile Internet stimulate stronger demand for higher data-rate services beyond the capability of 2G systems which offer maximum transmission speed of 64kbps. Wideband code division multiple access (W-CDMA) was adopted as a wireless access scheme for Third Generation (3G) communication systems. The first commercial 3G services have been launched in 2001 in Japan by NTT DoCoMo, and global scale introduction is under way. W-CDMA offers a maximum transmission speed of 2Mbps in the forward link.

In W-CDMA system, all users communicate simultaneously on the same frequency band thus creating mutual interference. This mutual interference is categorized into interference from other users' signals, multiple access interference (MAI) and interference from delayed paths (of other users' and own signal's), multipath interference (MPI). Consequently, the system capacity is determined by the total interference power in the system. This problem is especially significant in the forward link due to introduction of high data-rate services such as high-speed data downloading and Internet broadcasting in the near future. In addition, common channels which are transmitted at high power and without fast transmission power control (fast TPC) are potential sources of MPI. Although the use of orthogonal variable spreading factor (OVSF) codes establishes orthogonality among channels within same propagation path, the interference from different paths, MPI, are large thus severely limits the system capacity. Therefore, suppression of MPI is important in increasing the system capacity.

MPI cancellation techniques and adaptive antenna array beam forming (AAA-BF) receiver are effective for suppressing MPI. However, the former is not practical for mobile station because AAA-BF requires more than two antennas. So far, several MPI cancellation

* Doctor's Thesis, NAIST-IS-DT0161037, Department of Information Systems, Graduate School of Information Science, Nara Institute of Science and Technology, February 6, 2004

techniques such as minimum mean squared error (MMSE) equalizer and multipath interference canceller (MPIC) were proposed in the literature. MMSE equalizer requires very high computational complexity to obtain sophisticated performance. On the other hand, MPIC is interesting from practical implementation point of view because it is highly configurable to meet various constraints, such as hardware complexity. Therefore, in this thesis, configuration and algorithm for improving the performance of MPIC are proposed.

Firstly, this thesis proposes the application of MPIC to orthogonal code-multiplexed channels for single antenna transmission. The MPIC configuration proposed here capable of suppressing MPI from all physical channels included traffic channel (TCH). Therein, algorithms for improving the performance are proposed. Computer simulation results are shown to verify the effectiveness of the proposed MPIC.

Meanwhile, space time transmit diversity (STTD) for common control channel (CCH) and closed loop phase control (PC) transmit diversity scheme for TCH, which were adopted in the W-CDMA specification, are effective in improving the transmission performance even when using one branch receiver. The latter scheme is accompanied with antenna verification procedure at mobile station (MS) receiver to alleviate the effect of feedback bit information (FBI) decoding error. Thus, secondly, this thesis presents an extension of the MPIC receiver to be combined with STTD for CCH and closed loop phase control (PC) transmit diversity for TCH (hereafter the extended MPIC is called PTA-MPIC) to realize robust communication system in both interference-limited and noise-limited conditions. However, the performance of the PTA-MPIC receiver is affected by the accuracy of antenna verification due to MPI and background noise. Therefore, an antenna verification method utilizing dedicated pilot symbols after MPI from common channels and other channels/users are removed is proposed. The effectiveness of the proposed antenna verification method is elucidated by computer simulation.

The computer simulation results indicate that MPIC receiver is effective in improving the forward link transmission performance. Application of PTA-MPIC employing the proposed antenna verification to common channels only, reduces the required average transmit E_b/N_0 at average BER of 10^{-3} by about 3.3 dB. Furthermore, it is clarified that one-stage MPIC and two-stage PTA-MPIC are sufficient for serial construction and parallel construction, respectively. This result is very encouraging, from computational complexity perspective, for applying MPIC at mobile station.

Keywords : W-CDMA, forward link, multipath interference canceller, transmit diversity, antenna verification

論文概要

W-CDMA 下りリンクの直交多重チャネルにおける マルチパス干渉キャンセラに関する研究*

過去十年間における移動通信の急激なる成長は第 2 世代移動通信方式（2G）によるディジタル化が大きな寄与をしている。この成功の要因は、ディジタル化による高い経済性、高い周波数利用効率及びケイタイインターネットの実現である。これらの利点を生かして携帯電話は、単なる通話手段からあらゆる情報収集手段、娯楽享受のツールに変身した。

インターネットのブロードバンド化は、モバイルインターネットにおいてもよりブロードバンド化を必要とし、移動通信においても 2G の 64kbps から数 Mbps の伝送速度が必要となっている。このために開発されたのが第 3 世代移動通信方式（3G）であり、この 3G は広帯域符号分割多重方式（Wideband Code Division Multiple Access: W-CDMA）を通信方式として採用している。世界を先駆けて 2001 年に NTT ドコモが 3G の商用サービスを日本で開始し、現在世界中で導入が始まっている。W-CDMA の伝達速度は、高速移動環境および低速移動環境においてそれぞれ 384kbps および 2Mbps である。しかし、ユビキタスネットワークの進展により、移動通信は更なるブロードバンド化が必要になっている。

W-CDMA 方式では全ユーザが同じ周波数帯域を同時に利用して通信を行うため互いに干渉が生じる。この相互干渉は 2 種類あり、多元接続によるマルチアクセス干渉信号（multiple access interference: MAI）と多方向からの到来波(multipath)によるマルチパス干渉信号（multipath interference: MPI）とがある。従ってシステム容量（収容可能加入者数）は、システム内における上述の干渉電力をどれだけ抑圧できるかにより決まる。インターネット放送、WWW、高速データ等のブロード情報のダウンロードが多くなる下りリンクは厳しい干渉環境にある。また、一定な高送信電力で送信される共通チャネルが大きなマルチパス干渉源となる。同一伝搬路における他チャネルからのチャネル間干渉は直交拡散符号を用いているため零にできるものの他方向から数多く到来するマルチパス波(multipath)は直交していないため大きなマルチパス干渉信号になる。従ってシステム容量を増大するためにはマルチパス干渉信号を抑圧することが最も重要な課題となる。

マルチパス干渉信号の抑圧技術としては、適応アンテナアレー技術（adaptive

* 奈良先端科学技術大学院大学　情報科学研究科　情報システム学専攻　博士論文
NAIST-IS-DT0161037 2003 年 2 月 6 日

antenna array beam forming: AAA-BF）とマルチパス干渉抑圧技術がある。移動端末では小型化がまず、第一に要求されるため 2 本以上のアンテナを必要とする適応アレーアンテナは不適格である。マルチパス干渉抑圧技術は、最小平均二乗誤差（minimum mean squared error: MMSE）等化器とマルチパス干渉キャンセラ（multipath interference canceller: MPIC）がこれまでに提案されている。MMSE 等化器は高い性能があるが膨大な計算量（回路規模）が必要であるという欠点がある。そこで、本論文では MPIC の新しいアルゴリズム・構成法を提案し、MMSE 等化器と同等以上のマルチパス干渉除去能力の実現と優れた実装性を実証する。MPIC の利点は、様々な制限を満たすために柔軟に構成変更できる点にある。

まず、本論文では送信ダイバーシチ無しにおける直交多重チャネルへの MPIC の適用を提案すると共に性能向上のためのアルゴリズムを提案する。そして、有効性を確認するため計算機シミュレーション結果を示す。

一方、W－CDMA の仕様書に採用決定されている CCH 用の空間時間送信ダイバーシチ（STTD）および TCH 用の閉ループ型位相制御送信ダイバーシチが 1 ブランチアンテナ受信機における伝送特性向上に有効とされている。後者の閉ループ型位相制御送信ダイバーシチはフィードバック情報ビット（feedback information bit: FBI）の復調誤りによる性能劣化を防ぐためのアンテナベリフィケーションが備えてある。そこで、本論文では CCH 用の STTD および TCH 用の閉ループ型位相制御送信ダイバーシチと組み合わせるために MPIC を拡張し（以降、拡張した MPIC を PTA-MPIC と呼ぶ)、雑音制限或いは干渉制限された状況において良好な特性をもつ通信システムを実現する。しかし、PTA-MPIC 受信機の性能は雑音や MPI に影響されるアンテナベリフィケーションの精度によって劣化する。このため共通チャネルおよび他局からの MPI を取り除いた個別パイロットシンボルを用いた新しいアンテナベリフィケーション手法を提案する。提案アンテナベリフィケーション手法の有効性を検証するための計算機シミュレーション結果を示す。

提案した PTA-MPIC は、共通チャネルにのみ適用することにより、誤り率 10^{-3} の所要 E_b/N_0 を 3.3 dB 低減できることをシミュレーションにより実証した。これにより孤立セルシステム容量は 2 倍以上増大できる。更に、シリアル型 MPIC とパラレル型 PTA-MPIC にステージ数は 1 から 2 で十分であることを確認した。この結果は回路規模の大きな増大を伴わないため MPIC の移動端末への適用を可能であり、システム容量増大に大きく貢献できる。

キーワード：W-CDMA, 下りリンク、マルチパス干渉キャンセラ、送信ダイバーシチ、アンテナベリフィケーション

Acknowledgement

In the first place, I would like to express my sincere gratitude to Professor Heiichi Yamamoto for his constant support during my study at Communications Laboratory, previously Information Network Laboratory, at NAIST. Without his flexibility and understanding on various issues, my journey towards this thesis would be impossible.

I am very much grateful to Dr. Mamoru Sawahashi who introduced me to interference canceller research and supervised me throughout this study. His constant and generous advices, help and encouragement were great motivation to carry on this study.

I express my gratitude to Professor Masaki Koyama for his valuable comments and important suggestions concerning this thesis.

I would like also to express my gratitude to Associate Professor Minoru Okada who provided me with general knowledge in communication theory and practices, as well as fruitful discussion during the years and valuable comments and suggestions during writing this thesis.

I would like to extend my gratitude to Dr. Kenichi Higuchi of NTT DoCoMo who patiently guiding me throughout this thesis work and provided me with technical discussion on related subjects.

I am grateful to Dr. Satoru Fukumoto of NTT DoCoMo who helped me in the simulation of transmit diversity and his help during my stay in NTT DoCoMo in 2001.

I am indebted to Dr. Kenichi Chinen of Japan Advanced Institute of Science and Technology, Japan, for his help with the programming aid while he was with our laboratory as Assistant Professor.

I extend my gratitude to Assistant Professors Dr. Masato Saito and Dr. Takao Hara of Communications Laboratory for their fruitful discussions on related subjects.

I would like to thanks to all members of Communications Laboratory –past and presents– who made my stay at NAIST comfortable and pleasant.

This study was supported in part by Ministry of Education, Culture, Sports, Science and Technology, Government of Japan, NTT DoCoMo, Heiwa Nakajima Foundation and NAIST 21st Century COE Program, hereby acknowledged.

Personally, I would like to express my deepest gratitude to my mother, parents in law and my brothers and sisters who constantly encouraged me to carry out this study. Last but not least, thanks to my wife Nurul and our son Hilmi for their company throughout the years.

Contents

List of Figures and Tables

List of Abbreviations

AAA-BF	Adaptive Antenna Array Beam Forming
AAA-TD	Adaptive Antenna Array Transmit Diversity
AMPS	Advanced Mobile Phone Service
BER	Bit Error Rate
BPSK	Binary Phase Shift Keying
BS	Base Station
CCH	Common Control Channel
CCPCH	Common Control Physical Channel
CEIGU	Channel Estimation and Interference Replica Generation Unit
CPICH	Common Pilot Channel
DS-CDMA	Direct Spread Code Division Multiple Access
DPCH	Dedicated Physical Channel
EIA	Electronic Industries Alliance
FBI	Feedback Information
FDD	Frequency Division Duplex
FDMA	Frequency Division Multiple Access
GSM	Global System for Mobile Communications
HSDPA	High Speed Downlink Packet Access
IC	Interference Canceller
IRGU	Interference Replica Generation Unit
IRW	Interference Rejection Weight
IS-95	Interim Standard 95
MAI	Multiple Access Interference
MF	Matched Filter
MMSE	Minimum Mean Squared Error
MPI	Multipath Interference
MPIC	Multipath Interference Canceller
MPIRGU	Multipath Interference Replica Generation Unit
MS	Mobile Station
MSIC	Multistage Interference Canceller
NMT	Nordic Mobile Telephone
NTT	Nippon Telegraph and Telephone
ODMA	Opportunity Driven Multiple Access
OFDMA	Orthogonal Frequency Division Multiple Access
OVSF	Orthogonal Variable Spreading Factor

PDC	Personal Digital Cellular
PICH	Common Pilot Channel
PTA-MPIC	Per Transmit Antenna Multipath Interference Canceller
QoS	Quality of Service
QPSK	Quadrature Phase Shift Keying
SCH	Synchronization Channel
SF	Spreading Factor
SIR	Signal to Interference Ratio
STTD	Space Time Transmit Diversity
TCH	Traffic Channel
TDMA	Time Division Multiple Access
TIA	Telecommunications Industry Association
TPC	Transmit Power Control
TSTD	Time Switched Transmit Diversity
UE	User Equipment
USDC	United States Digital Cellular
W-CDMA	Wideband Code Division Multiple Access
WTDMA	Wideband Time Division Multiple Access
WMSA	Weighted Multi-Slot Averaging
3GPP	Third Generation Partnership Project

Chapter One

Introduction

Digital wireless and cellular history opened in 1940s when the first commercial mobile telephony service began in the United States. During the first four decades the mobile communication technology did not make notable progress until the introduction of Advanced Mobile Phone Service (AMPS) in the United States in 1978, NTT Cellular in Tokyo area in 1979 and Nordic Mobile Telephone (NMT)-450 systems in Northern European countries in 1981. These systems employed analog modulation schemes and are often referred to as the first generation (1G) mobile communication systems. They mainly served voice communications although low bit rate of 9.6 kbps (circuit switched) data communication was possible.

Second generation (2G) systems, adopting digital technology, were introduced during 1991 in the United States as U.S. Digital Cellular (USDC), and during1992 in Europe as Global System for Mobile (GSM) communications. Meanwhile, Japan introduced its 2G communication system in 1993 which is now called Personal Digital Cellular (PDC) [1]. Significant reduction of mobile station (MS) size and change of subscription policy made mobile communications more practical and affordable to the population thus stimulated the remarkable growth of subscriber number at the early stage. Later on, the introduction of data communication services, pioneered by *i-mode* services in Japan early in 1999, played an important role to the tremendous growth of the industry since it transformed a mobile phone from a mere voice communication device into an interactive infotainment terminal. As of September 2003, the number of cellular subscribers recorded 78 millions (almost doubled since the introduction of *i-mode* services) in Japan and more than one billion worldwide [2]. However, it is important to note that the adoption of digital technology which provided high spectral efficiency was the key factor behind this success.

The data communication services evolution to mobile multimedia ones and emerging mobile Internet is very likely to stimulate further the demand for higher data-rate services. Careful study on the third generation (3G) offered traffic characteristics conducted by UMTS Forum revealed that the traffic overall asymmetry ranges from 0.15 to 0.77 according to the service offered. In this respect, traffic overall asymmetry is defined as the ratio between total Service Category (namely, mobile internet access, rich voice, etc.) of the reverse link and that of the forward link [3]. As an example, an overall traffic asymmetry of 0.77 means that the ratio of the forward link traffic to the reverse link traffic is approximately 6:4. When all Service Categories are aggregated, the overall asymmetry is

0.43, i.e., the reverse link to the forward link traffic ratio is 3:7.

Due to inherent limitation of 2G systems to provide high data-rate services, candidates for the so-called 3G system have emerged. There were wideband code division multiple access (W-CDMA), wideband time division multiple access (WTDMA), TDMA/CDMA, orthogonal frequency division multiple access (OFDMA) and opportunity driven multiple access (ODMA) [3]. Third generation systems are designed for multimedia communication: with them person-to-person communication can be enhanced with high quality images and video, and access to information and services on public and private networks will be enhanced by the higher data rates and new flexible communication capabilities [4]. As such, it has the following requirements:

- Bit rates up to 2 Mbps
- Variable bit rate to offer bandwidth on demand (BoD)
- Multiplexing of services with different quality requirements on a single connection
- Delay requirements from delay-sensitive real time traffic to flexible best-effort packet data
- Support of asymmetric reverse link and forward link traffic
- High spectrum efficiency considering cellular system.

W-CDMA technology has emerged as the most widely adopted third generation air interface and finally adopted as one of the radio interface for frequency division duplex (FDD) mode [5]. Its specification has been created in the third generation partnership project (3GPP), which is the joint standardization project of the standardization bodies from Europe, Japan, Korea, the USA and China. In 2001 NTT DoCoMo initiated the first 3G services and global scale introduction is underway. At the first phase of introduction, in the forward link it supports variable maximum information bit rates up to 144kbps, 384kbps and 2Mbps in vehicular, pedestrian and indoor environments, respectively.

W-CDMA is derived from direct spread code division multiple access (DS-CDMA), a second generation system known as TIA/EIA/IS-95A (hereafter IS-95A) standard, hence shares many of the properties (in this thesis both terms are used interchangeably whenever appropriate, i.e., cause no confusion). In the DS-CDMA system, all communicating users share the same frequency bandwidth simultaneously. Therefore, multiple access interference (MAI) and multipath interference (MPI) in a multipath fading environment which constitute the total interference power limit the system capacity. Especially in the forward link, where the amount of traffic is expected to grow much larger than that of the reverse link as is envisaged in the UMTS Forum report [3].

In the forward link, orthogonal variable spreading factor (OVSF) codes [6] are used.

Thus, orthogonality among channels is achieved in the absent of multipath propagation. Nevertheless, the presence of multipath propagation causes MPI which severely degrades the bit error rate (BER) performance. Especially, large MPI arises from high-rate users and common channels which transmit at high power without fast transmit power control (fast TPC). Consequently, it is important to suppress the interference to increase the system capacity.

Table 1. 1 Comparison of MPI suppression techniques

Method	MPI suppression capabilities	Complexity Constraint	Extension to other cells' MUI suppression
Adaptive antenna array beam forming (AAA-BF)	Depend on the number of antennas and DOA of the multipath signals	Impractical since two or more antennas need to be installed at mobile terminal	Restricted by the allowable number of antennas
Zero Forcing/ MMSE Equalizer	Degraded in low E_b/N_0 region due to channel estimation error	Increases with increasing maximum path delay	Requires strict timing control among BS's
Nonlinear MPIC	Less degraded in low E_b/N_0 region owing to successive channel estimation	Linearly increases with increasing number of stages and resolvable paths	Easily extended to suppress other cells' MUI

There are several techniques to suppress MPI, such as adaptive antenna array beam forming (AAA-BF) receiver and MPI canceling technologies as listed in Table 1.1. AAA-BF receiver dynamically adjusts the antenna array pattern to optimize some characteristics of the received signal. This yields multiple beams that can be made to have high gain and low sidelobes, or controlled bandwidth. Consequently, interfering signals having a direction of arrival different from that of the desired signal can be suppressed. This technique requires two or more antennas which is impractical for mobile station application. On the other hand, MPI canceling technologies offer MPI suppression while requiring only one antenna. These technologies suppress MPI by restoring the spreading code orthogonality or explicitly regenerate the interfering signal replicas and subtract them from the received signal. Thus far, several algorithms have been proposed for canceling MPI in the forward link [7] - [12]. Here, discussion on blind algorithms, such as [7] [8], are excluded because in W-CDMA system pilot channel is available for estimating the propagation channel condition, thus eliminates the benefit of such algorithms. Zero forcing (ZF) criterion and minimum mean squared error (MMSE) criterion based channel

equalizers were proposed in [9] [10]. Petré et al. reported in [11] that their proposed algorithm has exactly the same performance as that of single user chip equalizer proposed in [9]. For example, to obtain sophisticated performance, MMSE equalizer requires matrix inversion of the channel matrix of size $(NQ+W-1)\mathrm{x}(NQ)$, where N, Q and W are the transmission burst length, spreading factor and channel impulse response length. The performance of this method depends on the accuracy of channel estimation, thus make it difficult to apply when the background noise power is large, i.e., low signal energy per bit to background noise spectrum density ratio (E_b/N_0).

Meanwhile, multipath interference canceller (MPIC) receiver is an interesting choice from practical implementation point of view. MPIC for canceling data packet channels in High Speed Downlink Packet Access (HSDPA) was proposed in [13]. Operational principles of MPIC are generation of interference replica, i.e., replica of received signal at each resolved path, of each user/channel and subtraction of generated MPI replica from the received signal. The performance of MPIC receiver is determined by the accuracy of generated MPI replica. Specifically, to generate MPI replica the following information need to be estimated:

- Tentative decision data
- Channel estimate
- Received timing of each path

In addition, the performance of this type of MPIC also depends on the number of stages because by iteratively performing MPI replica generation the accuracy and hence the overall performance of MPIC is improved. However, increasing the number of stages linearly increases the receiver complexity and processing delay. Thus, the central issues pertaining to MPIC are how to improve the MPI replicas and reduce the number of stages. Simultaneous pursuit of these issues is surely a tough challenge. Although the aforementioned issues are exactly the same with interference canceller (IC) in the reverse link channel, and have been dealt with in numerous papers, e.g., [14], [15], in the literature, the application of similar techniques in the forward link channels has its own aspects due to the different characteristics of both channels.

This thesis deals with MPIC for the orthogonal code-multiplexed forward link channels in the W-CDMA system. This paper, firstly, propose the application of MPIC to orthogonal code-multiplexed channels in the forward link. Therein, common pilot channel (PICH) is used for channel estimation for generating MPI replicas because it has large transmission power, thus yielding higher accuracy. In addition, weighted multi-slot averaging (WMSA) [25] channel estimation filter is applied to increase further the channel

estimation accuracy. Because traffic channel instantaneous amplitude is different from that of PICH, especially when fast transmit power control (TPC) is applied, the amplitude ratio of both channels is measured and with which the channel estimates obtained from common pilot channel are scaled (note that to generate accurate MPI replicas phase and amplitude variations of the channel are required). To minimize the number of stages, serial type MPIC, i.e., MPI replica generation is performed in the order of received power, is considered although this costs longer processing delay. Finally, prioritization to channels with higher received power to be cancelled is proposed to abate the increase in processing complexity. Extensive computer simulations are performed to confirm the effectiveness of the proposed MPIC receiver.

Meanwhile, transmit diversity in the forward link is effective in mitigating the degradation in transmission performance due to fading even when using a one branch receiver. Space time transmit diversity (STTD) was adopted for common control channel (CCH) and closed loop type PC transmit diversity was adopted for the traffic channel (TCH) in W-CDMA specifications [10]. It is conjectured that combination of the MPIC at mobile station and closed loop phase control (PC) transmit diversity at base station transmitter is beneficial in improving the BER performance of TCH in both noise-limited and interference-limited channels.

In closed loop type PC transmit diversity, the base station transmitter, control the transmit carrier phase of the signal from Antenna 1 and Antenna 2 according to decoded feedback information (FBI) sent by mobile station via the reverse link channel. If decoding error of the FBI bit occurs, the accuracy of channel estimates is affected, leading to performance degradation. This factor also affects the performance of MPIC receiver which relies on the accuracy of these channel estimates. To alleviate the effect of FBI bit decoding errors, antenna verification, i.e., verification of transmit carrier phase slot by slot, is performed at mobile station. Principally, antenna verification is performed by collating the channel estimate obtained from dedicated pilot symbols (transmitted on each TCH) to that obtained from PICH, both from Antenna 2. Therefore, the accuracy depends on the accuracy of TCH channel estimates and of PICH channel estimates.

This paper, extend MPIC receiver by combining it with transmit diversity at the base station (BS) transmitter, considering parallel type one, i.e., MPI replicas generation are performed simultaneously, to reduce the processing delay. More specifically, an MPIC configuration based on MPI replica generation per transmit antenna (called PTA-MPIC) associated with STTD for the CCH, which exploits tentative decision data after STTD decoding, and with closed-loop type PC transmit diversity for the DPCH employing tentative decision data after diversity combining is presented. Next, an antenna verification method is proposed. The proposed method utilizes dedicated pilot symbols after MPI from

common channels and other dedicated physical channels are removed by MPIC. In the proposed method, since the carrier modulation phase is estimated using the dedicated pilot symbols after MPI suppression, the estimation accuracy is improved. Computer simulation results are shown to confirm that the proposed antenna verification method is effective in reducing the antenna verification error.

Finally, in the thesis, it is emphasized that comprehensive channel structure as dictated in the 3GPP standardization, i.e., common pilot channel (PICH), CCH and synchronization channel (SCH) in addition to TCHs is adopted in the evaluations. This is important from implementation point of view as it provides concrete figures of the improvement offered.

The outline of this thesis is as follows.

Chapter 2 presents the principles of modulation and demodulation in DS-CDMA system. Next, features of W-CDMA system that make it excels existing 2G systems, such as soft (softer) handover, fast transmit power control (fast TPC) are explained. Then operational principles of MPIC are introduced followed by highlighting open problems that are dealt with in this thesis.

Chapter 3 presents a proposal of MPIC for orthogonal multiplexed channels in the W-CDMA forward link, assuming single antenna transmission. Note that different notification to that of 3GPP Specifications are used for reason that will be made clear therein. Several algorithms to improve the performance are proposed. Computer simulation results are shown to confirm the effectiveness of the proposed receiver.

Chapter 4 presents an MPIC configuration based on MPI replica generation per transmit antenna (called PTA-MPIC) associated with STTD for the CCH, which exploits tentative decision data after STTD decoding, and with closed-loop type PC transmit diversity for the TCH employing tentative decision data after diversity combining, in the W-CDMA forward link. Next, this chapter proposes transmitter carrier phase verification, i.e., an antenna verification method used in PC transmit diversity, that utilizes the dedicated pilot symbols in a TCH after the PTA-MPIC removes the MPI components. Similarly to the previous chapter, computer simulation results are shown to confirm the beneficial effect of the combination of MPIC and transmit diversity, and the effectiveness of the proposed antenna verification method.

Chapter 5 summarizes the achievements and highlights future research directions.

Chapter Two

W-CDMA: Principles and Features

2.1 DS-CDMA Principles

W-CDMA is derived from DS-CDMA system which is adopted in IS-95A standard, a second generation communication system thus, share many of the properties. DS-CDMA is a wireless multiple access method by use of spectrum spreading. In contrast to frequency division multiple access (FDMA) which utilizes frequency space or time division multiple access (TDMA) which utilizes time space (hereafter narrowband (nonspread) transmission), DS-CDMA system utilizes code space to realize multiple access. Fig. 2.1 illustrates the principle of modulation and demodulation in DS-CDMA. In DS-CDMA system, each user is assigned a unique spreading code (from a set of codes with sufficiently low cross correlation property) which has much wider bandwidth than the information data to be transmitted. Users multiply their transmit data with the assigned spreading code resulting in expansion of the spectrum of the transmit data equal to that of the spreading code (W-CDMA has bandwidth of 5MHz and DS-CDMA IS-95A has a bandwidth of 1.25 MHz). The ratio of the bandwidth of the spreading code and the transmit data (not considering bandwidth expansion due to channel coding) is called *spreading factor (SF).* At the receiver, the received signal is correlated with the same spreading code used at the transmitter to recover the transmit data (this process is called despreading). By despreading, the received signal power of other user is suppressed by a factor of, on average, *SF*.

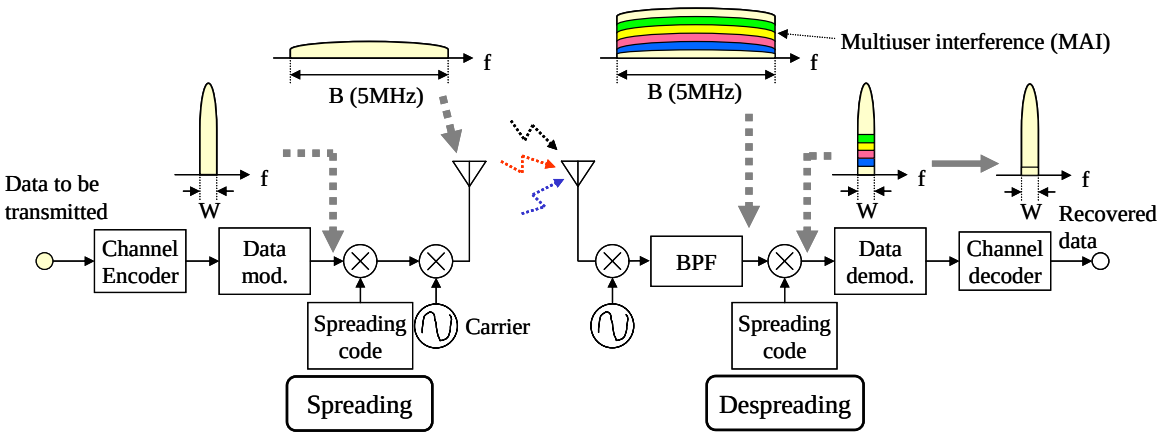

Fig. 2.1DS-CDMA principle

In mobile environment, there exist multiple propagation paths between a base station and a mobile station creating multipath propagation. Moreover, reflectors and scatterers at the proximity of mobile station cause random combining of incoming waves which generate fading, because their time arrival is virtually the same (to be precise, is within one chip period) therefore can not be separated one from another. The combined signal undergoes random phase and amplitude variations. If there are incoming waves whose delays are more than one chip period, these waves can be separated from the previous ones. Thus, more than one multipath signal is detected at the receiver. This is called multipath fading or frequency selective fading. Under such circumstance, it is generally difficult to assign orthogonal spreading codes. Consequently, after despreading signal components from different path(s) and different channel(s) are observed as interference. The interference power increases proportionally with increasing number of users. Fig. 2.2 illustrates the signal to interference power Ratio (SIR) concept in DS-CDMA systems. Thus, for a given quality of service (QoS) in terms of SIR value, the maximum interference power is determined. In other words the number of users that can be served is determined by the interference power.

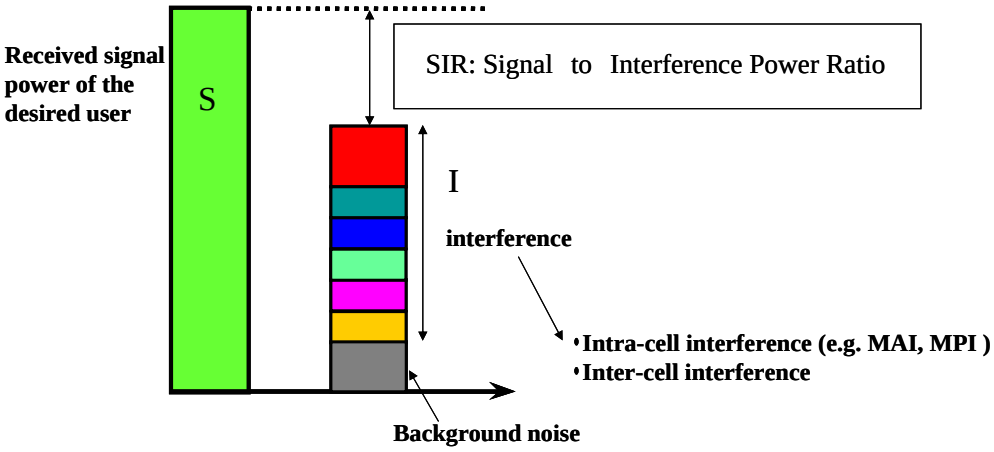

Fig. 2.2 Signal to interference power spectrum density ratio

2.2 W-CDMA Features

Unlike nonspread transmission which allocates disjoint slot (in frequency or time) to different users, DS-CDMA allocates spreading code and use the same frequency bandwidth simultaneously. This principle of DS-CDMA makes it beneficent for cellular communications. Since the same frequency can be used at adjacent cells (sectors), the overall system capacity is increased significantly. This feature is called Universal

Frequency Reuse which underlies all other features. Universal frequency reuse greatly simplifies the task of channel allocation and eliminates the need for frequency plan revision every time a new cell is introduced. This is not the case for nonspread transmission. The W-CDMA has many features that constitute its excellence against 2G systems. These features are listed in Table 2.1.

Table 2.1 W-CDMA features

Features	Description
Base station synchronization	Asynchronous operation
Duplexing	Frequency/time
Chip rate/Bandwidth	3.84Mcps/5Mhz
Multirate transmission	Multicode (reverse link)/ OVSF (forward link)
Multiuser detection	Supported by the standard, optional in the implementation
Transmission power control	Closed loop and open loop
Diversity	Open loop transmit diversity (Common channels)/ Closed loop transmit diversity (DPCH)

2.2.1 Fast TPC

It was explained in Section 2.1 that the interference power of an interfering user can be suppressed by a factor of *SF*. However, this interference suppression effect may become insufficient when the interfering user signal received at much higher power. This phenomenon is called near far effect, where the signal of a user far from a base station is masked by the signal of interfering user close to the base station.

Moreover, it is generally difficult to maintain orthogonality between users due to the random propagation delay between transmitting users (reverse link) and to multipath propagation (i.e., there exist several paths from the transmitter to the receiver), see Fig. 2.3. The former gives rise to multiple access interference (MAI) and the latter gives rise to multipath interference (MPI). As such, it is important to maintain the received signal of each user to be as low as possible while satisfying the required transmission quality to minimize the mutual interference power. The procedure of controlling the transmit power so as to meet the required transmission quality is called fast transmit power control (fast

TPC; it has feedback command frequency of 1500 Hz which is almost twice that of IS-95A, thus capable of tracking larger channel fluctuation). The transmitter varies the transmit power inversely proportional to channel fading variations; hence the channel becomes an essentially non-fading channel as seen by the receiver.

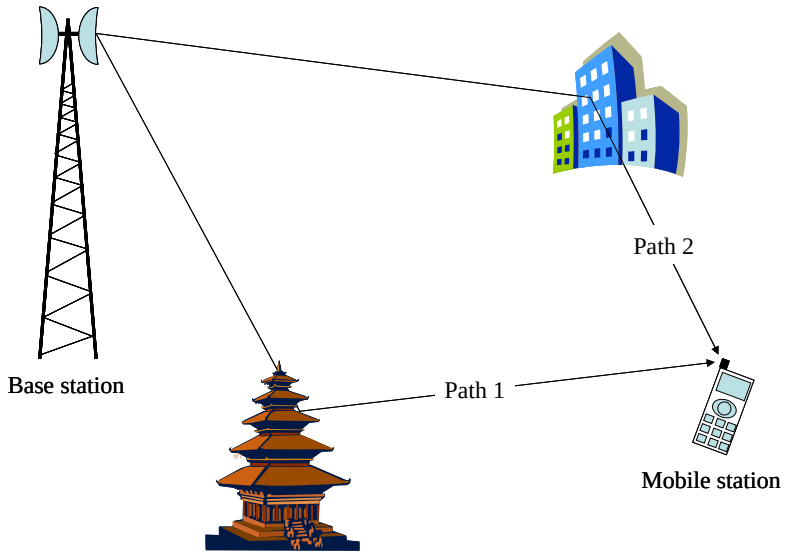

Fig. 2.3 Multipath propagation (forward link channel)

2.2.2 Inter-Base Station Asynchronous Operation

W-CDMA uses two-layer spreading both in the forward and reverse link. Information data symbol sequence is first spread by channelization code generated from Walsh sequences. An ingenious method for channelization code generation was proposed in [6] that realizes variable spreading factor while maintaining orthogonality. A channelization code has repetition period equals the symbol period of the information data (short code). This operation spread the bandwidth of the transmit data by a factor of *SF*. Channelization code function to separate different physical channels transmitted from the same terminal/cell. On top of spreading, scrambling code is used. Scrambling operation does not increase the signal bandwidth because scrambling code has the same chip rate as the channelization code. Scrambling code function to separate terminals (reverse link) or sector/cells (forward link). 512 codes are selected from Gold code family of period 2^{18}-1 to be used as scrambling codes in the forward link. This choice enables inter-base station asynchronous operation which contributes to easy deployment from outdoor to indoor environment since no outer timing source is required.

Inter-base station asynchronous operation feature is not available for the IS-95A systems because the same scrambling code but with different phase offset is assigned to

adjacent BS to ease the synchronization task [17]. The use of 512 scrambling codes in W-CDMA systems, however, makes the synchronization task become difficult. Because a MS must determine one out of 512 scrambling codes in a short time. Fortunately, this problem can be solved by a three-step cell search method proposed in [18]. This task can be simplified further if a mobile station informed a subset of scrambling code to search from.

2.2.3 Multipath Diversity by Coherent Rake Receiver

W-CDMA chip rate is 3.84 Mcps and, correspondingly, the chip duration is 0.26 μs . This is equivalent to path length difference of 78 m. Received signals with path difference greater than 78 m will be detected or resolved as different paths. Thus, more multipath component can be resolved even in small cell, which is not possible with IS-95A whose chip duration is 0.81 μs (= path length difference of 245 m). Fig. 2.4 shows the block diagram of coherent Rake combiner. Dispersed signal energy at each resolved path (i.e., paths detected by path searcher block, not shown in the figure) is collected by first correlated the received signal with the spreading code replica (i.e., the same spreading code as used at the transmitter) and weighted by the complex conjugate of respective channel gain (or channel estimate) and coherently combined (maximal ratio combining, MRC) for subsequent signal processing. A Rake finger consists of a correlator, channel estimator and channel compensator.

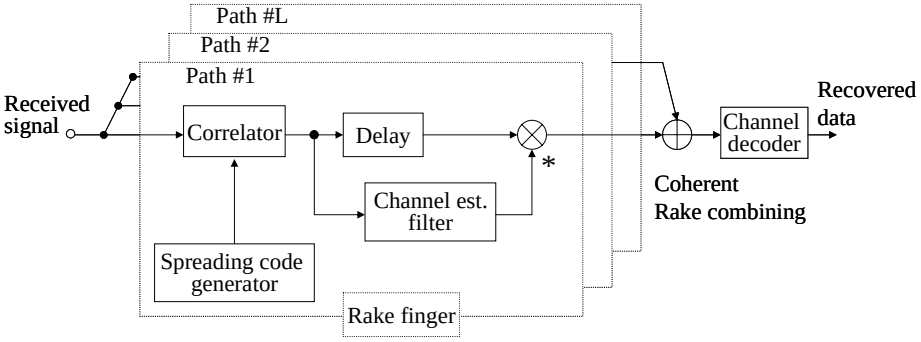

Fig. 2.4 Coherent Rake combiner

Fig. 2.5 shows the required average transmit E_b/N_0 at average bit error rate (BER) of 10^{-3} as a function of the number of paths in a Rayleigh fading channel in the forward link channel. In the figure, the performance when maximum Doppler frequencies, f_D, were 5Hz and 160Hz, relevant to moving speed of approximately 2.5 km/h and 86 km/h, respectively, assuming carrier frequency of 2 GHz, are shown. The required average transmit E_b/N_0 at average BER of 10^{-3} monotonically decreases by increasing the number of paths from one

to four and almost constant by increasing the number of paths further. Increasing the number of paths decreases the average power of each path, thus decreases the channel estimation accuracy. However, it is evident that in the forward link case accurate channel estimation is possible. Thanks to accurate channel estimation derived from CPICH. Further, we note, that the effect of multipath diversity is larger when f_D=5Hz than that when f_D=160Hz because at low f_D channel coding and interleaving effect is rather small.

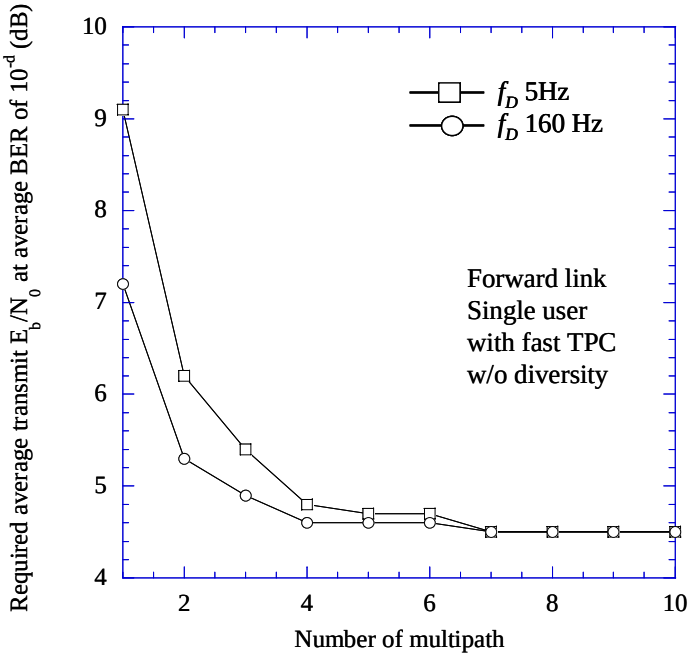

Fig. 2.5 Multipath diversity effect in Rayleigh fading channel (uniform delay profile)

2.2.4 Orthogonal Spreading Code

Unlike the reverse link channel, where transmitters (users) are dispersed across the service area thus difficult, if not impossible, to maintain symbol level synchronism amongst the channels, forward link channels are transmitted from the same BS thus symbol level synchronism is easily achieved. Taking advantage of this symbol level synchronism, orthogonality amongst the channels can be established by employing orthogonal spreading codes, namely Walsh-Hadamard codes or orthogonal Gold codes. Walsh-Hadamard code has advantage of structured generation as illustrated in Fig. 2.6 which is important to realizing multi rate transmission because orthogonality amongst channels with same *SF* and amongst those with different *SF*s are easily established. In the Figure $c_{i,k}$ represent a

spreading code with *SF* of *i* ($i=2^{n-1}$;*n* is the order of the Walsh-Hadamard matrix) and code index *k* ($1 \le k \le i$). The generation of the spreading codes with *SF* of *i* can be done by generating Walsh-Hadamard matrices recursively as

$$H_n = \begin{bmatrix} H_{n-1} & H_{n-1} \\ H_{n-1} & -H_{n-1} \end{bmatrix} \tag{2.1}$$

$$H_1=[1] \tag{2.2}$$

where H_n is Walsh-Hadamard matrix of size 2^{n-1} ($n > 0$; note that H_n is a square matrix). Then, the first spreading code of *SF* $i(=2^{n-1})$ $c_{i,1}$ is the first row of H_n, the second spreading code $c_{i,2}$ is the second row of H_n and so forth. Thus, for *SF* of *i* the number of spreading codes is *i*.

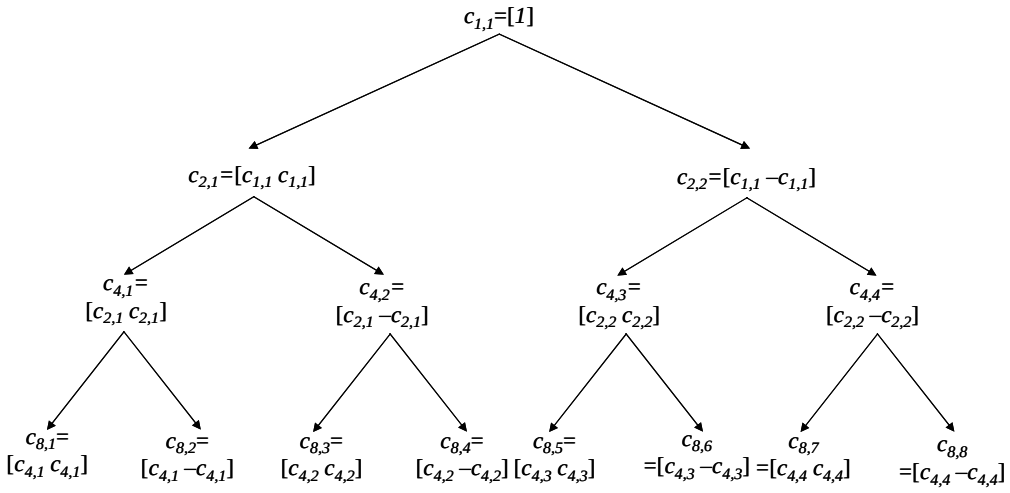

Fig. 2.6 Spreading code tree

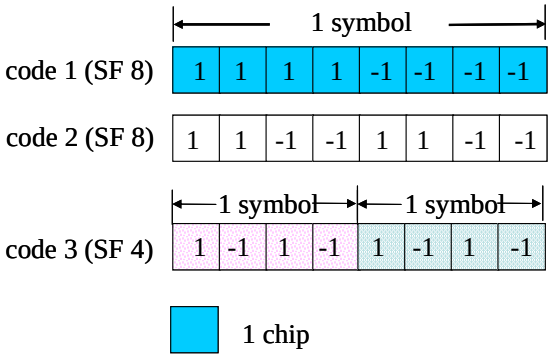

Fig. 2.7 Spreading code orthogonality

The orthogonality amongst spreading codes with same SF can easily be traced from the row-wise orthogonality of H_n. Orthogonal spreading codes of arbitrary length can be easily generated using the spreading code tree. In addition, to maintain orthogonality amongst spreading codes of different *SF*s it is essential that a code $c_{i,k}$ at any given node is in use than any code stems from that node must not be assigned to user with higher *SF*, i.e., lower data rate. A code at certain node from which other codes of higher SF are generated from is called mother code. In other words, borrowing this term, to establish orthogonality amongst spreading codes with different *SF*s those codes must not have the same mother code. This generation method yields OVSF code which was proposed in [6]. In the figure the generation of spreading codes with SF up to eight is shown. However, the spreading code generation for higher *SF* is straightforward.

Fig. 2.7 exemplifies the orthogonality amongst spreading codes with arbitrary *SF*. First, the orthogonality of spreading codes with same *SF* is explained. Consider code1 and code2 with *SF* of eight. Note that orthogonality is defined at symbol level, i.e., after despreading at the receiver. Therefore, to verify the orthogonality between code1 and code2 we can cross-correlate, i.e., multiply the spreading codes chip by chip and sum up over the symbol length, see Eq. (2.3). Simple calculation yields zero which implies orthogonality. On the other hand, to verify orthogonality amongst spreading codes of different *SF*s, the verification needs a slight modification. In this example, I consider code1 of length eight (longer code) and code3 of length four (shorter code). When considering the longer code, the cross-correlation is performed over two-period of the shorter code. On the other hand, when considering the shorter code the cross-correlation is performed over half-period of the longer code. Identically to the case of same *SF*, the cross-correlation is zero thus implies orthogonality. To summarize, the calculation of cross-correlations $C_{j,k}$ are formulated as,

$$C_{2,1} = C_{1,2} = \sum_{i=1}^{8} c_1(i) * c_2(i) \tag{2.3}$$

$$C_{1,3} = \sum_{i=1}^{8} c_1(i) * c_3(i \,(\mathrm{mod}\, 4)) \tag{2.4}$$

$$C_{3,1} = \sum_{i=1}^{4} c_3(i) * c_1(i) \tag{2.5}$$

where *j*, *k* are the spreading code indices and c_j represents *j*-th spreading code.

2.2.5 Soft (Softer) Handover

During soft (or softer) handover the communication between mobile station and BSs take place concurrently via *N* air interface channels, one for each cell (sector) separately. This

requires the use of *N* channelization codes in the forward link, one for each connection. The received signals are processed in similar manner to multipath reception, except that different code is generated at each Rake finger. Soft (softer) handover take place where there is overlap between cells' (sectors') coverage, i.e., at cell boundaries. This feature is important in improving the forward link quality at cell edge. The counterpart of this technique in the reverse link is called site diversity. Transmit signal from mobile station is received by *N* base station, channel decoded independently at each base station. Afterwards, the hard decision data sequence along with the reliability information is sent to the radio network controller (RNC). The RNC then select the best sequence, one out of *N* sequences (diversity selection combining). It is reported in [19] that the choice of reliability information affects the system performance.

2.2.6 Flexibility of Providing Variable Rate Services

W-CDMA provides variable rate services from as low as 7.5 kbps to as high as 2 Mbps with good granularity. This very wide range of transmission data rate services is possible because transmission data rate can be changed easily by changing the spreading factor while maintaining the spreading bandwidth constant. This feature is also important from the resource utilization point of view, because high granularity will reduce excessive radio resource allocation.

2.2.7 Transmit Diversity

As it was clear from 2.2.3, diversity is important in improving the transmission performance of a mobile communication system. Transmit diversity is beneficent in improving the quality of mobile reception, i.e., forward link channel, without increasing the complexity of mobile terminal.

In the transmit diversity, the same information data is sent via two transmit antennas having spatial correlation less than unity. Two types of transmit diversity, namely open loop and closed loop types, were adopted in the W-CDMA specification [21]. Basically, closed loop type differs from open loop type in that feedback from mobile station is required. The mobile station periodically informs the channel condition to the base station according to which the base station controls the transmit signal. On the other hand, open loop type controls the transmit signal according to a fix rule regardless of the channel condition. Thus, it can be easily conjectured that the closed loop type can better utilize the channel at the expense of feedback.

In [22], it was reported that open loop type transmit diversity, namely space time transmit diversity (STTD), is suitable for channel without fast TPC such as common control channel because the achievable gain diminish when combined with fast TPC. In the 3GPP

specification, the open loop type, namely time switch transmit diversity (TSTD) is applied to synchronization channel (SCH) and STTD is applied to common control physical channel (CCPCH) and dedicated physical channel (DPCH). Meanwhile, the closed loop type one is applied to the DPCH.

(a) Open Loop

Figure 2.8 illustrates the operation of STTD encoding. In the Figure a segment of the transmit symbol sequence consisting of two consecutive symbols is considered. The transmit symbols $s(1)$ and $s(2)$ are input to the STTD encoder. From the input, then the encoder generates two sequences which are the original one, i.e., $s(1)$ and $s(2)$, and the complex-conjugate of $s(1)$ and negative complex-conjugate of $s(2)$ whose order is reversed.

The block diagram of base station transmitter and mobile station receiver for STTD are shown in Fig. 2.9(a) and (b), respectively. At the transmitter (see Fig. 2.9(a)), the transmit data after channel encoder is STTD encoded [23] resulting in two different transmit sequences. These transmit sequences are spread by the same spreading code, and then code multiplexed with respective spread CPICH sequence to obtain the transmit signals for Antenna 1 and Antenna 2.

At the receiver (see Fig. 2.9(b)), the received signal is simultaneously despread using matched filter (MF) of DPCH and CPICH. Using the output of CPICH matched filter, independent channel estimation for Antenna 1 and Antenna 2 are performed. Next, the complex conjugate of channel estimate is multiplied with DPCH matched filter output to compensate the channel variations. These two sequences are input to STTD decoder and followed by a channel decoder to recover the transmit data. Note that the STTD scheme does not incur any bandwidth redundancy, thus preserves the transmission rate.

Another open loop type transmit diversity is TSTD which is considered for the SCH. In this scheme, the transmit antenna is periodically switched from one antenna to the other. This simplicity is required not to incur additional complexity for synchronization tasks.

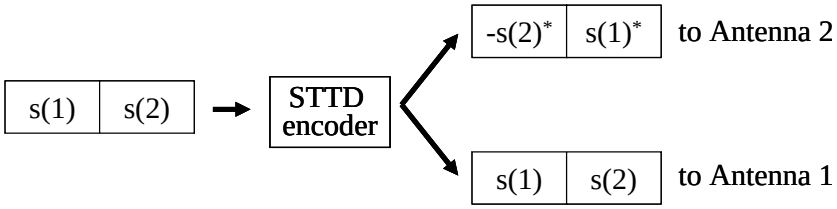

Fig. 2.8 Operation of STTD encoding

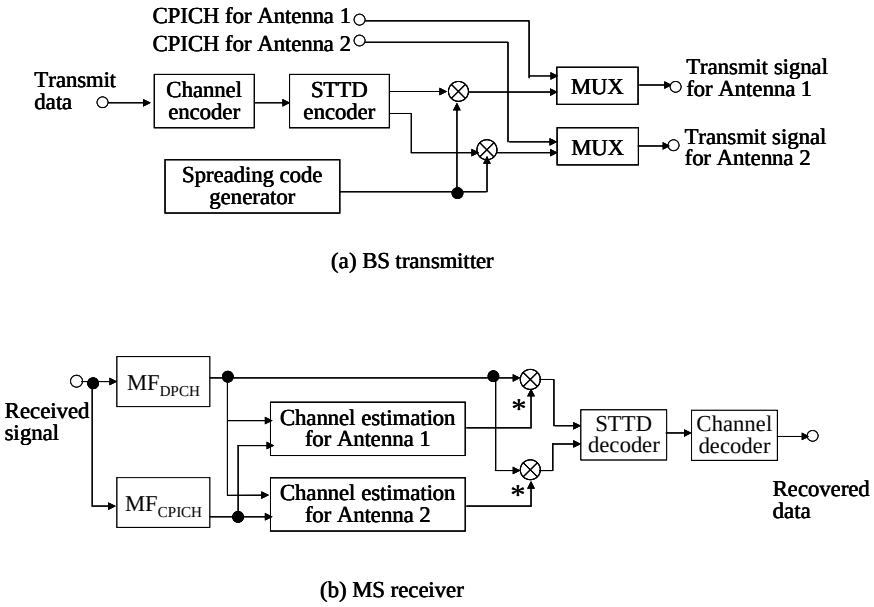

Fig. 2.9 Block diagrams for STTD transmitter and receiver

(b) Closed Loop

Figure 2.10 (a) and (b) show the block diagrams of transmitter and receiver for closed loop phase control transmit diversity. At the base station transmitter, the transmit data after channel encoder is split into two identical transmit sequences. These sequences are then multiplied with respective complex weights, $W_{1,n} = A_{1,n} \exp\{j\phi_{1,n}\}$ and $W_{2,n} = A_{2,n} \exp\{j\phi_{2,n}\}$ where $A_{1,n} = A_{2,n} = \sqrt{1/2}$ and $\phi_{1,n} = 0$ and $\phi_{2,n} = \{\pm\pi/4, \pm 3\pi/4\}$ according to decoded feedback information (FBI) bit received from mobile station. Since the feedback channel rate is 1.5 kbps (1 bit per slot), two consecutive FBI bits is used to obtain control resolution of $\pi/4$. Note, that this operation is possible due to constellation rotation at MS. If FBI decoding error does not occur the BS employs the same complex weights as commanded by the MS, thus maximize the instantaneous received signal power at the MS. Then, spreading is performed followed by code multiplexing with respective despread CPICH sequences to obtain the transmit signals for Antenna 1 and Antenna 2.

At the MS receiver, similarly to open loop type, the received signal is simultaneously despread using matched filter of DPCH and CPICH and channel estimation is performed independently for Antenna 1 and Antenna 2. However, unlike the open loop type, by comparing the phase difference of the received signal from Antenna 1 and Antenna 2, FBI bit is generated and informed to the BS about transmit carrier phase that will maximize the instantaneous received power at the next slot. After channel compensation, then coherent

Rake combining is performed followed by channel decoder to recover the transmit data. It is intuitive that the performance is affected by the feedback channel accuracy. Indeed, it is true that errors in the feedback channel (the BER is about 5% which corresponds to acceptable quality for voice communications) reduce the obtainable diversity effect. To alleviate the effect, antenna verification is performed at the MS.

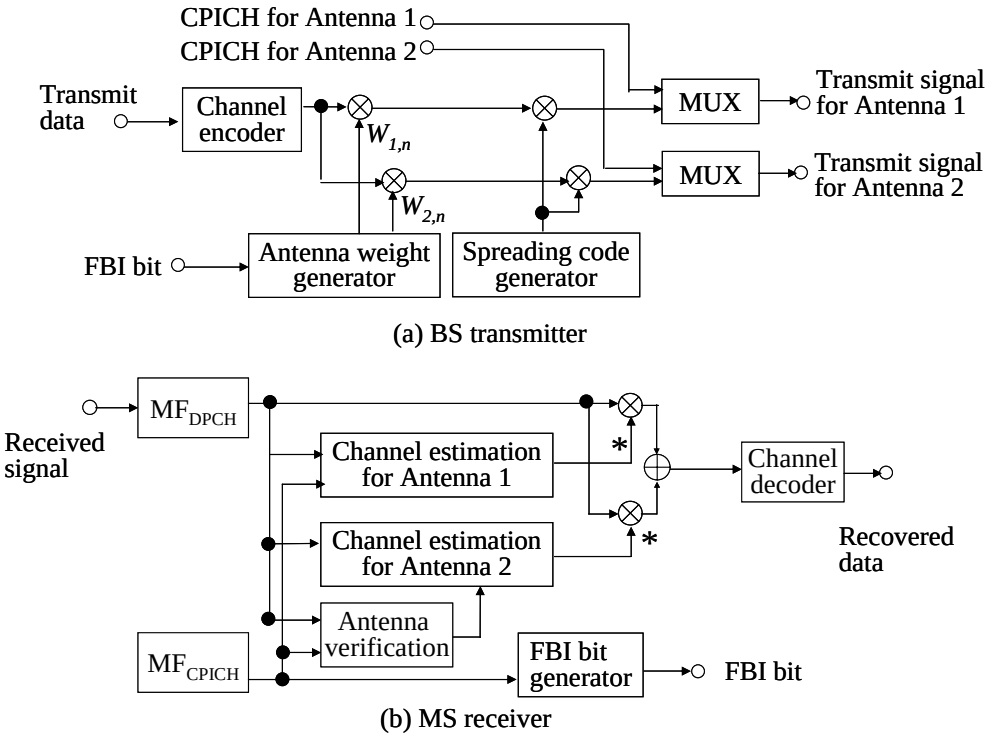

Fig. 2.10 Block diagrams of transmitter and receiver for closed loop phase control transmit diversity

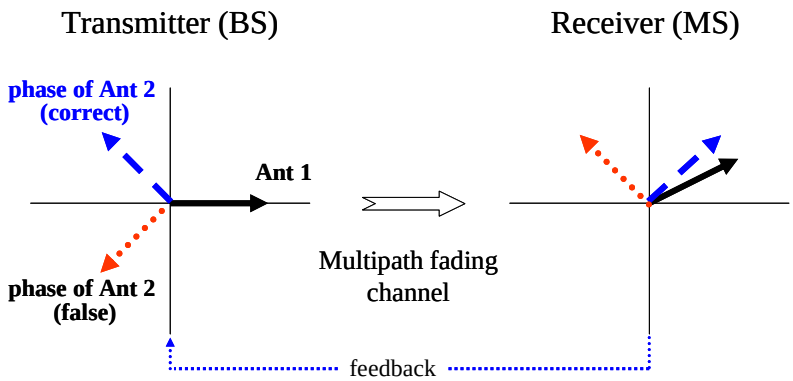

Fig. 2.11 Operation of antenna verification

Fig. 2.11 describes the operation of antenna verification at MS. The transmitted and received carrier phases of signal from Antenna 1 are shown in solid lines. The transmitted and received carrier phases when the feedback is correct and in error are shown in broken lines and dotted lines, respectively (note that the amplitude variation is ignored for simplicity).

First, let's consider the case when the feedback is correct. The BS then uses transmitted carrier phase as shown in the broken line at the left. At the MS, the transmitted signals from Antenna 1 and Antenna 2 are received almost co-phased, thus maximizing the instantaneous received power. The MS can demodulate the signal correctly because the transmitted carrier phase of Antenna 2 is correctly compensated for.

On the other hand, when feedback error occurs the BS uses different transmitted carrier phase to that commanded by the MS as illustrated by the dotted line in the Figure. This results in degradation of instantaneous received power. Consequently, the MS erroneously demodulate the signal because the transmitted carrier phase of Antenna 2 is not correctly compensated for. To alleviate this effect, the MS detects the actual transmitted carrier phase of Antenna 2 by collating the channel estimates obtained from dedicated pilot symbols to that obtained from CPICH.

2.3 MPIC

From the discussion in Section 2.1 it is clear that the capacity of CDMA system is limited by the interference power in the system. Therefore, it is important to suppress the interference power to increase the system capacity. Although characteristics of forward link and reverse link are different, the former can be considered as a special case of the latter. That is, all channels in the forward link are aligned in time and travel the same propagation path(s). Taking advantage of the time alignment among the channels, the use of orthogonal spreading codes, namely OVSF codes described in Section 2.4, establish orthogonality among the channels, i.e., eliminate inter-channel interference. However, due to multipath propagation, which is common in mobile communication environment, each channel suffers from severe MPI especially from high rate users and other-cell interference.

Multipath interference canceller (MPIC) stemmed from multistage interference canceller (MSIC), originally devised for the reverse link. Operational principles of MPIC are generation of interference replica, i.e., replica of received signal at each resolved path of each user, and subtraction of it from the received signal before performing data decision of the desired user. Note that MPI replica of other users at the same path need not to be cancelled. To generate MPI replica we can use Rake coherent combiner soft output or Rake coherent combiner output after hard decision. In this thesis MPIC employing hard decision in, assuming coherent detection is considered. Although this causes propagation of decision

error, the effect can be alleviated by using interference rejection weight. Thus, to generate MPI replica the following information need to be estimated:

- Channel estimate (channel gain)
- Tentative decision data
- Received timing of each path

Generally, MPIC has multistage construction in which MPI replica generation is performed recursively, yet refined input signal is used after MPIs from other channels and own channel are removed in the subsequent stages.

Based on the order of MPI generation and subtraction, there are serial type and parallel type. Each has its own advantages and disadvantages. Each will be described in detail shortly.

Fig.2.12 shows the operational principles of serial type MPIC. Because of different circumstances of the first stage and later ones, both will be described briefly. At the first stage, the received power of each channel is measured and then channels are ordered in the order of decreasing received power (hereafter channel ranking). Channel with highest received power is first processed because it is the least affected by MPI and therefore most reliable tentative decision data is possible. As a result, accurate MPI replica can be generated. Next, channel with second highest received power is processed in similar manner to the strongest channel. The only difference is that the MPI replicas of the strongest channel are removed from the received signal input to MPI replica generator. Using this enhanced signal, the MPI replicas are generated more reliably. At last, the generated MPI replicas of all channels but the weakest one are removed from the received signal. Then, the MPI replicas of the weakest channel are generated. Accurate MPI replica of the weakest channel is possible because MPI from stronger channels are removed from the input signal. Note that only MPI replicas of stronger channels than that to be processed are cancelled because MPI replicas of weaker ones than that to be processed are not yet available. At the second stage and after, similar processes are performed, yet more accurate MPI replica is generated because enhanced input signal after the MPI removal is used. Note that MPI replica subtraction is performed so that the MPI replica of stronger channel generated at the same stage is used and that of weaker channel generated at the previous stage is used. The accuracy of generated MPI replicas is improved with increasing number of stages. After the last stage, the generated MPI replicas of all channels except that of the desired user are subtracted from the received signal. Then despreading followed by coherent Rake combining is performed to recover the transmit data.

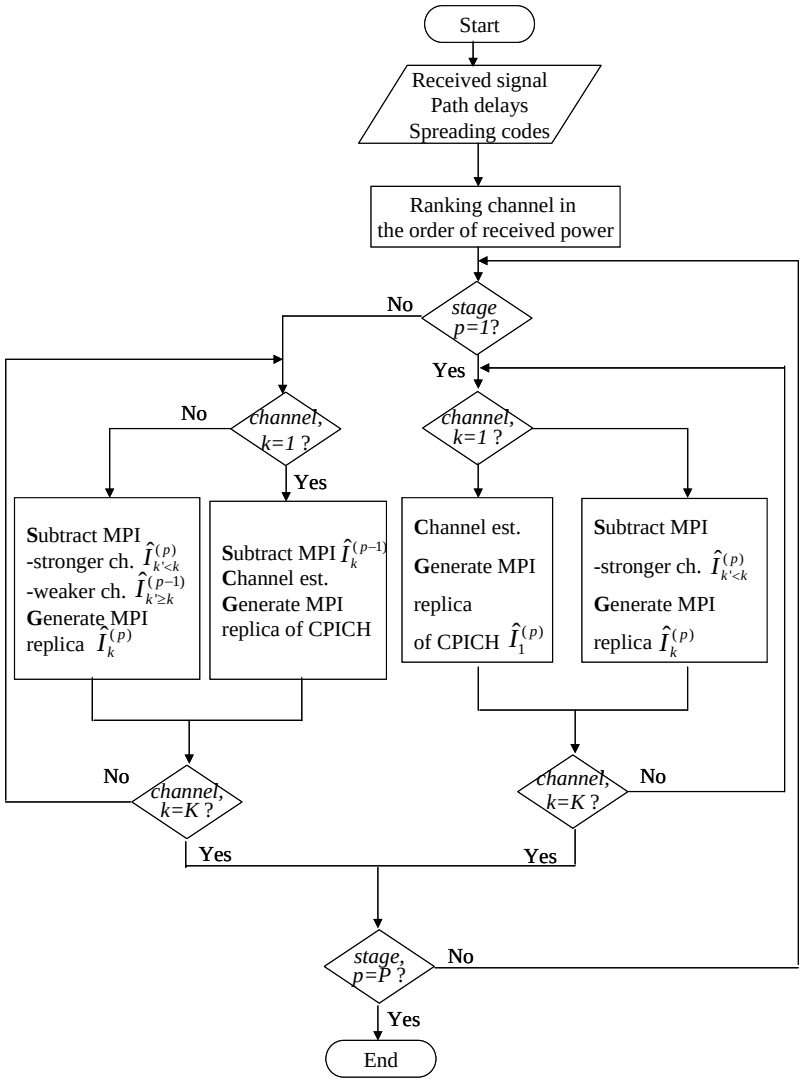

Fig. 2.12Operational principles of serial type MPIC

Serial MPIC has advantage of good performance, in term of achievable BER, because MPI replica generation is performed successively in the order of the channels reliability, i.e., received signal power. Another advantage is low hardware complexity. However, it has disadvantage of longer processing delay.

Next, parallel type MPIC is discussed. Fig.2.13 shows flowchart describing the operational principles of parallel type MPIC. Similarly to serial type MPIC, the operations at the first stage and later ones are different. At the first stage, unlike the serial type MPIC, channel ranking is not performed. MPI replicas of all channels are simultaneously generated using the received signal without MPI replica subtraction. Since the reliability of each channel varies one from another, accordingly so does the accuracy of generated MPI replica. At second stage and after, MPI replicas generated at previous stage are subtracted from the

received signal before regenerates MPI replicas of each channel. Similarly to the serial type MPIC, after the last stage, the generated MPI replicas of all channels except that of the desired user are subtracted from the received signal. Then despreading followed by coherent Rake combining is performed to recover the transmit data.

Parallel MPIC, in contrast to serial MPIC, has advantage of shorter processing delay because all channels are processed simultaneously. However, it has disadvantages of inferior performance compared to serial MPIC and high hardware complexity. The comparison of both types of MPIC is listed in Table 2.2.

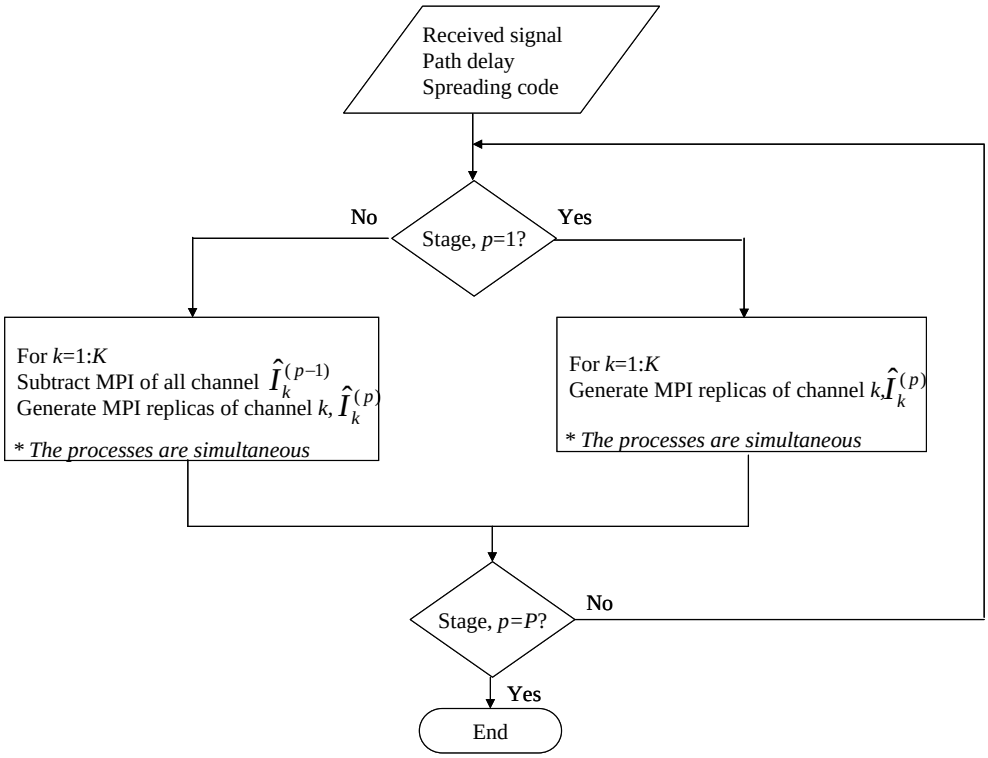

Fig. 2.13 Operational principles of parallel type MPIC

Table 2.2 Comparison between serial and parallel MPIC

	Serial MPIC	Parallel MPIC
BER performance	Good	Inferior
Complexity	Low	High
Processing delay	Long	short

In the following, important issues pertain to MPIC receiver and factors which affect the performance are discussed. Channel estimate is required for compensating the fading variations before coherent Rake combining to obtain tentative decision data and generating MPI replica. Therefore, it is crucial to achieve accurate channel estimate to improve the overall performance of MPIC receiver. Channel estimate is obtained from pilot symbols. Basically, the accuracy of channel estimation depends on the power allocated to the pilot symbols. Higher power yields more accurate channel estimate, but is power inefficient because pilot symbols do not carry any information. Channel estimate accuracy also affected by the maximum Doppler frequency, f_D, ($f_D = v/\lambda$) where v is the moving speed and λ is the wavelength of the carrier frequency. At low f_D, the channel is highly correlated in time, therefore longer averaging period will average out noise hence yield accurate channel estimate. On the other hand, at high f_D the channel varies rapidly, thus shorter time averaging is desirable not to overlook the fading variations. A channel estimation filter called WMSA filter [25] was proposed for the reverse link channel. This filter varies the number of slots (a slot is a unit for performing channel estimation) to be coherently combined and their respective weights according to the fading variations, thus achieving accurate channel estimates.

Although channel estimation indeed affects the accuracy of tentative decision data, there is another technique to improve the accuracy. As pointed out previously, we can perform tentative decision data after channel decoding then, re-encode the tentative decision data sequence for generating the MPI replica. This technique, significantly improve the tentative decision data accuracy, but it needs to buffer one frame portion of the received signal thus incur processing delay of more than one frame duration (10ms).

The third factor that affects MPIC performance is received timing of each path. In this paper, the effect of received timing estimation error is not considered. Assuming that robust path search is possible [27], nevertheless subject to further investigation. Moreover, in the forward link common pilot channel with relatively large transmission power and without fast TPC is available for this purpose. Still further, in [35] is reported that MPIC can be made robust against received timing estimation error.

Although the aforementioned issues are exactly the same with IC in the reverse link channel, and have been dealt with in numerous papers in the literature, the application of similar techniques in the forward link channels has its own aspects due to the differences of both channels. Further, adaptation of MPIC structure when transmit diversity is employed and appropriate performance evaluations considering its aspects are required. Another important issue is the receiver complexity, since application at the mobile station is considered.

Chapter Three

Multipath Interference for Orthogonal-Code Multiplexed Channels in W-CDMA Forward Link

3.1. Introduction

This chapter proposes to employ a multipath interference canceller (MPIC) in orthogonal code multiplexed channels associated with orthogonal variable spreading factor (OVSF) short code assignment in the DS-CDMA forward link, and evaluates the bit error rate (BER) performance by computer simulation. Application of the MPIC has the following two advantages compared to adaptive antenna array transmit diversity (AAA-TD) at the base station (BS) transmitter at the sacrifice of increased complexity of the mobile station (MS) terminal. First, the MPIC suppresses MPI irrespective of the relative relation of the direction of arrivals (DOAs) between the desired signal and interfering signals, meanwhile, when the difference in DOA between the desired signal and interfering signals is within the beam width, almost no MPI suppression is gained in AAA-TD. Second, the MPIC decreases severe MPI from the common channels with larger transmission power since they are transmitted with an omni-directional antenna pattern and without fast TPC, while assuring the required quality with the prescribed outage probability depending on each system. However, AAA-TD cannot remove the MPI component within the generated transmit beam pattern.

In this chapter, I first propose to apply the MPIC to only the common channels because the performance improvement in the forward link is large by removing the MPIs from common channels. Moreover, I also propose to apply the MPIC to the prior dedicated channels with large transmission powers, i.e., high-rate traffic channels, in addition to the common channels, in order to limit the increase in the complexity of MS terminal.

The MPIC algorithm employed here is based on that originally proposed in [13]. However, the MPIC algorithm proposed here differs from [13] in the following two points. First, the original MPIC algorithm has a function to remove only the data packet channel called HS-DSCH (High Speed Downlink Shared Channel) with OVSF code spreading and with constant transmission power in HSDPA (High Speed Downlink Packet Access). Meanwhile, the MPIC algorithm here is extended to suppress MPI of all dedicated physical channels presented in Section 3.2 including non-orthogonal physical channel. Second, this chapter proposes the MPI suppression of limited number of traffic channels (TCHs) with priority based on the received signal power for restraining the increase of complexity of a MS terminal. Further, the proposed MPIC employs WMSA channel estimation filter to

further enhance the channel estimation accuracy which is essential to the performance. The detail comparison of the proposed MPIC and the HSDPA MPIC is listed in Table 3.1.

Table 3. 1 Comparison between HSDPA MPIC and the proposed MPIC

	Proposed MPIC	HSDPA MPIC
Functionality	1. Canceling multipath of own signal and other users' signal 2. Canceling orthogonal common channel 3. Canceling non-orthogonal physical channel	Multipath of common packet channel in HSDPA
Algorithm	1. Using CPICH and dedicated pilot for channel estimation 2. Using W-MSA channel estimation filter for further enhancement of channel estimation accuracy	Using CPICH of corresponding slot only for channel estimation

3.2 Transmitted Signal Representation

I consider the following four physical channels: pilot channel (PICH), common control channel (CCH), synchronization channel (SCH), and TCH. The frame structures of these four physical channels are illustrated in Fig. 3.1. The radio frame length is 10 msec and comprises 15 slots, each 0.667 msec. Ten data-unmodulated pilot symbols with the SF = 256, which are shared by communicating users within a cell, are included in each slot of PICH. Each slot of the CCH consists of N_d = 10 coded data symbols. Similarly, each slot of the dedicated TCH comprises N_p = 16 dedicated pilot symbols and N_d = 144 coded data symbols. In addition, the symbol rates of the CCH and TCH become 15 ksps and 240 ksps, respectively (note that the symbol rate means the total symbol rate of the physical channel including pilot symbols similar to the definition in 3GPP (3^{rd} Generation Partnership Project) standard [20]). Thus, the spreading factor, which is the ratio of the chip rate to the symbol rate, of the CCH and TCH is SF = 256 and 16, respectively. Finally, each slot of the SCH consists of the 10 known-data-modulated symbols with the SF = 256 (thus, the symbol rate is 15 ksps).

A simplified block diagram of the transmitter of a BS assumed here is illustrated in Fig. 3.2. Within four physical channels, three channels except the SCH are spread by the combination of a scrambling code with the repetition period of one radio frame (= 38400-chip length) and a short OVSF code with the repetition period of SF, similar to the

2-layered spreading codes in W-CDMA [5]. Meanwhile, the SCH is spread only by the short code (thus, note that the SCH is not orthogonal to other physical channels). The scrambling code is generated by truncating the Gold sequence with the length of 2^{41} chips. Further, Walsh-Hadamard sequence was used as OVSF code. The resultant chip rate is 3.84 Mcps.

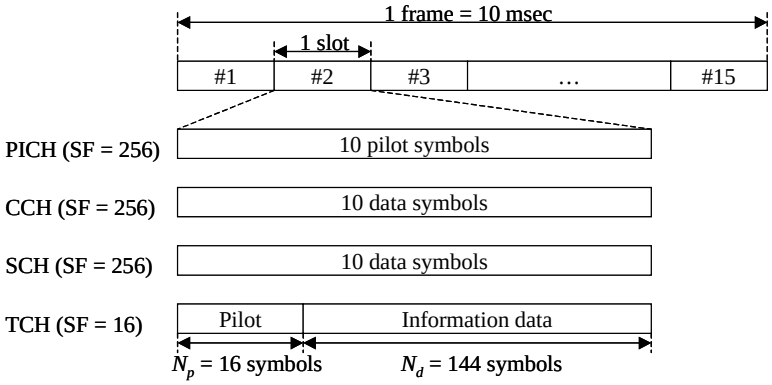

Fig. 3.1 Frame Structure

The four channels are characterized as follows. Note that although the physical channels having the identical features are defined in 3GPP (3rd Generation Partnership Project) standard [20], I use different notations in the paper because I focus on the transmission property of each physical channel in itself.

- PICH: The PICH is data-modulated by the known modulation phase at the receiver, i.e., bearing no data information, and spread by the combination code of a cell-specific scrambling code and OVSF code. Aside from this, the PICH is transmitted with constant transmission power.
- CCH: The CCH bears the information data, thus the symbol sequence is data-modulated (note that tentative data decision is required to generate an MPI replica in the MPIC as explained in Section 3.3). It is spread by the cell-specific scrambling code and OVSF code. In addition, the CCH is also transmitted at constant transmission power.
- SCH: The SCH is data-modulated by the known modulation phase at the receiver and transmitted at constant transmission power. However, it is spread only by the short code. This means that the SCH is non-orthogonal to the other channels.
- TCH: The TCH bears information data; therefore, it is data-modulated and is spread by the cell-specific scrambling code and OVSF code. Dissimilar to the CCH, the TCH is transmission-power-controlled so that the required SIR after Rake combing is satisfied.

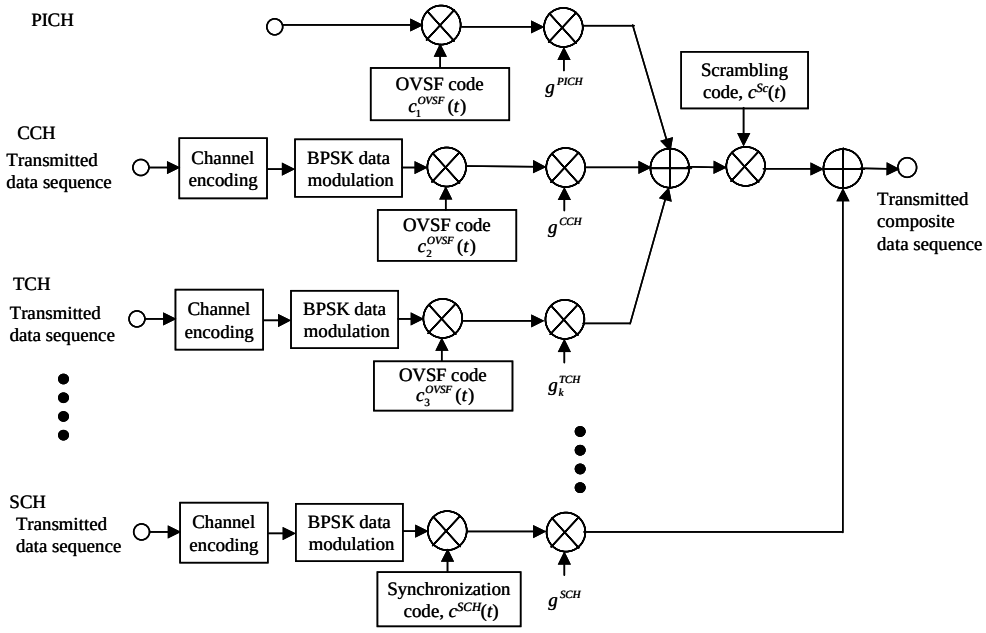

Fig. 3.2 Base station transmitter configuration

In the paper, I assume that $d^{PICH}(t) = \sum_{i=-\infty}^{\infty} g^{PICH} \cdot u(t/T^{PICH} - i)$ for the PICH, where g^{PICH} and T^{PICH} are the amplitude and symbol duration of the PICH, respectively, and u (t) is the step function such that $u(t) = 1$ for $0 \le t < 1$, and otherwise, $u(t) = 0$. I express the data-modulated signal waveform of the CCH, SCH, and the *k*-th TCH as $d^{CCH}(t) = \sum_{i=-\infty}^{\infty} g^{CCH}(i) \cdot \exp\left[j\phi^{CCH}(i)\right] \cdot u(t/T^{CCH} - i)$, $d^{SCH}(t) = \sum_{i=-\infty}^{\infty} g^{SCH}(i) \cdot \exp\left[j\phi^{SCH}(i)\right] \cdot u(t/T^{SCH} - i)$, $d_k^{TCH}(t) = \sum_{i=-\infty}^{\infty} g_k^{TCH}(i) \cdot \exp\left[j\phi_k^{TCH}(i)\right] \cdot u(t/T_k^{TCH} - i)$, respectively, where T^{CCH}, T^{SCH} and T^{TCH}, and g^{CCH}, g^{SCH} and g^{TCH} are the symbol duration and amplitude of the CCH, SCH and TCH, respectively. Further, $\phi^{CCH}(i)$, $\phi^{SCH}(i)$, and ϕ_k^{TCH} are the narrowband data modulation of CCH, SCH, and *k*-th TCH, respectively and they are expressed as $\phi^{CCH}(i), \phi^{SCH}(i), \phi_k^{TCH}(i) \in \{q\pi; q = 0,1\}$ since I assumed BPSK (Binary Phase Shift Keying) data modulation.

Let $c_k^{OVSF}(t) = \sum_{i=-\infty}^{\infty} \exp[j\phi_k^{'}(i)] \cdot u(t/T_c - i)$ and $c^{Sc}(t) = \sum_{i=-\infty}^{\infty} \exp[j\phi_{Sc}^{'}(i)] \cdot u(t/T_c - i)$ be

the spreading signal waveform of the OVSF code and that of the in-phase (I)/quadrature (Q) components of the cell-specific scrambling code. In those notations, T_c denotes the chip duration and $N = T/T_c$ is the *SF*. Furthermore, $\phi_k^{'}(i) \in \{q\pi; q = 0,1\}$ are the BPSK modulation phases. Similarly, let $c^{SCH}(t) = \sum_{i=-\infty}^{\infty} \exp[j\phi_{SCH}^{'}(i)] \cdot u(t/T_c - i)$ be the spreading signal waveform of the SCH, assuming the BPSK modulation phase such that $\phi_{SCH}^{'}(i) \in \{q\pi; q = 0,1\}$. Then, the combined spreading code sequence is represented as $c_k^{Spread}(t) = c_k^{OVSF}(t)c^{Sc}(t)$, and the transmitted signal *s(t)* is given as

$$s(t) = d^{PICH}(t)c_1^{Spread}(t) + d^{CCH}(t)c_2^{Spread}(t) + \sum_{k=1}^{K} d_k^{TCH}(t)c_{k+2}^{Spread}(t) + d^{SCH}(t)c^{SCH}(t) \qquad (3.1)$$

3.3 MPIC

The transmitted signals represented in Equation (3.1) propagate through a multipath-fading channel and are received at a MS receiver employing the proposed MPIC. Antenna diversity reception was not used in the evaluation. The received signal is represented as

$$r(t) = \sum_{l=1}^{L} \xi_l(t)s(t - \tau_l) + n(t) \qquad (3.2)$$

where ξ_l and τ_l are the complex-valued channel gain and the time delay of the *l*-th path. Term *n(t)* is the additive Gaussian noise component with one-sided spectrum density N_0. The structure of the proposed MPIC is illustrated in Fig. 3.3. Each stage of MPIC comprises an MPI replica generation unit, called MPIRGU, of the PICH, CCH, and TCH. For the SCH, an interference replica of the same propagation path and that of the MPI are generated in this unit. Thus, I refer to this as an interference replica generation unit (IRGU) for the SCH. A block diagram of the MPIRGU of the PICH is shown in Fig. 3.4. In each MPIRGU, the input sample sequence of each antenna is despread by a matched filter (MF) into the resolved multipath components. The complex fading envelope, i.e., the channel gain of each path, is derived from the despread signal of the PICH. The channel gain of the *n*-th slot, $\hat{\xi}_l^{(1)}(n)$, is obtained by coherently accumulating the despread signal of three successive slots as shown in the next equation. For channel estimation filter, I applied WMSA channel estimation filter as shown in Fig. 3.5 [25], in which the channel estimate, i.e., coherent accumulation of the despread symbols of the PICH at each slot is weighted by

the real-value weight and coherently combined. I used weights such as $\alpha_1 = 0.27$, $\alpha_1 = 0.27, \alpha_0 = 0.46$ and $\alpha_{-1} = 0.27$ [25].

$$\hat{\xi}_l^{(1)}(n) = \sum_{i=-1}^{1} \frac{\alpha_i}{\sqrt{|\, d^{PICH} \,|^2 T_{Slot}}} \int_{(n+i)T_{slot}+\hat{\tau}_l}^{(n+i+1)T_{slot}+\hat{\tau}_l} r(t) \cdot c_1^{Spread*}(t-\hat{\tau}_l) dt \tag{3.3}$$

where the despread signal of each slot is weighted by weighting factor α_i. The MPI of the PICH is then computed using the channel gain in Equation (3.3) as

$$\hat{I}_{PICH,l}^{(1)}(t-\hat{\tau}_l) = \hat{\xi}_l^{(1)}(t) d^{PICH}(t-\hat{\tau}_l) \cdot c_1^{Spread}(t-\hat{\tau}_l) \quad . \tag{3.4}$$

As shown in Fig. 3.3, for the input signal of MPIRGU of the CCH, the generated MPI replica of the PICH is subtracted from the received signal. The structure of the MPIRGU for the CCH, SCH, and TCH is shown in Fig. 3.6. The despread data sequence of the *m*-th symbol of the *n*-th slot associated with the *l*-th path of the CCH in MPIRGU is given as,

$$z_{CCH,l}^{(1)}(n,m) = \frac{1}{T^{CCH}} \int_{nT_{slot}+mT^{CCH}+\hat{\tau}_l}^{nT_{slot}+(m+1)T^{CCH}+\hat{\tau}_l} \left[r(t) - \sum_{\substack{l'=1 \\ l' \neq l}}^{L} \alpha_{PICH} \hat{I}_{PICH,l'}^{(1)}(t-\hat{\tau}_{l'}) \right] \cdot c_2^{Spread*}(t-\hat{\tau}_l) dt \tag{3.5}$$

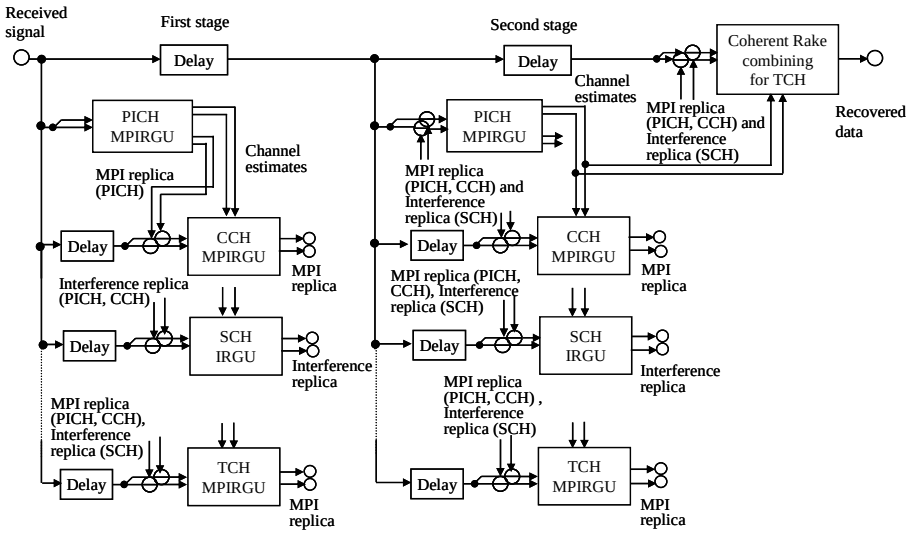

Fig. 3.3 Block diagram of MPIC

where, α_{PICH} denotes the real-valued interference rejection weight (IRW) ($0 < \alpha \leq 1$) [28] for the MPI of the PICH. In a real propagation channel, the accuracy of the generated interference replica is degraded due to channel estimation error and data decision error. Thus, by using a weighting factor that is smaller than 1.0, the impact of the interference replica error is mitigated. By multiplying the complex conjugate of the channel estimate, $\hat{\xi}_l^{(1)}(n)$, with the despread data sequence of the resolved path component in Equations (3.5), the *L*-path components are coherently Rake-combined. The data sequences after Rake combining of the *m*-th symbols of the *n*-th slot for the CCH, $\hat{d}_{CCH}^{(1)}(n,m)$ is expressed as,

$$\hat{d}_{CCH}^{(1)}(n,m) = \sum_{l=1}^{L} z_{CCH,l}^{(1)}(n,m) \cdot \hat{\xi}_l^{(1)*}(n) \quad , \tag{3.6}$$

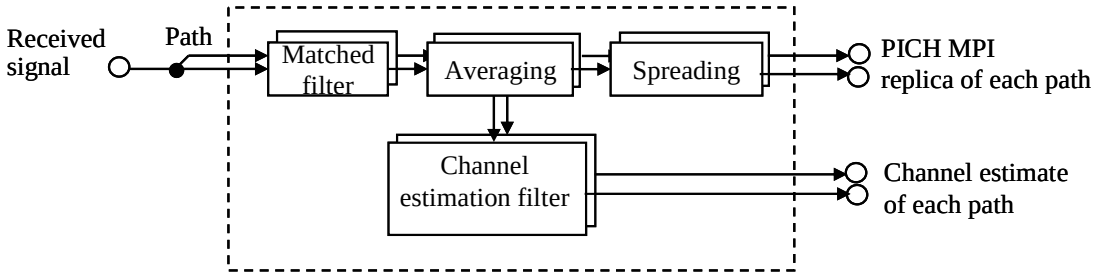

Fig. 3.4 Block diagram of MPIRGU of PICH

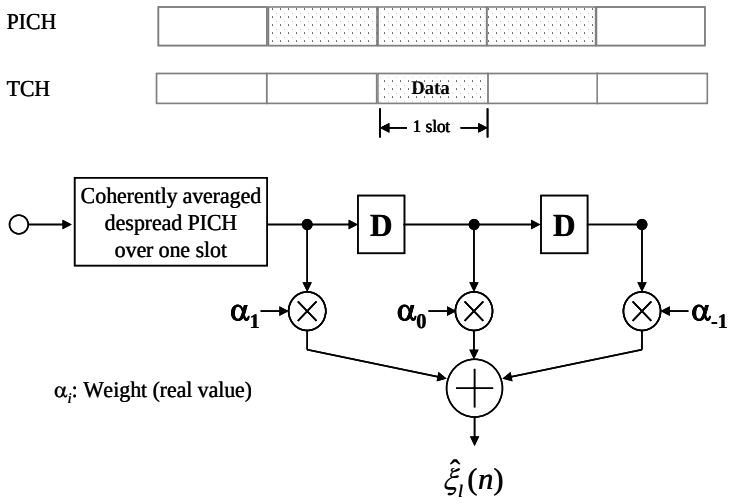

Fig. 3.5 Principle of channel estimation filter

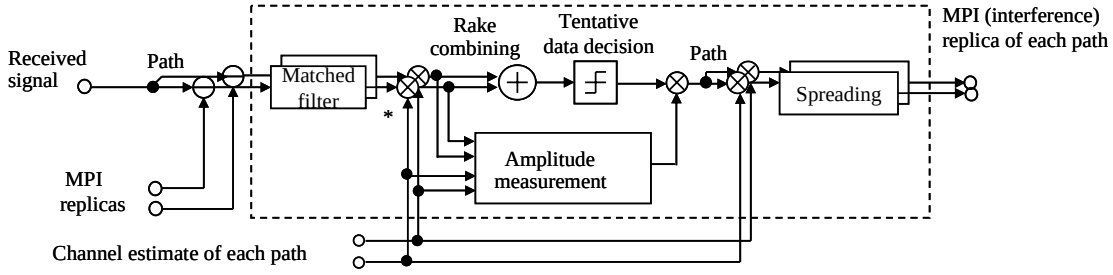

Fig. 3.6 Block diagram of MPIRGU for CCH and TCH, and IRGU for SCH

where * denotes the complex conjugate. Thus, the Rake-combined data sequence is tentatively decided to generate the binary data sequence. By using the binary decision data sequence after Rake combining, $\tilde{d}_{CCH}^{(1)}(n,m)$, i.e., reverse data modulation, the data demodulation of the Rake combined data sequence is removed. Therefore, the MPI replica of the CCH associated with *l*-th path is generated as,

$$\hat{I}_{CCH,l}^{(1)}(t-\hat{\tau}_l) = \hat{\xi}_l^{(1)}(t)\tilde{d}_{CCH}^{(1)}(t-\hat{\tau}_l)\cdot c_2^{Spread}(t-\hat{\tau}_l) \quad . \tag{3.7}$$

Employing the spread data sequence, nevertheless, in which the MPI replicas of the PICH and CCH are removed, the interference replica, i.e., MPI replica in addition to the replica in the same propagation path, is produced based on the similar processing as in the CCH. The despread data sequence of the *m*-th symbol of the *n*-th slot associated with the *l*-th path of the SCH in IRGU is expressed as,

$$\begin{aligned} z_{SCH,l}^{(1)}(n,m) = \frac{1}{T^{SCH}} \int_{nT_{slot}+mT^{SCH}+\hat{\tau}_l}^{nT_{slot}+(m+1)T^{SCH}+\hat{\tau}_l} \Bigg[& r(t) - \sum_{l'=1}^{L} \Big(\alpha_{PICH}\hat{I}_{PICH}(t-\hat{\tau}_{l'}) \\ & + \alpha_{CCH}\hat{I}_{CCH,l'}^{(1)}(t-\hat{\tau}_{l'}) \Big) \Bigg] \cdot c^{SCH*}(t-\hat{\tau}_l)dt \end{aligned} \tag{3.8}$$

where, α_{PICH} denotes the IRW for the MPI of the CCH. Then, based on the binary decision data sequence of SCH, the channel estimate in equation (3.1), the interference replica of the SCH associated with *l*-th path is derived as,

$$\hat{I}_{SCH,l}^{(1)}(t-\hat{\tau}_l) = \hat{\xi}_l^{(1)}(t)\tilde{d}_{SCH}^{(1)}(t-\hat{\tau}_l)\cdot c^{SCH}(t-\hat{\tau}_l) \quad . \tag{3.9}$$

Finally, the MF in the MPIRGU of the TCH despreads the signal, in which the MPI replica of the PICH and CCH, and interference replica of the SCH are all subtracted from the received signal. Then, the despread data sequence of the *m*-th symbol of the *n*-th slot associated with the *l*-th path of the *k*-th TCH ($1 \le k \le K$) at the first stage is expressed as

$$z_{k,l}^{(1)}(n,m) = \frac{1}{T^{TCH}} \int_{nT_{slot}+mT^{TCH}+\hat{\tau}_l}^{nT_{slot}+mT^{TCH}+\hat{\tau}_l} \left[r(t) - \sum_{\substack{l'=1 \\ l' \neq l}}^{L} \left(\alpha_{PICH} \hat{I}_{PICH,l'}^{(1)}(t-\hat{\tau}_{l'}) + \alpha_{CCH} \hat{I}_{CCH,l'}^{(1)}(t-\hat{\tau}_{l'}) \right) - \sum_{l'=1}^{L} \alpha_{SCH} \hat{I}_{SCH,l'}^{(1)}(t-\hat{\tau}_{l'}) \right] \cdot c_{k+2}^{Spread*}(t-\hat{\tau}_{l'}) dt$$

for *k*-th TCH, where $1 \le k \le K$ (3.10)

where, α_{SCH} denotes the IRW for the interference of the SCH. Then, the data sequences after Rake combining of the *m*-th symbols of the *n*-th slot for the *k*-th TCH $\hat{d}_k^{(1)}(n,m)$ is represented as

$$\hat{d}_k^{(1)}(n,m) = \sum_{l=1}^{L} z_{k,l}^{(1)}(n,m) \cdot \hat{\xi}_l^{(1)*}(n) \quad \text{for } k\text{-th TCH, where } 1 \le k \le K \tag{3.11}$$

By using the binary decision data sequence after Rake combining, $\tilde{d}_k^{(1)}(n,m)$, and channel estimate $\hat{\xi}_l^{(1)}(n)$, the MPI replica associated with the *l*-th path can be calculated as

$$\hat{I}_{k,l}^{(1)}(t-\hat{\tau}_l) = \hat{\xi}_l^{(1)}(t) \tilde{d}_k^{(1)}(t-\hat{\tau}_l) \cdot c_k^{Spread}(t-\hat{\tau}_l) \tag{3.12}$$

In the evaluation when the transmission power control (TPC) is not used for TCH, the amplitude of the transmitted signal of TCH, g_k^{TCH} is a constant value similar to those of PICH, CCH, and SCH. However, when TPC is employed in TCH, the value of g_k^{TCH} changes slot by slot. Thus, the amplitude or power of the received signal of TCH of each slot is determined by g_k^{TCH} and channel gain due to fading. Therefore, instantaneous amplitude of received signal at each slot must be estimated in order to generate the MPI replica of TCH. Then, I calculated the amplitude ratio of the PICH to TCH, i.e., g^{PICH} / g_k^{TCH} of each slot in the amplitude measurement block in Fig.3.6.

At the second stage, the channel estimation is performed for the data sequence of PICH, in which the generated MPI replicas of the PICH, CCH, SCH, and TCH (including the own path replica for SCH) are subtracted from the received signal. Thus, when the MPI replicas are ideally generated and subtracted from the received signal, only the PICH signal associated with the target path remains. Therefore, the channel estimate of the *n*-th slot at the second stage is given as

$$\hat{\xi}_l^{(2)}(n) = \sum_{i=-1}^{1} \frac{\alpha_i}{\sqrt{|\, d^{PICH}\,|^2\, T_{slot}}} \int_{(n+i)T_{slot}+\hat{\tau}_l}^{(n+i+1)T_{slot}+\hat{\tau}_l} \left[r(t) - \sum_{\substack{l'=1 \\ l' \neq l}}^{L} \left(\alpha_{PICH} \hat{I}^{(1)}_{PICH,l'}(t-\hat{\tau}_{l'}) + \alpha_{CCH} \hat{I}^{(1)}_{CCH,l'}(t-\hat{\tau}_{l'}) \right.\right.$$
$$\left.\left. + \sum_{k=1}^{K} \alpha_{TCH} \hat{I}^{(1)}_{k,l'}(t-\hat{\tau}_{l'}) \right) - \sum_{l'=1}^{L} \alpha_{SCH} \hat{I}^{(1)}_{SCH,l'}(t-\hat{\tau}_{l'}) \right] \qquad (3.13)$$
$$\cdot\, c_1^{Spread*}(t-\hat{\tau}_l)\, dt$$

The despreading operation by the MF of the CCH, TCH, and SCH at the second stage is conducted in a similar manner to that for the first stage as shown from Equations (3.5) and (3.6). The Rake combining for the TCH at the second stage is also identical to that at the first stage, yet, the more refined MPI replicas than those in the first stage are employed. Finally, in the last stage, the Rake-combined data sequence is de-interleaved and soft-decision Viterbi decoded to recover the transmitted data sequence. In the scheme, since the channel estimation and data decision are updated at each stage, the accuracy of the MPI replica is improved from the resulting enhancement of the channel estimation and decreasing data decision error. By combining the MPIC with orthogonal code multiplexing, when the data decision error occurs in a certain code channel, this decision error can be corrected in successive stages due to the improved SIR.

3.4 Simulation Configuration

The major radio link parameters assumed in the simulations are given in Table 1. The transmitted data sequence of the TCH is, after appending six tail bits, channel-coded using a convolutional code with a rate of 1/3 and a constraint length of seven bits. The coded data sequence is block-interleaved over one frame length (=10 msec). The data demodulation channel of the TCH and CCH are BPSK. Thus, since *SF* = 16, the processing gain, which is defined as the ratio of the chip rate to the information bite rate, becomes *Pg* = 16x3 = 48, where 3 is the bandwidth spreading factor due to convolutional coding. After being segmented into the assigned slot length, the data sequence is packed into the radio frame of the TCH, PICH, and CCH, and then spread by the combination of a cell-specific scrambling

code and OVSF short code. These three channels and the SCH, which is spread only by the OVSF short code, are code-multiplexed to generate the composite transmitted signal in the forward link.

In the simulations, an *L*-path channel model with equal average received power, in which each path suffers independent Rayleigh fading with the maximum Doppler frequency, f_D, in hertz was assumed. Chip and packet frame synchronizations were assumed to be ideally performed.

SIR-based fast TPC [29], [30] was employed for the dedicated TCH in the forward link. To reduce the TPC time delay, Rake combining for SIR measurement was performed independently from that for data demodulation. Signal power *S* and the instantaneous interference plus background noise power, *I*, associated with each slot were measured over N_p pilot symbols. The average of *I* was obtained using a first order filter with forgetting factor μ of 0.99375. The average received signal energy per bit-to-interference power spectrum density ratio (E_b/I_0) after Rake combining, which was calculated as E_b/I_0 = SIR + 10log(3) dB since channel coding with the rate of 1/3 was used, was compared with the target E_b/I_0 value. If the measured value was above (below) the target, the TPC command was sent to the BS to lower (raise) the transmitted power by 1 dB at the beginning of the next slot. The TPC delay had one-slot duration.

Table 3.2 Simulation parameters

Chip rate		3.84 Mcps
Symbol rate	PICH, SCH, CCH	15 ksps
	TCH	240 ksps
Spreading code	Spreading	OVSF code
	Scrambling	Gold code (2^{41}-1)
Modulation	Data	BPSK
	Spreading	BPSK
Spreading factor	PICH, SCH, CCH	256
	TCH	16
Channel model		Equal average power *L*-path Rayleigh fading
Channel estimation		WMSA channel estimation filter
Channel Coding (TCH)		Convolutional coding (R=1/3, k=7)/ soft decision Viterbi decoding
Diversity		*L*-finger Rake diversity

The number of active users throughout the simulations, with an exception of Fig. 3.16, was assumed to be ten that indicates that the evaluated system was near its capacity. In this respect, I defined system capacity as the number of users satisfying their respective QoS requirements, assuming MF-based Rake receiver and interfering users with equal average transmit power. For example, assuming a required QoS of average BER of 10^{-3}, namely voice conversation, the maximum number of users producing BER floor immediately below BER of 10^{-3} was 10 as shown in Fig. 3.10. This assumption is considered appropriate to justify the validity of MPIC because the performance depends on the interference power.

3.5 Simulation Results

3.5.1 MPI Suppression Effect of Each Channel

The average received E_b/N_0 for achieving the average BER of 10^{-3} applying the MPIC only to the PICH is plotted in Fig. 3.7 as a function of the ratio of transmit E_b/N_0 of the PICH to that of the TCH, $\Delta_{PICH/TCH}$. The performance with the MF-based Rake receiver is also shown for comparison. The ratios of the average transmit E_b/N_0 of the CCH and the SCH to that of the TCH were set to $\Delta_{SCH/TCH}$ = 3 dB and $\Delta_{CCH/TCH}$ = 5 dB, respectively. It was assumed that L = 2 and f_D = 80 Hz. The interference rejection weighting factor of the MPI replica was assumed to be α_{PICH} = 1.0. Figure 3.7 shows that although the required average transmit E_b/N_0 at the average BER of 10^{-3} with the MF-based Rake receiver is first decreased as $\Delta_{PICH/TCH}$ is increased due to the improvement in the channel estimation accuracy, it is abruptly degraded as $\Delta_{PICH/TCH}$ is increased further, since the MPI from the PICH increased. Meanwhile, from the figure, it is found that an almost constant required received E_b/N_0 is achieved according to the average transmit E_b/N_0 of the PICH as it increases. This indicates that the MPIC sufficiently suppresses the severe MPI from the PICH.

Next, the average received E_b/N_0 at the average BER of 10^{-3} using MPIC for the CCH in addition to the PICH is plotted in Fig. 3.8 as a function of the ratio of the average transmit E_b/N_0 of the CCH to that of the TCH, $\Delta_{SCH/TCH}$. From the results in Fig. 3.7, $\Delta_{PICH/TCH}$ was set to 0 dB. It was assumed that $\Delta_{SCH/TCH}$ = 3 dB, L = 2, f_D = 80 Hz, and $\alpha_{PICH} = \alpha_{CCH} = 1.0$. The figure shows that the required received E_b/N_0 with the MF-based Rake receiver is remarkably increased as $\Delta_{CCH/TCH}$ is increased, and that the average BER of 10^{-3} is not achieved due to severer MPI from the CCH when $\Delta_{CCH/TCH}$ is above 5 dB, assuming the 10 TCHs with SF = 16 are multiplexed. However, it is clear that almost a constant required received E_b/N_0 is achieved using MPIC since the severe MPI from the CCH is removed. When $\Delta_{CCH/TCH}$ = 5 dB, the required average received E_b/N_0

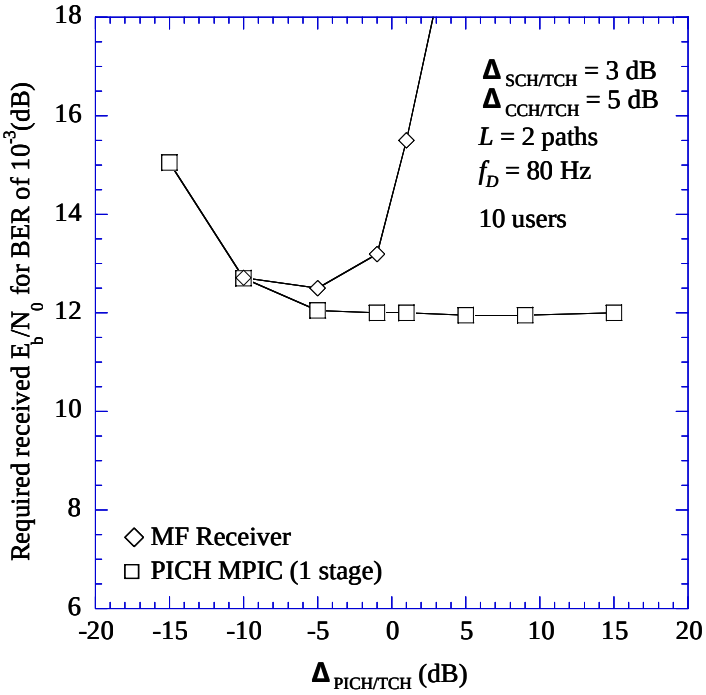

Fig. 3.7 Required average received E_b/N_0 as a function of $\Delta_{PICH/TCH}$

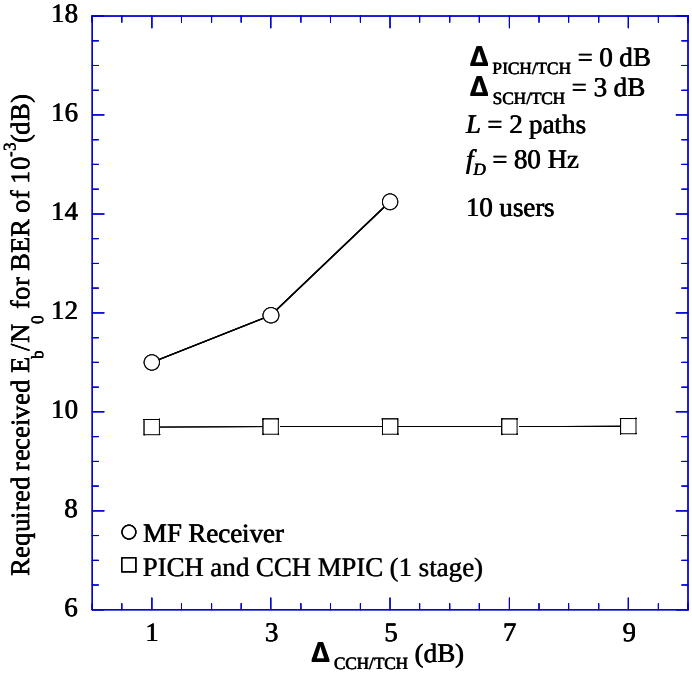

Fig. 3.8 Required average received E_b/N_0 as a function of $\Delta_{CCH/TCH}$

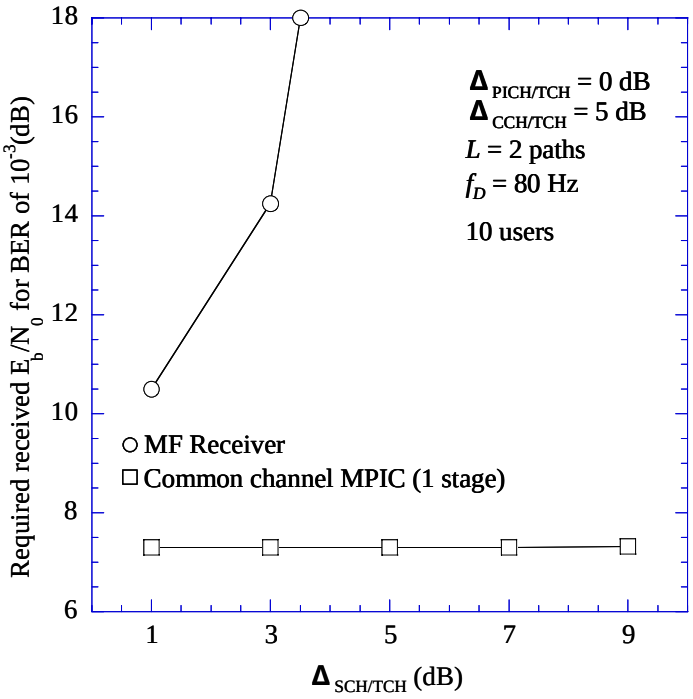

Fig. 3.9 Required average received E_b/N_0 as a function of $\Delta_{SCH/TCH}$

when the MPIC is used for the PICH and the CCH is decreased by approximately 3.0 dB compared to the case when it is used only for the PICH.

Further, the average received E_b/N_0 at the average BER of 10^{-3} using the MPIC for the SCH in addition to the PICH and CCH is plotted in Fig. 3.9 as a function of the ratio of the average transmit E_b/N_0 of the SCH to that of the TCH, $\Delta_{SCH/TCH}$. It was assumed that $\Delta_{PICH/TCH}$ = 0 dB, $\Delta_{CCH/TCH}$ = 5 dB, L = 2, and f_D = 80 Hz. It is evident that for the MF-based Rake receiver, as $\Delta_{SCH/TCH}$ is increased, the required average received E_b/N_0 is significantly degraded due to the severe interference from both the same propagation path and the delayed path. However, the figure shows that by applying the MPIC, almost a constant required received E_b/N_0 is achieved since the MPI in addition to the interference within the same propagation path is sufficiently suppressed. The required average received E_b/N_0 with MPIC suppression for the SCH in addition to the PICH and the CCH is further decreased by approximately 2.2 dB compared to the case with MPI suppression for the PICH and the CCH in Fig. 3.8.

3.5.2 Influence of the Number of Stages

The average BER performance with the function of the number of stages of the MPIC as a parameter is plotted in Fig. 3.10 as a function of the average received E_b/N_0 of the TCH.

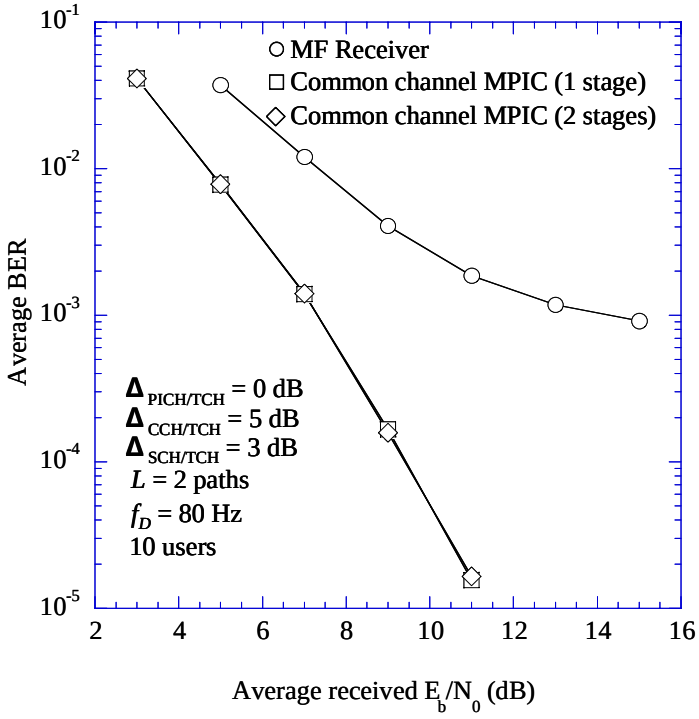

Fig. 3.10 Average BER performance of MPIC for MPI canceling of only common channels

Table 3.3 Complexity comparison between 1-stage MPIC and MF-based Rake receiver

	MF without MPIC	1-stage MPIC	
		Common channels only	All channels
Despreading	N_s x SF x 2 x L	N_s x SF x 4 x L	N_s x SF x (K+3) x L
Channel compensation	N_s x L	N_s x 2 x L	N_s x (K+1) x L
Multiplication of channel		N_s x 3 x L	N_s x (K+2) x L
Multiplication of interference rejection weight		N_s x 3 x L	N_s x (K+3) x L
Re-spreading		N_s x SF x 3 x L	N_s x SF x (K+3) x L
Total	$N_sL(2SF+1)$	$N_sL(7SF+8)$	$N_sL\{2SF(K+3)+3K+6\}$
Example (N_s = 160, SF = 16, L = 2, K = 10)	10560	38400	144640

From the results in Subsection 3.5.1, I set $\Delta_{PICH/TCH}$ = 0 dB, $\Delta_{CCH/TCH}$ = 5 dB, and $\Delta_{SCH/TCH}$ = 3 dB. It was also assumed that $\alpha_{PICH} = \alpha_{CCH} = \alpha_{SCH} = 1.0$, L = 2, and f_D = 80 Hz. Figure 3.10 clearly shows that the BER performance at the second stage was almost identical to that at the first stage. This is because an accurate MPI replica was generated at the first stage output due to the refined channel estimation and due to a decrease in the number of data decision errors since the transmit signal energy per symbol of the common

channel was much larger than that of the TCH. The required received E_b/N_0 at the average BER of 10^{-3} using MPIC for the PICH, the CCH, and SCH was decreased by approximately 6.5 dB compared to that with MF-based Rake receiver. This result suggests that by canceling MPI only from the PICH, CCH, and SCH, the achievable BER performance is largely improved by a relatively simple MPIC application.

Here, I compare the processing complexity of MPIC to that of the MF-based Rake receiver based on the number of operations of complex-valued multiplications (hereafter simply multiplications). The number of multiplications needed for each constituent process of the MPIC with 1-stage for MPI canceling of only common channels and that of the MF-based Rake receiver is listed in Table 3.2. In the MPIC, operations such as inverse-modulation required for decision-feedback channel estimation, multiplication of estimated channel gain to the decision data symbols, multiplication of the interference rejection weight, and re-spreading to regenerate the MPI replica are added to the operations needed for the MF-based Rake receiver. Finally, based on the number of multiplications listed in Table 3.2, I calculated the total number of multiplications of the MPIC and that of the MF-based Rake receiver which are also shown in the Table. It indicates that the complexity of the 1-stage MPIC for MPI canceling of only the common channels is almost 3.6 fold that of the MF-based Rake receiver. Thus, was can say that by applying 1-stage MPIC for MPI canceling of only the common channels is practical in improving the forward link BER performance.

3.5.3 Influence of the Interference Rejection Weight

Next, I investigate the effect of the interference rejection weight, α, when the MPI of a CCH and SCH was removed from the received signal, on the achievable BER performance. The average BER performance as a function of IRW $\alpha_{CCH}, \alpha_{SCH}$ is plotted in Fig. 3.11 with L as a parameter assuming that the α_{PICH} was 1.0. It was assumed that $\Delta_{PICH/TCH}$ = 0 dB, $\Delta_{CCH/TCH}$ = 5 dB, $\Delta_{SCH/TCH}$ = 3 dB, and f_D = 80 Hz. The average received E_b/N_0 was set to 7 dB. Figure 3.11 shows that the BER performance for L = 2 is improved most when $\alpha_{CCH} = \alpha_{SCH} = 1.0$. Meanwhile, for L = 3 and 4, almost the best BER performance is obtained with $\alpha_{CCH} = \alpha_{SCH} = 0.9$ because the accuracy of the generated interference replica is slightly degraded due to the increasing channel estimation error caused by the decreased received signal power per path. However, since the improvement from $\alpha_{CCH} = \alpha_{SCH} = 1.0$ is small, I used the parameters of $\alpha_{CCH} = \alpha_{SCH} = 1.0$ in the following evaluations.

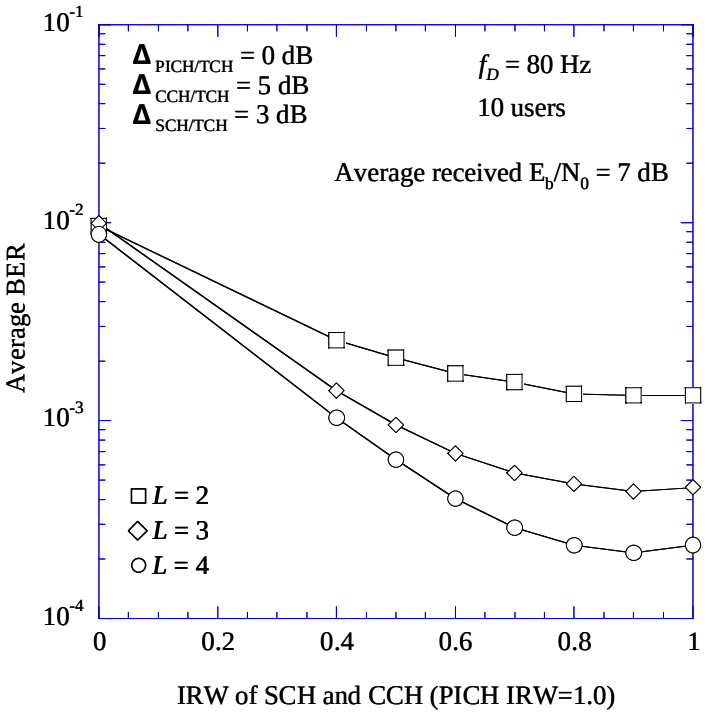

Fig. 3. 11 Optimum IRW for CCH and SCH

3.5.4 Rake Time Diversity Effect for L and f_D

Figure 3.12 shows the required average received E_b/N_0 for satisfying the average BER of 10^{-3} when the MPIC for the common channels is applied and fast TPC is not employed. The required average received E_b/N_0 is plotted as a function of f_D with L as a parameter using the parameters of $\Delta_{PICH/TCH}$ = 0 dB, $\Delta_{CCH/TCH}$ = 5 dB, $\Delta_{Int/Des}$ = 3 dB and $\alpha_{PICH} = \alpha_{CCH} = \alpha_{SCH} = 1.0$. The figure shows that the required average received E_b/N_0 is monotonously decreased as f_D became larger thanks to the improving channel coding effect associated with the increasing interleaving effect. It was reported in [30] that the required average received E_b/N_0 at the average BER of 10^{-3} with the MF-based Rake receiver is decreased most when L = 3 without antenna diversity reception. This is because when L is increased further beyond 3, the increasing MPI and channel estimation error offset the improving Rake diversity effect. However, it is clear from Fig. 3.12 that by using MPIC which suppresses MPI from the common channels having a larger transmit power than that of the TCH, the required average received E_b/N_0 is decreased as L is increased owing to the increasing Rake diversity effect. This implies that the Rake diversity effect is effectively derived without the impact of MPI. It is evident that the required average received E_b/N_0 with MPIC for the common channels at the average BER of 10^{-3} is decreased by approximately 1.0 (0.5) dB when L is increased from 2 (3) to 3(4) at f_D = 80 Hz.

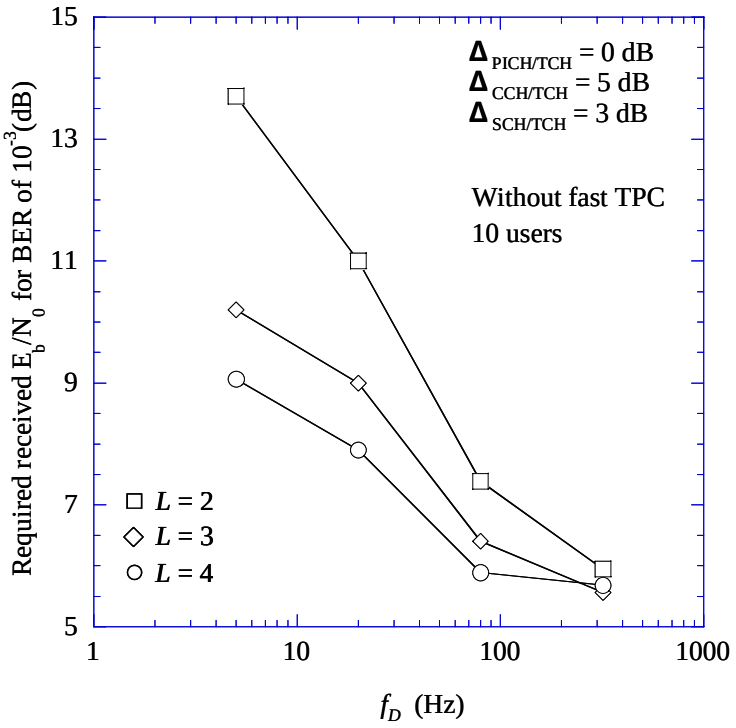

Fig. 3.12 Required average received E_b/N_0 as a function of f_D (without fast TPC)

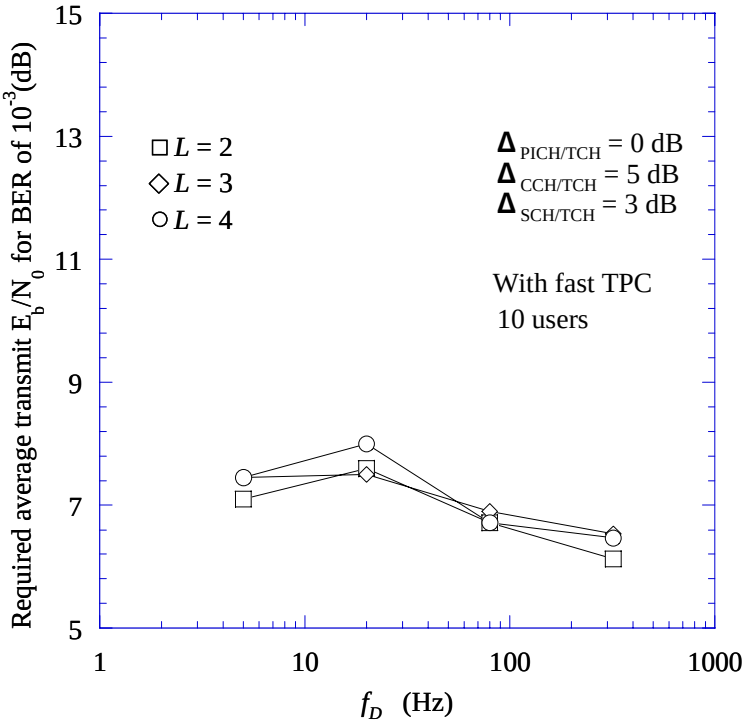

Fig. 3. 13 Required average transmit E_b/N_0 as a function of f_D. (With fast TPC)

Figure 3.13 shows the required average transmit E_b/N_0 at the average BER of 10^{-3} when MPIC for the common channels is employed and fast TPC is used. The simulation conditions except for the use of fast TPC were the same as those in Fig. 3.12. Compared to the results in Fig. 3.12, the required transmit E_b/N_0 for smaller values of f_D is remarkably reduced by the fast TPC effect. As a result, an almost constant required average transmit E_b/N_0 performance is achieved over wide range of f_D from 5 Hz to 300 Hz. Dissimilar to the case without fast TPC, the Rake time diversity effect is relatively diminished by the fast TPC and channel coding effect even with MPIC.

3.5.5 MPI Suppression Effect of TCH

Finally, I investigated the BER performance when the MPIC removed MPI of the TCHs in addition to the common channels. The average BER performance when MPIC was used in both the common channels and TCHs is plotted in Fig. 3.14 as a function of the average received E_b/N_0 without fast TPC. The parameters of the transmit power ratios and IRWs were identical to those used in Fig. 3.10. It was assumed that L = 2, and f_D = 80 Hz. The BER performance with MPIC for only the common channels and without MPIC, i.e., MF-based Rake receiver, is also shown for comparison.

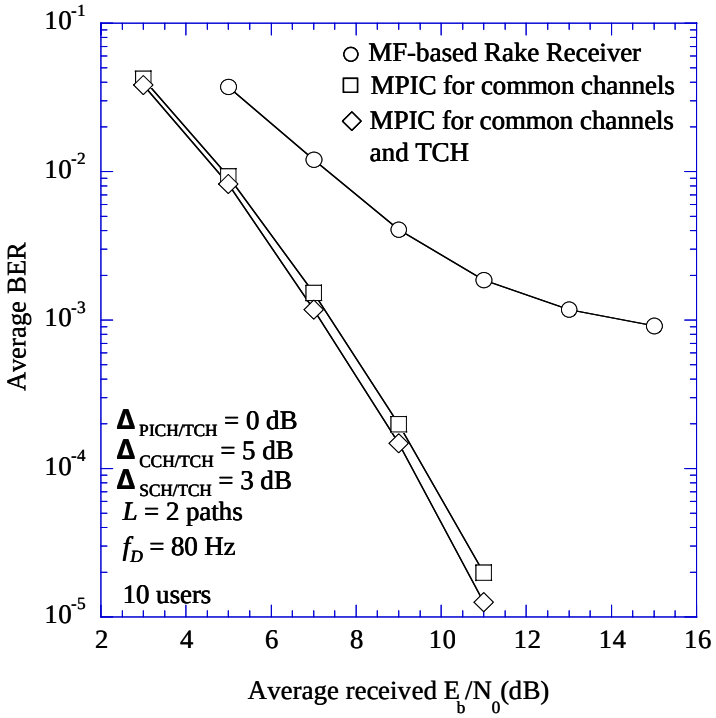

Fig. 3.14 Average BER performance with MPIC for low-rate TCH in addition to common channels (without fast TPC)

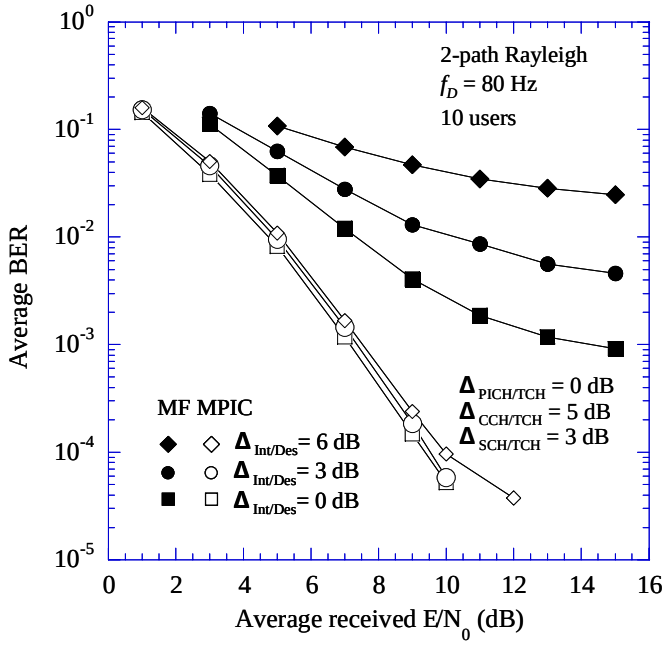

Fig. 3.15 Average BER performance with MPIC for high-rate TCH in addition to common channels (without fast TPC.)

The figure shows that the improvement in the required received E_b/N_0 at the average BER of 10^{-3} with the MPIC for the common channels and TCHs from that with MPIC for only the common channels is only approximately 0.3 dB. This is because the MPI from the TCHs, which has the same symbol rate as that of the desired TCH, is small. Therefore, in an environment where the symbol rates of all interfering users is as low as that of the desired user, I conclude that it is sufficient to apply MPIC which suppress MPI from only the common channels.

On the other hand, Fig. 3.15 shows the average BER performance as a function of the average received E_b/N_0 with MPIC for both the common channels and TCHs when the transmit power of 9-interfering TCHs were $\Delta_{Int/Des}$ dB greater than that of the desired TCH (this situation means that a larger number of high rate users with large transmit power exist). Other simulation conditions were the same as those as in Fig. 3.14. In contrast to Fig. 3.14, the average BER performance was degraded as $\Delta_{Int/Des}$ was increased due to the increased MPI. Considering the diversification of non-voice communication services, it is natural to observe the beneficial effect of MPIC in several plausible scenarios. First, I consider the case of high-rate interfering users ($\Delta_{Int/Des}$ = 3, 6 dB) with somewhat lower QoS requirement, i.e., BER of 10^{-2}, equivalent to average packet error rate (PER) of approximately 10^{-1}, after channel coding. However, services offered at this QoS must

incorporate retransmission scheme governed by higher layer. The proposed MPIC for all channels reduced the required average received E_b/N_0 by about 5.3 dB when the value of $\Delta_{Int/Des}$ was 3 dB. Moreover, while MF-based Rake receiver could not realize the required QoS when $\Delta_{Int/Des}$ = 6 dB, the MPIC for all channels realized the required QoS at almost the same average received E_b/N_0 with the case when $\Delta_{Int/Des}$ was 3 dB (Note that a decrease in required average received E_b/N_0 for any given QoS can be translated into system capacity increase). Next, I consider the case of low-rate interfering users ($\Delta_{Int/Des}$ = 0 dB) with high QoS requirement of average BER of 10^{-4}. This results in error free transmission when the block codes such as Reed-Solomon code is concatenated with the convolutional code. As it is evident from the figure, MF-based Rake receiver could not achieve the required BER. On the other hand, the proposed MPIC for all channels satisfactorily suppressed the MPI from the common channels as well as other interfering channels. Thus, the proposed MPIC was effective even when considering the diversified services, i.e. non-voice communications with various QoS requirements.

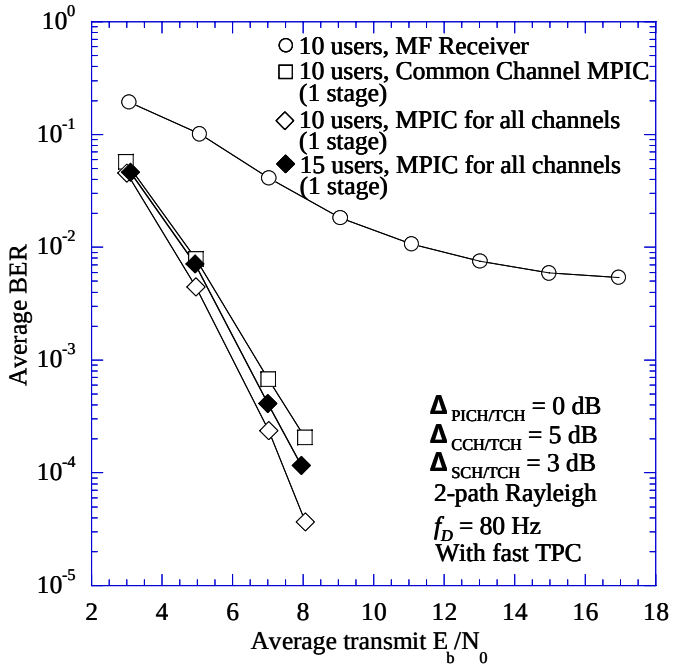

Fig. 3.16 Average BER performance with MPIC for low-rate TCH in addition to common channels (with fast TPC)

The average BER performance when MPIC for both common channels and TCHs was applied is plotted in Fig.16 as a function of the average transmit E_b/N_0 with fast TPC. It was assumed that the symbol rates for all TCHs were identical to that of the desired user and the number of simultaneous active interfering users was 9 and 14. Compared to the results in Fig. 10, the decrease in the average transmit E_b/N_0 at the average BER of 10^{-3} when the MPIC both for the common channels and TCHs is compared to that with the MPIC only for the common channels is within 0.5 dB. The figure shows that the increase of the required transmit E_b/N_0 at the average BER of 10^{-3} for 14 interfering TCHs from that of the case with 9 interfering TCH is within 0.5 dB since the MPIC removes the MPI effectively. This increase in the required transmit E_b/N_0 is caused by the errors of the generated MPI replica mainly due to the channel estimation error. It is show in Table 2 that the complexity of the 1-stage MPIC for MPI canceling of 10 TCHs in addition to the common channels is almost 13 fold that of the MF-based Rake receiver.

Meanwhile, Fig. 3.17 shows the average BER performance as a function of the average received E_b/N_0 with MPIC for both the common channels and TCHs when the transmit power of 9-interfering TCHs were $\Delta_{Int/Des}$ dB greater than that of the desired TCH. Similar observation as that of Fig. 3.15 revealed that when considering high-rate interfering

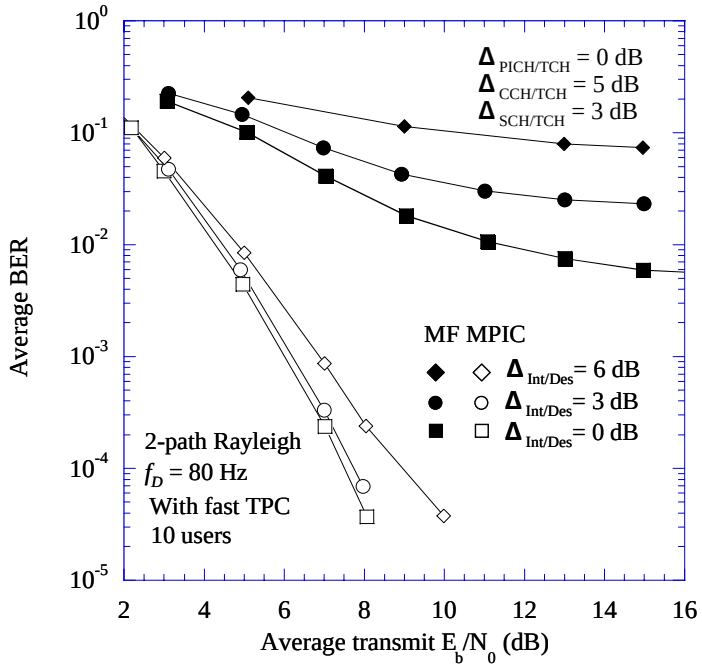

Fig. 3. 17 Average BER performance with MPIC for high-rate TCH in addition to common channels (with fast TPC)

users ($\Delta_{Int/Des}$ =3,6 dB) with somewhat lower QoS (average BER of 10^{-2}), the MF-based Rake receiver could not realize the required QoS due to severe MPI from the common channels and high-rate users. On the other hand, the MPIC for all channels removed the MPI satisfactorily, thus achieved the required QoS. Furthermore, observation on low-rate interfering users ($\Delta_{Int/Des}$ =0 dB) with high QoS requirement of average BER of 10^{-4} affirmed the effectiveness of the MPIC for all channels. Consequently, it is concluded that MPIC receiver retained its effectiveness when fast TPC is applied to the TCH.

3.6. Conclusion

This chapter proposed an MPIC for orthogonal multiplexed channels in the W-CDMA forward link and evaluates by computer simulation the BER performance improvement due to the MPI suppression effect by MPIC. The simulation results show that a one-stage MPIC, which removes the MPI from the PICH, CCH, and SCH, achieves a sufficient MPI suppression effect. The required received E_b/N_0 of the TCH at the average BER of 10^{-3} with the MPIC for the common channels is decreased by approximately 6.5 dB compared to that with the MF-based Rake receiver (the transmit E_b/N_0 ratio of each common channel to TCH: $\Delta_{PICH/TCH}$ = 0 dB, $\Delta_{CCH/TCH}$ = 5 dB, $\Delta_{SCH/TCH}$ = 3 dB, without fast transmit power control and antenna diversity reception). It is also showed that by using the MPIC, the required transmit E_b/N_0 at the average BER of 10^{-3}, when the ratio of the average transmit E_b/N_0 of the desired user to 9-interfering users is $\Delta_{Int/Des}$ = 6 dB with fast TPC, is increased only by approximately 0.6 dB compared to that when $\Delta_{Int/Des}$ = 0dB. Further observation on the MPIC performance considering diversification of non-voice communication services, revealed that the MPIC for all channels is effective when high-rate users with somewhat lower QoS requirement or low-rate users with high QoS requirement exist in the system. This implies that the preferential MPI suppression from high-rate TCHs which limits the increase in complexity of the mobile terminal is effective in increasing link capacity in the forward link.

Chapter Four

Antenna Verification Method for Multipath Interference Canceller Based on Replica Generation per Transmit Antenna with Phase Control Transmit Diversity in W-CDMA Forward Link

4.1. Introduction

In the previous chapter I have proposed an MPIC optimized for the forward link and clarified via computer simulations the strong MPI suppression effect of it. The proposed MPIC has serial structure which shows good MPI suppression capability at the cost of long processing delay. It was also shown that the MPIC exhibits sufficient performance with only one iteration. However, it cannot gain a diversity effect in the multipath Rayleigh fading channel (note that the multipath diversity or Rake combining diversity gain is offset by the large MPI), where the influence of the residual MPI components and that of the background noise are distinct.

Meanwhile, transmit diversity in the forward link is effective in mitigating the degradation in transmission performance due to fading even when using a one-branch receiver at the MS. Among transmit diversity schemes, the closed-loop type, which controls the carrier phase or/and amplitude of the parallel signals transmitted from two antennas according to a feedback information (FBI) bit sent via the reverse link, was adopted for the TCH [16] in the W-CDMA specifications. In this chapter, I focus on closed-loop type phase control (PC) transmit diversity employing weighting factors $W^{(1)}(n) = e^{j\phi^{(1)}(n)}$ and $W^{(2)}(n) = e^{j\phi^{(2)}(n)}$ that are calculated according to the FBI bit sent via the reverse link (this scheme is called Mode 1 in the W-CDMA specification). In the PC transmit diversity scheme, the transmitted carrier phase of the second antenna is controlled with the control resolution of $\pi/2$ slot-by-slot. It is therefore conjectured that the combination of the MPIC at the MS receiver and transmit diversity at the BS transmitter is beneficial in improving the BER performance both in the interference-limited and noise-limited channels, i.e., the influence of the MPI is relatively small, in multipath Rayleigh fading environments. As is well known, it was decided in the 3rd Generation Partnership Project (3GPP) specifications that open-loop type PC transmit diversity is applied to common channels (more precisely, the Space Time Transmit Diversity (STTD) method for Common Control Channels (CCH) and Time Switched Transmit Diversity (TSTD) for Synchronization Channel (SCH),

respectively), and closed-loop type transmit diversity is used for the TCH associated with each communicating user.

Then, considering the MPIC configuration exploiting STTD for common channels, two methods are considered for generating MPI replicas in the MPIC. The first method is to decide a tentative data modulation phase before STTD decoding and generate the MPI replica associated with each path based on the tentative decision data symbols. The second method performs STTD decoding using the channel estimate and derives tentative data modulation. Then, the STTD encoding is performed and the MPI replica for each path is generated using the channel estimate. In the first method, although the STTD decoding and re-encoding are not needed, all the received composite symbol replicas are generated from the channel estimate and all the data modulation candidates corresponding to two transmitter antennas are estimated. Then, the tentative data modulation, i.e., decision data symbols from two antennas, are simultaneously obtained by Maximum Likelihood Detection (MLD). Thus, it is conjectured that that the MPI replica generation method using the tentative decision data symbols before STTD decoding accompanies a higher degree of computational complexity than that of the method using STTD decoding and encoding.

Therefore, in this chapter, I choose the MPI generation method using the tentative data decision after STTD decoding and STTD re-encoding to the MPIC for CCH. Then, I present the actual MPIC configurations with MPI replica generation per transmitter antenna (PTA-MPIC hereafter) for open-loop type PC transmit diversity for common channels and closed-loop type PC transmit diversity for TCH in the W-CDMA forward link, and investigate the BER performance of the TCH using PTA-MPIC. In the PTA-MPIC, to generate the MPI replicas for the two transmission antennas, we use the channel gain of each resolved path of the transmitted signals estimated by the PICH, the received path timing, and the tentative decision data symbol after combining the two diversity branches transmitted from the two antennas.

Furthermore, since decoding errors of the FBI bit occur in the reverse link, the MS verifies the transmitted carrier phase of each slot of the TCH with the carrier phase of the PICH as a reference (this verification of the transmitted carrier phase of the TCH is called antenna verification). Nevertheless, due to the antenna verification error caused by MPI and background noise, the effect of PC transmit diversity is reduced. Therefore, in this chapter I propose transmitter carrier phase verification, i.e., an antenna verification method used in PC transmit diversity, that utilizes the received dedicated pilot symbols in the TCH after MPI from the common channels and that from other TCHs are removed by the MPIC. In the proposed antenna verification method, since the carrier modulation phase is estimated using the pilot symbols of the TCH after MPI suppression, the estimation accuracy is improved.

4.2. Transmitted Signal Representations

I consider in the paper the following four physical channels: PICH, CCH, SCH, and TCH. The frame structures of these four physical channels are illustrated in Fig. 4.1. The radio frame length is 10 msec and comprises 15 0.667-msec long slots. The PICH, which is shared by communicating users within a cell, is data-modulated by the known modulation phase at the receiver, i.e., it bears no data information. Ten pilot symbols with the spreading factor of SF = 256 are included in each slot of the PICH. The CCH bears the information data, thus the symbol sequence is data-modulated (note that tentative data decision is required to generate an MPI replica in the MPIC as explained in Section 4.3). Each slot of the CCH consists of N_d = 10 coded data symbols and similarly, each slot of the TCH comprises N_p = 16 dedicated pilot symbols and N_d = 144 coded data symbols. The symbol rates of the CCH and TCH become 15 ksps and 240 ksps, respectively (note that the symbol rate represents the total symbol rate of the physical channel including pilot symbols similar to the definition in the 3GPP standard [20]. Thus, the spreading factors of the CCH and TCH are SF = 256 and 16, respectively. Finally, each slot of the SCH consists of one data-modulated symbol with the SF = 256 (thus, the symbol rate is 1.5 ksps).

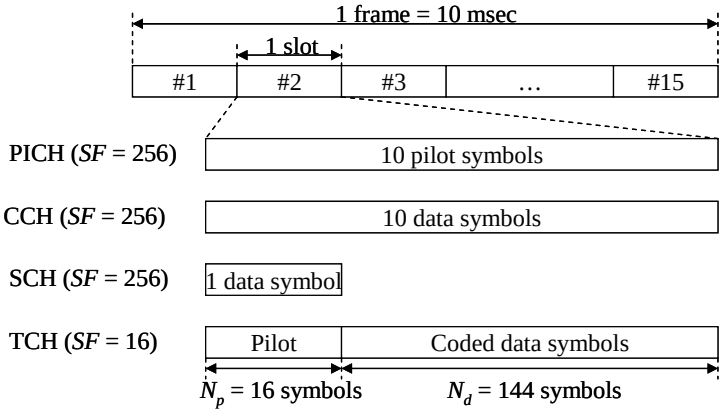

Fig. 4.1 Forward link frame structure

A simplified block diagram of the transmitter of the BS assumed in this chapter is illustrated in Fig. 4.2. Within the four physical channels, three channels except the SCH are spread by the combination of a scrambling code with the repetition period of one radio frame (= 38400-chip length) and a short OVSF code with the repetition period of SF, similar to the two-layered spreading codes in W-CDMA [21]. Meanwhile, the SCH is spread only by a short synchronization code (thus, this means that the SCH is non-orthogonal to the other channels). The scrambling code is generated by truncating the Gold sequence with the length of 2^{41}-1 chips. Furthermore, a Walsh-Hadamard sequence

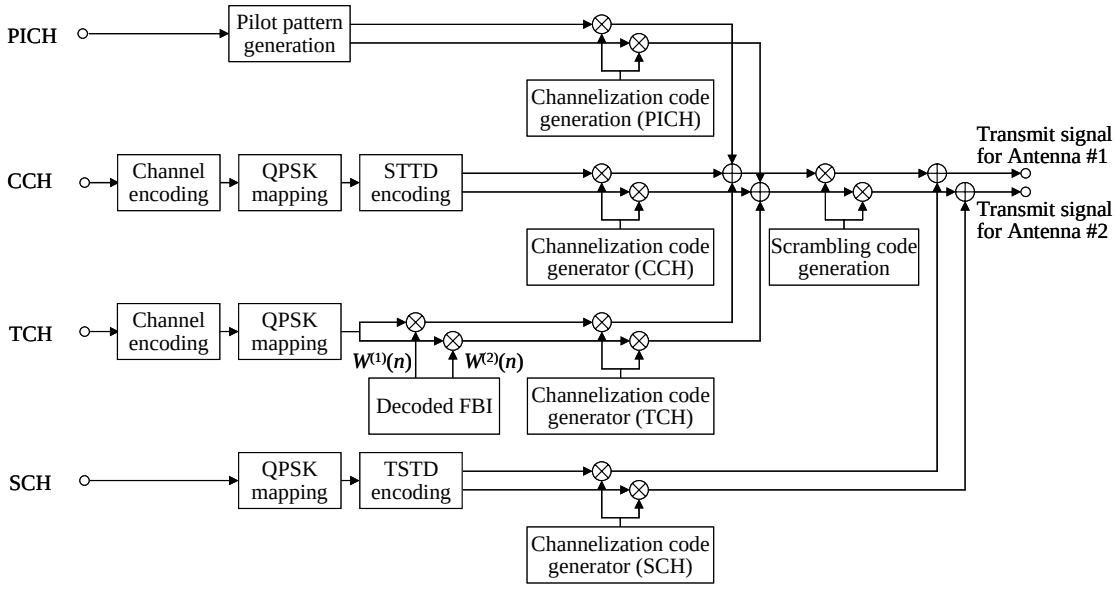

Fig. 4.2 Transmitter configuration at base transceiver station (BTS)

was used as the OVSF code. The resultant chip rate was 3.84 Mcps. The PICH, CCH, and SCH are transmitted at constant transmission powers. Meanwhile, the SIR-based fast TPC is applied to the TCH so that the required SIR after Rake combing is satisfied.

In order to mitigate the performance degradation due to multipath fading, I applied open-loop transmit diversity called STTD [23], [32] to the CCH and time space transmit diversity (TSTD) [33] to the SCH, respectively. Two PICH sequences with the orthogonal data modulation transmitted from two antennas are commonly used for closed-loop type PC transmit diversity for the TCH and for STTD for the CCH. Then, let q be the index of the transmission antenna such that q = 1 or 2 and $\phi_q^{PICH}(i)$ is the transmitted carrier phase of the pilot symbols, which takes the orthogonal values from $\{\pm\pi/4 \text{ or } \pm 3\pi/4\}$ for the PICH, since I employed Quadrature Phase Shift Keying (QPSK) data modulation. Thus, the data-modulated signal waveform of the PICH associated with the q-th transmission antenna is expressed as $d_q^{PICH}(t) = \sum_{i=-\infty}^{\infty} g^{PICH} \cdot \exp\left[j\phi_q^{PICH}(i)\right] \cdot u(t/T^{PICH} - i)$, where g^{PICH} and T^{PICH} are the amplitude and symbol duration of the PICH, respectively, and u (t) is the step function such that $u(t) = 1$ for $0 \le t < 1$, and otherwise, $u(t) = 0$. Similarly, I express the data-modulated signal waveform of the CCH, SCH, and the k-th TCH as $d_q^{CCH}(t) = \sum_{i=-\infty}^{\infty} g^{CCH}(i) \cdot \exp\left[j\phi_q^{CCH}(i)\right] \cdot u(t/T^{CCH} - i)$, $d_q^{SCH}(t) = \sum_{i=-\infty}^{\infty} g_q^{SCH}(i) \cdot \exp\left[j\phi^{SCH}(i)\right] \cdot u(t/T^{SCH} - i)$ and

$d_{k,q}^{TCH}(t) = \sum_{i=-\infty}^{\infty} g_k^{TCH}(i) \cdot \exp\left[j(\phi_{k,q}^{TCH}(i) + \phi_k^{(q)}(i))\right] \cdot u(t/T_k^{TCH} - i)$, respectively, where T^{CCH} , T^{SCH} , T^{TCH} and g^{CCH} , g_q^{SCH} , g_k^{TCH} are the symbol duration and amplitude associated with the *q*-th transmission antenna of the CCH, SCH with TSTD, and the *k*-th TCH, respectively. Furthermore, $\phi_q^{CCH}(i)$, $\phi^{SCH}(i)$, and $\phi_{k,q}^{TCH}$ are the data-modulated carrier phases of the CCH after STTD encoding, SCH, and the *k*-th TCH, and are expressed as $\phi_q^{CCH}(i), \phi^{SCH}(i), \phi_{k,q}^{TCH}(i) \in \{(2q-1)\pi/4; q = 1,2,3,4\}$, respectively, since I assumed QPSK data modulation. Here, I assumed that $\phi_{k,q}^{TCH}(i)$ is the orthogonal pattern between two transmission antennas over N_p-pilot symbol duration at the beginning of each slot and that the condition such that $\phi_{k,1}^{TCH}(i) = \phi_{k,2}^{TCH}(i)$ is maintained over the remaining coded-data symbol duration. Finally, $\phi_k^{(q)}(i)$ denotes the carrier phase of the TCH transmitted from the *q*-th antenna, which is controlled by the PC transmit diversity. After appending the dedicated pilot channel and packing them into a slot format, the QPSK symbol sequence of each data channel is multiplied by weighting factors $W^{(1)}(n) = e^{j\phi^{(1)}(n)}$ and $W^{(2)}(n) = e^{j\phi^{(2)}(n)}$, where $\phi^{(1)}(n) = 0$, $\phi^{(2)}(n) = \in \{(2q-1)\pi/4; q = 1,2,3,4\}$, for the *n*-th slot, which is calculated according to the FBI bit sent via the reverse link every slot for the two transmit antennas. Then, the weight-multiplied data sequence is multiplied with the spreading code. The spread TCHs for the two transmit antennas are code-multiplexed with the PICH, CCH, and SCH with a constant transmission power (without fast TPC).

Let $c_k^{OVSF}(t) = \sum_{i=-\infty}^{\infty} \exp[j\phi_k^{'}(i)] \cdot u(t/T_c - i)$ and $c^{Sc}(t) = \sum_{i=-\infty}^{\infty} \exp[j\phi_{Sc}^{'}(i)] \cdot u(t/T_c - i)$ be the spreading signal waveform of the OVSF code and that of the in-phase (I)/ quadrature (Q) components of the cell-specific scrambling code. In these notations, T_c denotes the chip duration and $N = T/T_c$ is the *SF*. Furthermore, $\phi_k^{'}(i) \in \{(2q-1)\pi/2; q = 0,1\}$ is the BPSK modulation phases and $\phi_{Sc}^{'}(i) \in \{(2q-1)\pi/4; q = 1,2,3,4\}$ is the QPSK modulation phases. Similarly, let $c^{SCH}(t) = \sum_{i=-\infty}^{\infty} \exp[j\phi_{SCH}^{'}(i)] \cdot u(t/T_c - i)$ be the spreading signal waveform of

the SCH, assuming that the modulation phase is BPSK, for example, $\phi'_{SCH}(i) \in \{q\pi; q = 0,1\}$. The combined spreading code sequence is represented as $c_k^{Spread}(t) = c_k^{OVSF}(t)c^{Sc}(t)$, and the transmitted signal from the *q*-th antenna, $s_q(t)$, is given as

$$s_q(t) = d_q^{PICH}(t)c_1^{Spread}(t) + d_q^{CCH}(t)c_2^{Spread}(t) + \sum_{k=1}^{K} d_{k,q}^{TCH}(t)c_{k+2}^{Spread}(t) + d_q^{SCH}(t)c^{SCH}(t) \quad (4.1)$$

4.3. PTA-MPIC

The transmitted signals represented in Equation (4.1) propagate through a multipath-fading channel and are received at a MS receiver employing the PTA-MPIC. Antenna diversity reception was not used in the evaluation. The received signal is represented as

$$r(t) = \sum_{q=1}^{2}\sum_{l=1}^{L} \xi_{q,l}(t)s_q(t-\tau_l) + n(t) \quad (4.2)$$

where $\xi_{q,l}$ and τ_l are the complex-valued channel gain and the time delay of the *l*-th path transmitted from the *q*-th antenna. Here, we assume that the time delays of the corresponding paths transmitted from two antennas are identical. This assumption is reasonable because we confirmed using the implemented W-CDMA transceiver with transmit diversity that the time delay difference of the corresponding paths from two antennas is within the duration of the four-time over-sampled chip rate clock signal [34]. Term $n(t)$ is the additive Gaussian noise component with one-sided spectrum density N_0.

The structure of the overall MPIC is illustrated in Fig. 4.3. Each stage of the MPIC comprises an MPI replica generation unit, which is called MPIRGU, for the PICH, CCH, and TCH. Meanwhile for the SCH, interference replicas of all resolved paths including the same propagation path and that of the MPI are generated in this unit, because the orthogonality between the SCH and other channels is not accomplished. Thus, we refer to this as an interference replica generation unit (IRGU) for the SCH.

A block diagram of the MPIRGU of the PICH is shown in Fig. 4.4. In each MPIRGU, the input sample sequence of each antenna is despread by a MF into the resolved multipath components. At the first stage, the received signal is directly input to the MPIRGU of the PICH of the *l*-th path, $r_l^{(1)}(t)$, *i.e.*, $r_l^{(1)}(t) = r(t)$. The complex fading envelope, *i.e.*, the

channel gain of each path, is derived from the despread signal of the PICH. The channel gain of the *n*-th slot associated with the *q*-th antenna, $\hat{\xi}_{q,l}^{(1)}(n)$, is obtained by coherently accumulating the despread symbols of the PICH within each slot as

$$\hat{\xi}_{q,l}^{(1)}(n)=\frac{1}{\sqrt{|\,d^{\,PICH}\,|^2 T_{Slot}}}\int_{nT_{slot}+\hat{\tau}_l}^{(n+1)T_{slot}+\hat{\tau}_l} r_l^{(1)}(t)\cdot d_q^{PICH*}(t)\cdot c_1^{Spread*}(t-\hat{\tau}_l)dt\,, \tag{4.3}$$

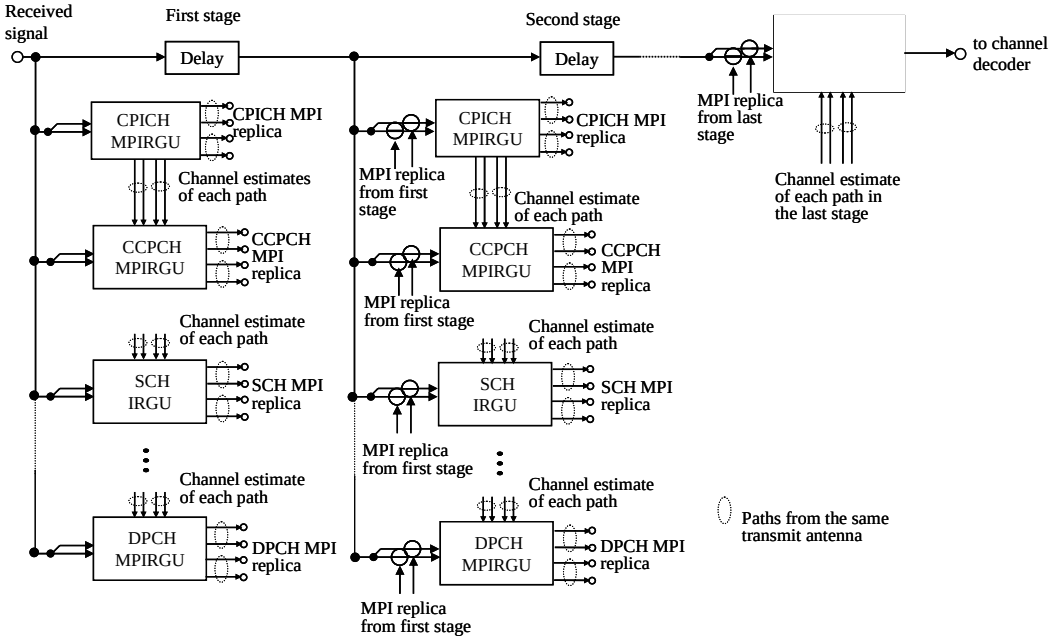

Fig. 4.3 Block diagram of PTA-MPIC associated with PC transmit diversity

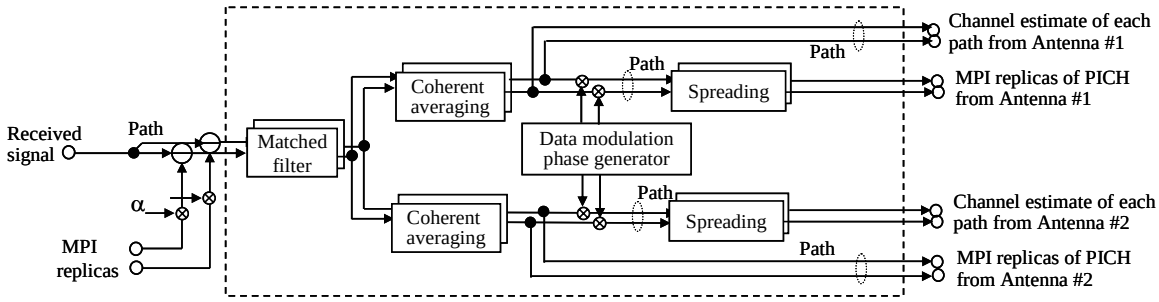

Fig. 4.4 Block diagram of MPIRGU for PICH

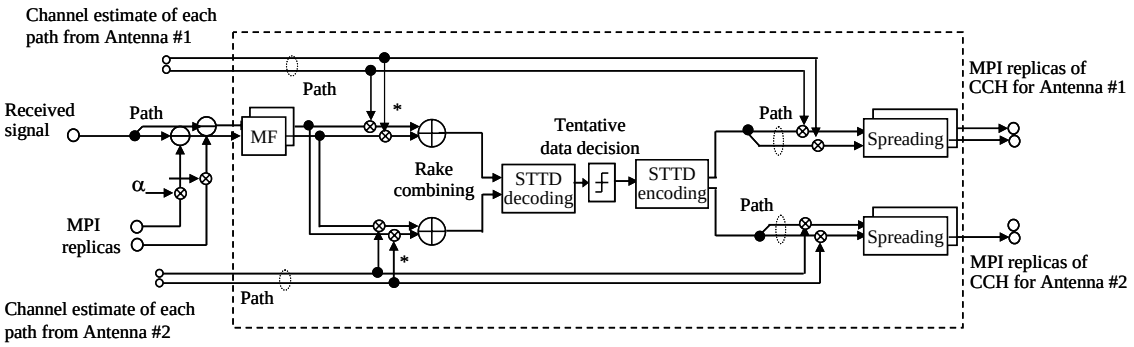

Fig. 4.5 Block diagram of MPIRGU for CCH

where * denotes the complex conjugate. Term $\hat{\tau}_l$ is the estimated time delay of the *l*-th path and we assume that $\hat{\tau}_l$ is ideally estimated at the receiver in the subsequent evaluations in Section 4.6. The MPI of the PICH is then computed using the channel gain in Equation (4.3) as

$$\hat{I}^{(1)}_{PICH,q,l}(t-\hat{\tau}_l) = \hat{\xi}^{(1)}_{q,l}(t) d_q^{PICH}(t-\hat{\tau}_l)\cdot c_1^{Spread}(t-\hat{\tau}_l) \quad . (4.4)$$

The structure of the MPIRGU for the CCH with STTD is shown in Fig. 4.5. The despread data sequence of the *m*-th symbol of the *n*-th slot associated with the *l*-th path of the CCH in MPIRGU is given as

$$z^{(1)}_{CCH,l}(n,m) = \frac{1}{T^{CCH}} \int_{nT_{slot}+mT^{CCH}+\hat{\tau}_l}^{nT_{slot}+(m+1)T^{CCH}+\hat{\tau}_l} r_l^{(1)}(t)\cdot c_2^{Spread*}(t-\hat{\tau}_l)dt \quad (4.5)$$

By multiplying the complex conjugate of the channel estimate, $\hat{\xi}^{(1)}_{q,l}(n)$, with the despread data sequence of the resolved path component in Equation (4.5), the *L*-path components are coherently Rake-combined. The data sequences after Rake combining of the *m*-th symbol of the *n*-th slot for the CCH, $\hat{d}^{(1)}_{CCH,q}(n,m)$, is expressed as

$$\hat{d}^{(1)}_{CCH,q}(n,m) = \sum_{l=1}^{L} z^{(1)}_{CCH,l}(n,m)\cdot \hat{\xi}^{(1)*}_{q,l}(n) \quad . \quad (4.6)$$

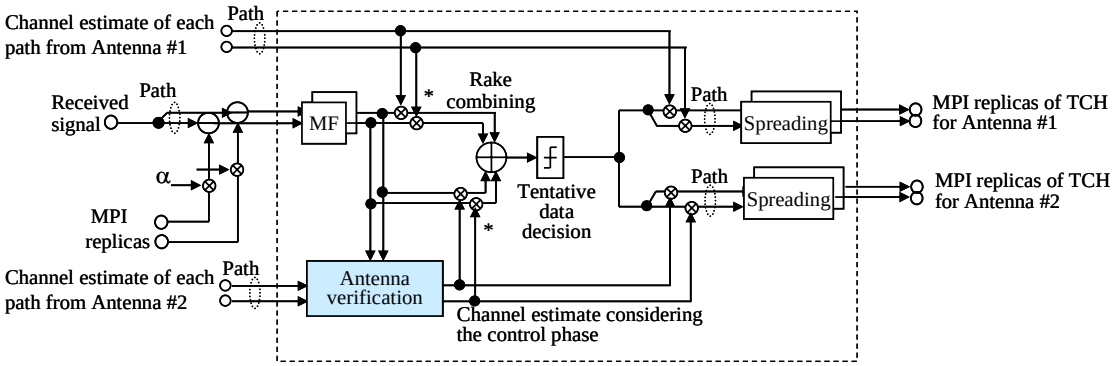

Fig. 4. 6 Block diagram of MPIRGU for TCH

STTD decoding is performed by using the parallel data sequence after Rake combining, $\hat{d}^{(1)}_{CCPCH,q}(n,m)$. Thus, after STTD decoding, the data sequence is tentatively decided to recover the data modulation of the CCH, and the data-modulated symbols at the *q*-th antenna, $\tilde{d}^{(1)}_{CCPCH,q}(n,m)$, are generated by re-encoding using STTD. In this way, by employing the tentative decision data symbols of the CCH after STTD decoding, i.e., after combining the branches transmitted from the two antennas, the data decision error is significantly reduced compared to the case when the tentative data decision is performed independently at each branch. Therefore, the MPI replica of the CCH associated with the *l*-th path and the *q*-th transmission antenna is generated as

$$\hat{I}^{(1)}_{CCH,q,l}(t-\hat{\tau}_l) = \hat{\xi}^{(1)}_{q,l}(t)\tilde{d}^{(1)}_{CCH,q}(t-\hat{\tau}_l)\cdot c_2^{Spread}(t-\hat{\tau}_l) \quad . \tag{4.7}$$

Since we assume that the transmitted carrier phase in the data modulation of the SCH is known at the receiver following the SCH in the W-CDMA air interface, the MPI replica of the SCH associated with the *l*-th path and the *q*-th transmission antenna is generated as

$$\hat{I}^{(1)}_{SCH,q,l}(t-\hat{\tau}_l) = \hat{\xi}^{(1)}_{q,l}(t)\cdot d_q^{SCH}(t-\hat{\tau}_l)\cdot c^{SCH}(t-\hat{\tau}_l) \quad . \tag{4.8}$$

Finally, the MF in the MPIRGU of the TCH shown in Fig. 4.6 despreads the signal $r_l^{(1)}(t)$, and the despread data sequence of the *m*-th symbol of the *n*-th slot associated with the *l*-th

path of the *k*-th CCH ($1 \le k \le K$) at the first stage is expressed as

$$z_{k,l}^{(1)}(n,m) = \frac{1}{T^{TCH}} \int_{nT_{slot}+mT^{TCH}+\hat{\tau}_l}^{nT_{slot}+(m+1)T^{TCH}+\hat{\tau}_l} r_l^{(1)}(t) \cdot c_{k+2}^{Spread*}(t-\hat{\tau}_l)dt$$

for the *k*-th TCH, when $1 \le k \le K$. (4.9)

Next, the channel gain of the signal transmitted from each antenna of the TCH, $\hat{\xi}_{k,q,l}^{(1)}(n)$, is calculated using pilot symbols in *k*-th TCH as follows.

$$\hat{\xi}_{k,q,l}^{(1)}(n) = \frac{1}{N_P} \sum_{m=1}^{N_P} z_{k,l}^{(1)}(n,m) \cdot \exp[-j\phi_{k,q}^{TCH}] \quad . \tag{4.10}$$

Then, $\hat{\xi}_{q,l}^{(1)}(n)$ and $\hat{\xi}_{k,q,l}^{(1)}(n)$ are averaged to obtain the channel estimate for Rake combining for TCH as

$$\overline{\xi}_{k,q,l}^{(1)}(n) = \{\hat{\xi}_{q,l}^{(1)}(n) \cdot \exp[j\hat{\phi}_k^{(q)}] + \hat{\xi}_{k,q,l}^{(1)}(n)\}/2, \tag{4.11}$$

where $\hat{\phi}_k^{(q)}$ is the estimate of transmitted carrier phase of the *q*-th antenna, which is updated in the PC transmit diversity. Actually, the $\hat{\phi}_k^{(q)}$ value is estimated in the antenna verification process since FBI bit decoding errors in the reverse link occur as explained in Section 4.4. The data sequences after Rake combining of the *m*-th symbol of the *n*-th slot for the *k*-th TCH, $\hat{d}_k^{(1)}(n,m)$, are represented as

$$\hat{d}_k^{(1)}(n,m) = \sum_{l=1}^{L} z_{k,l}^{(1)}(n,m) \cdot (\overline{\xi}_{k,1,l}^{(1)}(n) + \overline{\xi}_{k,2,l}^{(1)}(n))^*$$

for the *k*-th TCH, where $1 \le k \le K$ (4.12)

By using the recovered data modulation of the *k*-th TCH, $\tilde{d}_k^{(1)}(n,m)$, and the channel

estimation, $\hat{\xi}_{q,l}^{(1)}(n)$, the MPI replica associated with the *l*-th path can be calculated as

$$\hat{I}_{k,q,l}^{(1)}(t-\hat{\tau}_l) = \hat{\xi}_{q,l}^{(1)}(t)\tilde{d}_{k,q}^{(1)}(t-\hat{\tau}_l)\cdot c_{k+2}^{Spread}(t-\hat{\tau}_l) \tag{4.13}$$

Since SIR-based fast TPC is employed in the TCHs, and the value of g_k^{TCH} changes slot by slot, the amplitude or power of the received signal of the TCH of each slot is determined by g_k^{TCH} and the channel gain due to fading. Therefore, the instantaneous amplitude of the received signal at each slot must be estimated in order to generate the MPI replica of the TCH. We calculated the amplitude ratio of the TCH to PICH, i.e., g_k^{TCH} / g^{PICH} of each slot.

At the second stage, the channel estimation is performed by using the chip sequence of PICH, in which the generated MPI replicas of the PICH, CCH, SCH, and TCH (including the own-path replica for SCH) are subtracted.

$$\begin{aligned} r_l^{(2)}(t) = r(t) - \sum_{q=1}^{2}\Bigg(\sum_{\substack{l'=1 \\ l'\neq l}}^{L}\Big(& \hat{I}_{PICH,q,l'}^{(1)}(t-\hat{\tau}_{l'}) + \hat{I}_{CCH,q,l'}^{(1)}(t-\hat{\tau}_{l'}) \\ & + \sum_{k=1}^{K}\alpha_{TCH}\hat{I}_{k,q,l'}^{(1)}(t-\hat{\tau}_{l'})\Big) - \sum_{l'=1}^{L}(\hat{I}_{SCH,q,l'}^{(1)}(t-\hat{\tau}_{l'}))\Bigg) \end{aligned} \tag{4.14}$$

where α_{TCH} is the real-valued interference rejection weight ($0 < \alpha_{TCH} \le 1$) for TCH, which alleviates the impact of generation error of the MPI replica. Therefore, the channel estimate of the *n*-th slot at the second stage is given as

$$\hat{\xi}_{q,l}^{(2)}(n) = \frac{1}{\sqrt{|d^{PICH}|^2 T_{Slot}}}\int_{nT_{slot}+\hat{\tau}_l}^{(n+1)T_{slot}+\hat{\tau}_l} r_l^{(2)}(t)\cdot d_q^{PICH*}(t)\cdot c_1^{Spread*}(t-\hat{\tau}_l)dt \tag{4.15}$$

The despreading operation by the MF of the CCH, TCH, and SCH at the second stage is performed in the similar manner to that for the first stage as shown in Equations (4.5) and (4.6). The Rake combining for the TCH at the second stage is also identical to that at the

first stage, yet, MPI replicas that are more refined than those in the first stage are generated. Similarly, the input signal at the *p*-th stage ($p \geq 2$) in which the MPI replica generated in the previous stage is subtracted, is denoted as

$$r_l^{(p)}(t) = r(t) - \sum_{q=1}^{2} \left(\sum_{\substack{l'=1 \\ l' \neq l}}^{L} \left(\hat{I}_{PICH,q,l'}^{(p-1)}(t-\hat{\tau}_{l'}) + \hat{I}_{CCH,q,l'}^{(p-1)}(t-\hat{\tau}_{l'}) + \sum_{k=1}^{K} \alpha_{TCH} \hat{I}_{k,q,l'}^{(p-1)}(t-\hat{\tau}_{l'}) \right) - \sum_{l'=1}^{L} \hat{I}_{SCH,q,l'}^{(p-1)}(t-\hat{\tau}_{l'}) \right) . \quad (4.16)$$

After the last stage, all generated MPI replica of other channels as well as own MPI replica are subtracted from the received signal. The signal after MPI replica subtraction is input to the MF and despread. Consequently, the Rake-combined sequence is de-interleaved and soft-decision Viterbi decoded to recover the transmitted data sequence. In the scheme, since the channel estimation and data decision are updated at each stage, the accuracy of the MPI replica is improved from the resulting enhancement of the channel estimation and decreasing data decision error.

4.4. Proposed Antenna Verification Method Coupled with MPIC

In this section, I explain the operations of PC transmit diversity and the conventional antenna verification method for the MF-based Rake receiver and the PTA-MPIC. I also propose an improved antenna verification method using the pilot channel after removing MPI. At the MS receiver, the received carrier phase and amplitude at each slot of the PICH associated with each transmission antenna is measured by accumulating the despread pilot symbols of each path within a slot as $\hat{\xi}_q^{(1)}(n) = \sum_{l=1}^{L} \hat{\xi}_{q,l}^{(1)}(n)$. Then, from the differences in the carrier phases and amplitudes of the separated signals from the two transmission antennas, the FBI bits are generated and informed to the BS, which updates the transmitted carrier phase at the second antenna with the accuracy of $\pi/2$. The transmitted carrier phase of the second antenna is controlled so that the carrier phases of the received signals transmitted from two antennas are almost identical. More specifically, the FBI bit at the *n*-th slot, $b(n)$, is generated from the $\hat{\xi}_q^{(1)}(n)$ value. When the *n* value is even, $b(n) = 0$ in the case of $-\pi/2 \leq \arg(\hat{\xi}_1^{(1)}(n) \cdot \hat{\xi}_2^{(1)*}(n)) < \pi/2$ （otherwise, $b(n) = 1$） . Meanwhile when *n* is an odd

value, $b(n)=0$ in the case of $0 \le \arg(\hat{\xi}_1^{(1)}(n) \cdot \hat{\xi}_2^{(1)*}(n)) < \pi$ (otherwise, $b(n)=1$).

The BS updates the transmitted carrier phase of the TCH at the (n+1)-th slot associated with the second antenna, $\varphi^{(2)}(n+1)$, according to the decoded FBI bit $\hat{b}(n)$ as follows (note that when a decoding error does not occur, $\hat{b}(n)=b(n)$). When n is an even number, $\varphi^{(2)}(n+1)$ is set to $0(\pi)$ for $\hat{b}(n)=0$ (otherwise). Furthermore, when n is an odd number, $\varphi^{(2)}(n+1)$ is set to $\pi/2$ $(-\pi/2)$ for $\hat{b}(n)=0$ (otherwise). Therefore, the tentative carrier phase at the n-th and (n+1)-th slots is based on the decoded FBI bit. Finally, the transmitted carrier phase of the TCH at the (n+1)-th slot associated with the second antenna, $\phi^{(2)}(n+1)$, is derived as

$$\phi^{(2)}(n+1) = (\varphi^{(2)}(n) + \varphi^{(2)}(n+1))/2 \tag{4.17}$$

As mentioned earlier, since the decoding errors of the FBI bits occur in the reverse link, the MS verifies the transmitted carrier phase of each slot of the TCH. The tentative transmitted carrier phase at the n-th slot associated with Antenna #2 is obtained as follows [20].

When n is an even number,

$$\{\hat{\varphi}_k^{(1)}(n), \hat{\varphi}_k^{(2)}(n)\} = \{0,0\} \quad \text{in the case of}$$

$$2\sum_{l=1}^{L} \frac{1}{\sigma_l^2} \left\{ \sqrt{2}\,\mathrm{Re}\left(\gamma \hat{\xi}_{k,2,l}^{(p)}(n) \hat{\xi}_{2,l}^{(p)*}(n) \right) \right\} > \ln\left(\frac{\bar{p}(\varphi_k^{(2)}(n)=\pi)}{\bar{p}(\varphi_k^{(2)}(n)=0)} \right)$$

$$\{\hat{\varphi}_k^{(1)}(n), \hat{\varphi}_k^{(2)}(n)\} = \{0,\pi\}, \text{ otherwise} \tag{4.18}$$

When n is an odd number,

$$\{\hat{\varphi}_k^{(1)}(n), \hat{\varphi}_k^{(2)}(n)\} = \{0,-\pi/2\} \quad \text{in the case of}$$

$$-2\sum_{l=1}^{L} \frac{1}{\sigma_l^2} \left\{ \sqrt{2}\,\mathrm{Im}\left(\gamma \hat{\xi}_{k,2,l}^{(p)}(n) \hat{\xi}_{2,l}^{(p)*}(n) \right) \right\} > \ln\left(\frac{\bar{p}(\varphi_k^{(2)}(n)=-\pi/2)}{\bar{p}(\varphi_k^{(2)}(n)=\pi/2)} \right)$$

$$\{\hat{\varphi}_k^{(1)}(n), \hat{\varphi}_k^{(2)}(n)\} = \{0, \pi/2\}, \text{ otherwise} \tag{4.19}$$

Therefore, let P_{fbi_error} be the bit error rate of FBI bits in the reverse link.

Then, when *n* is an even number,

If the FBI bit of 1 is transmitted, $\bar{p}(\varphi_k^{(2)}(n) = \pi) = 1 - P_{fbi\_error}$, $\bar{p}(\varphi_k^{(2)}(n) = 0) = P_{fbi\_error}$

If the FBI bit of 0 is transmitted, $\bar{p}(\varphi_k^{(2)}(n) = \pi) = P_{fbi\_error}$, $\bar{p}(\varphi_k^{(2)}(n) = 0) = 1 - P_{fbi\_error}$

Meanwhile, when *n* is an odd number,

If the FBI bit of 1 is transmitted $\bar{p}(\varphi_k^{(2)}(n) = -\pi/2) = 1 - P_{fbi\_error}$, $\bar{p}(\varphi_k^{(2)}(n) = \pi/2) = P_{fbi\_error}$

If the FBI bit of 0 is transmitted, $\bar{p}(\varphi_k^{(2)}(n) = -\pi/2) = P_{fbi\_error}$, $\bar{p}(\varphi_k^{(2)}(n) = \pi/2) = 1 - P_{fbi\_error}$

where γ is the ratio of the SIR of the TCH to that of the PICH, σ_l^2 is the background noise plus interference power of the *l*-th path, and $\bar{p}(\cdot)$ denotes *a priori* probability. In the MPIC, the FBI bits of other user TCHs are unknown. Thus, when the FBI bits are unknown, the values of $p(\phi = \pi) = p(\phi = 0)$ in Equation (4.18) become 0.5. Then, the right term in Equation (4.18) becomes 0. Similarly, the right term in Equation (4.19) is 0 when the FBI bits are unknown.

Finally, from Equations (4.18) and (4.19), the transmitted carrier phase of TCH at the *n*-th slot associated with Antenna #2 is gained as

$$\hat{\phi}^1(n) = 0, \quad \hat{\phi}^{(2)}(n) = (\hat{\varphi}^{(2)}(n-1) + \hat{\varphi}^{(2)}(n))/2 = \{\pm\pi/4, \pm 3\pi/4, \}, \tag{4.20}$$

A block diagram of the MS receiver including the proposed antenna verification method using the signal after removing the MPI is shown in Fig. 4.7. In the proposed antenna verification method, the despread signal of the TCH after the MPI from the common channels is removed is employed to verify the transmitted carrier phase from Antenna #2. Here, the transmitted carrier phase of Antenna #2 is verified based on the following estimated values: the ratio of the SIR (note that the background noise is included in the interference component) of TCH to PICH, the background noise plus interference power for each path, and the channel gain of the TCH. The criteria for deciding the tentative carrier

modulation phase of the TCH with closed-loop PC transmit diversity, which are represented in Equations (4.18) and (4.19), are identical between the proposed antenna verification and the conventional antenna verification. The proposed method uses the pilot symbols in the TCH signal after PTA-MPIC suppresses the MPI. Therefore, in the proposed method, the accuracy of the antenna verification is improved due to the enhanced channel estimation, $\overline{\xi}_{k,q,l}^{(p)}(n)$, after removing the MPI from the common channels as well as the TCHs. Furthermore, since the FBI bits are generated using the received PICH signals with even higher transmission power than that of the TCH before MPI suppression, the proposed antenna verification method does not bring about a processing delay for closed-loop PC transmit diversity.

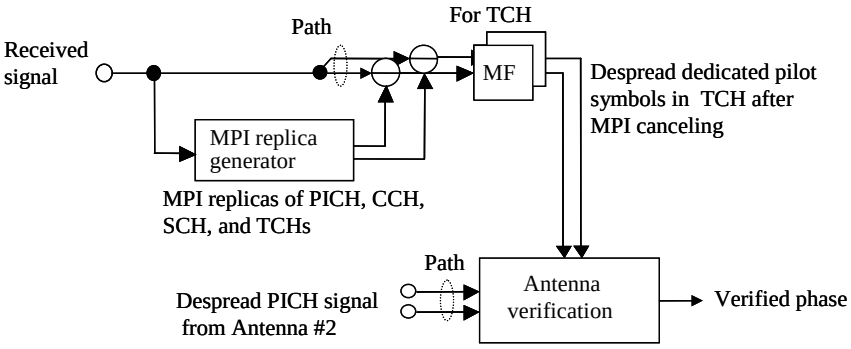

Fig. 4.7 Operation of antenna verification using pilot symbols after removing MPI

The closed loop-type fast TPC is applied to the TCH in the forward link similarly to that in the reverse link to mitigate the influence of MPI and other-cell interference. So, the transmission power of the TCH is minimized at a level such that the required received quality, e.g., the packet error rate or bit error rate is satisfied. Thus, when the number of simultaneous accessing TCHs is increased, each TCH suffers from greater MPI from the other TCHs. This brings about increasing estimation error in the carrier modulation phase employing the dedicated pilot symbols of the TCH in the antenna verification process. Consequently, the false estimation of the carrier modulation phase of the TCH leads to the degradation in the transmit diversity effect. Meanwhile, accurate estimation of the carrier modulation phases of the TCH is possible regardless of the number of simultaneous TCHs. Therefore, the proposed antenna verification method is effectual particularly when the number of simultaneous accessing TCHs is large, i.e., heavy channel load situation. Furthermore, the FBI bit for controlling the transmitter carrier modulation phase of the

second antenna is generated based on the estimation of the carrier modulation phase of the PICH with large transmission power before MPI suppression independently of the proposed antenna verification method. Thus, the proposed antenna verification method does not influence the control delay of the PC transmit diversity. The only disadvantage of the proposed antenna verification method is the additional processing delay in the MPIC after verifying the carrier modulation phase of the TCHs transmitted from the two antennas. However, since the MPIC processing is performed slot-by-slot, the additional processing delay using the proposed antenna verification method is only a few slot lengths.

4.5. Simulation Configuration

The major radio link parameters assumed in the simulations are given in Table 4.1. The transmitted data sequence of the TCH is, after appending six tail bits, channel-coded using a convolutional code with the rate of 1/3 and the constraint length of seven bits. The coded data sequence is block-interleaved over one frame length (= 10 msec). The data modulation method for the TCH and CCH are QPSK. Thus, since SF = 16, the processing gain, which is defined as the ratio of the chip rate to the information bite rate, becomes Pg = 16x3/2 = 24, where three is the bandwidth spreading factor due to convolutional coding. After being segmented into the assigned slot length, the data sequence is packed into the radio frame of the TCH, PICH, and CCH, and then spread by the combination of a cell-specific scrambling code and OVSF short code. These three channels and the SCH, which is spread only by the short code, are code-multiplexed to generate the composite transmitted signal in the forward link. We assumed that the number of transmit antennas was two when transmit diversity was applied. In the simulations, an L-path channel model with equal average received power, in which each path suffers independent Rayleigh fading with the maximum Doppler frequency, f_D, in hertz was assumed. Chip and packet frame synchronizations were assumed to be ideally performed.

SIR-based fast TPC [29], [30] was employed for the TCH in the forward link. To reduce the TPC time delay, Rake combining for SIR measurement was performed independently from that for data demodulation. Signal power S and the instantaneous interference plus background noise power, I, associated with each slot were measured over N_p pilot symbols. The average of I was obtained using a first order filter with forgetting factor $\mu = 0.99375$. The average received signal energy per bit-to-interference power spectrum density ratio (E_b/I_0) after Rake combining, which was calculated as E_b/I_0 = SIR + 10log(3/2) dB since channel coding with the rate of 1/3 and QPSK data modulation was used, was compared with the target E_b/I_0 value. If the measured value was above (below) the target, the TPC command was sent to the BS to lower (raise) the transmitted power by 1 dB at the beginning of the next slot. The TPC delay was one-slot duration.

Table 4.1 Simulation parameters

Chip rate		3.84 Mcps
Symbol rate	PICH	15 ksps
	CCH	15 ksps
	SCH	1.5 ksps
	TCH	240 ksps
Spreading code	Channelization	OVSF codes
	Scrambling	Truncated Gold code (38400 chips)
Modulation	Data	QPSK
	Spreading	QPSK
Transmission power ratio to DPCH	PICH	3 dB
	CCH	5 dB
	SCH	3 dB
Transmit diversity	CCH	STTD (Space-Time Block Coding Transmit Diversity)
	SCH	TSTD (Time Space Transmit Diversity)
	TCH	Closed-loop type PC (phase control) transmit diversity (Phase control resolution = $\pi/2$)
Channel estimation		Pilot-symbol assisted channel estimation
Channel coding		Convolutional coding (R = 1/3, k = 7) / Soft-decision Viterbi decoding
Multipath fading channel model		L-path Rayleigh with equal average power
FBI bit error rate in the reverse link		5%

In the throughput simulation evaluations, it was assumed that the ratio of the transmission power of the PICH, CCH, and SCH to the average transmission power of the TCH was $\Delta_{PICH/TCH}$ = 3 dB, $\Delta_{CCH/TCH}$ = 5 dB, and $\Delta_{SCH/TCH}$ = 3 dB, respectively. We also assumed ten active TCHs with identical symbol rates. We added the FBI bit decoded bit error of 5% with a random pattern in the reverse link.

The number of active users throughout the simulations, with an exception of Fig. 4.15, was assumed to be ten that indicates that the evaluated system was near its capacity. In this respect, I defined system capacity as the number of users satisfying their respective QoS requirements, assuming MF-based Rake receiver and interfering users with equal average transmit power. For example, assuming a required QoS of average BER of 10^{-3}, namely voice conversation, the maximum number of users producing BER floor immediately below BER of 10^{-3} was 10 as shown in Fig. 4.8. This assumption is considered appropriate to justify the validity of MPIC because the performance depends on the interference power.

4.6. Simulation Results

4.6.1 PTA-MPIC that suppresses MPI from common channels only

In this section, I investigate the average BER performance of the TCH for the desired user employing the PTA-MPIC, which only removes MPI from the common channels such as

PICH, CCH, and SCH (hereafter, called PTA-MPIC for the common channels), when STTD and PC transmit diversity are applied to the CCH and TCH, respectively. The number of stages in the PTA-MPIC was one for the common channels. This is because it is considered that the improvement by increasing the number of stages beyond one is small for the common channels, since the data modulations for the PICH and SCH were known at the MPIC receiver (data decision errors did not occur for the PICH and SCH). In the evaluations in this section, I assume ten simultaneous accessing TCHs and the identical average transmission powers for the ten TCHs (i.e., the ratio of the average transmission power of the desired user and that of an interfering user is set to $\Delta_{Int/Des}$ = 0 dB). Nevertheless, the instantaneous transmission powers of the ten TCHs are different, since fast TPC reflecting the respective instantaneous multipath fading is independently performed for each TCH.

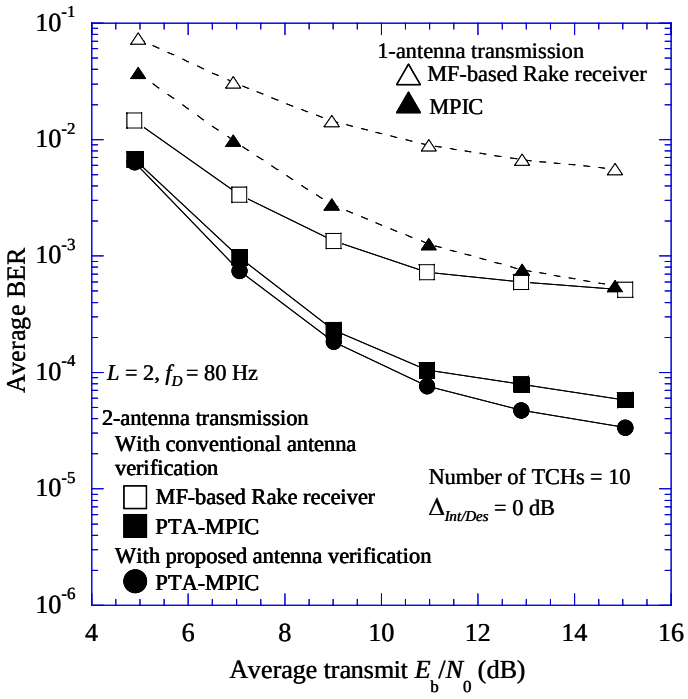

Fig. 4.8 Average BER performance employing PTA-MPIC for common channels as a function of the average transmit E_b/N_0

The average BER performance employing the PTA-MPIC for the common channels using the conventional antenna verification and the proposed antenna verification method using pilot symbols after removing MPI is plotted in Fig. 4.8 as a function of the average transmit E_b/N_0 for L = 2 and f_D = 80 Hz. The average BER performance of the MF-based

Rake receiver associated with PC transmit diversity and that using one-antenna transmission are also plotted in the figure for comparison. Figure 4.8 shows that the average BER performance employing the MF-based Rake receiver with the one-antenna transmission is significantly degraded due to the increasing MPI from the common channels and TCHs. However, I also find that by applying the PTA-MPIC to the common channels, the average BER performance is improved by one order of magnitude compared to that with the MF-based Rake receiver owing to the decreasing MPI from the common channels.

I find that the MF-based Rake receiver associated with PC transmit diversity can decrease the average transmit E_b/N_0 at the average BER of 10^{-3} by approximately 2 dB compared to the MPIC with one-antenna transmission. This is because the PC transmit diversity is superior to the PTA-MPIC in the noise-limited channels where the average transmit E_b/N_0 is low. It is further indicated that the required average transmit E_b/N_0 using the PTA-MPIC for the common channels together with PC transmit diversity is reduced by approximately 3.0 dB compared to that using the MF-based Rake receiver with PC transmit diversity. In addition, by applying the proposed antenna verification using the signal after removing MPI from the common channels, the required average transmit E_b/N_0 is further decreased by approximately 0.3 dB compared to that using the conventional antenna verification for the PTA-MPIC associated with the PC transmit diversity.

The average transmit E_b/N_0 at the average BER of 10^{-3} employing the PTA-MPIC associated with PC transmit diversity as a function of f_D is plotted in Fig. 4.9 for $L = 2$. Similarly to Fig. 4.8, the performance using MPIC with one-antenna transmission and that of the MF-based Rake receiver with PC transmit diversity are also given for comparison. Note that the MPIC for the common channels with one-antenna transmission could not realize the average BER of 10^{-3} when the f_D values were lower than approximately 60 Hz.

Figure 4.9 shows that the average transmit E_b/N_0 at the average BER of 10^{-3} using the MF-based Rake receiver with PC transmit diversity is smaller than that with MPIC for the common channels with one-antenna transmission when the f_D value is lower than approximately 100 Hz. However, it is conversely increased since the PC transmit diversity loop cannot track the fluctuations in the received signal level due to the fast fading where f_D is greater than 100 Hz. The figure shows that the combination of the PTA-MPIC for the common channels and PC transmit diversity can significantly reduce the required average transmit E_b/N_0 from a slow to fast fading channel up to approximately 200 Hz compared to that of the MF-based Rake receiver with PC transmit diversity. Furthermore, the required average transmit E_b/N_0 with the antenna verification employing the pilot symbols after removing MPI from the common channels can be decreased by approximately 0.3 dB compared to that with the conventional antenna verification in the PTA-MPIC associated

with PC transmit diversity. In the performance of the PTA-MPIC with PC transmit diversity, as f_D is increased, the required average transmit E_b/N_0 is first increased since the tracking ability of the SIR-based fast TPC for fading variation is degraded. Then, it is reduced owing to the increasing interleaving effect associated with channel coding.

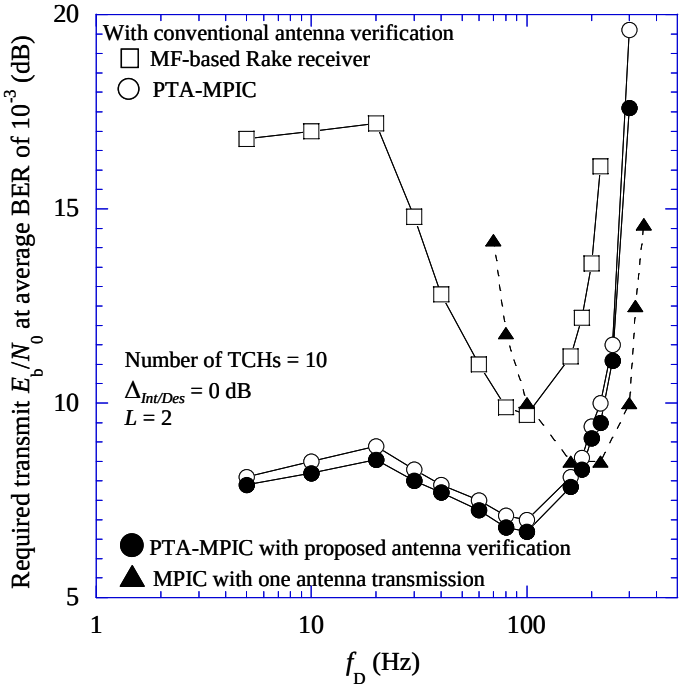

Fig. 4.9 Average transmit E_b/N_0 at the average BER of 10^{-3} employing PTA-MPIC for common channels as a function of f_D

Whereas, as f_D is further increased beyond around 100 Hz, it is again increased since the pilot channel-assisted channel estimation and PC transmit diversity loop fail to track the fast fading variation.

The average transmit E_b/N_0 for satisfying the average BER of 10^{-3} employing the PTA-MPIC for common channels and the PC transmit diversity is plotted in Fig. 4.10 as a function of the number of paths, L, for f_D = 80 Hz. Figure 4.10 shows that, as L is increased, the required average transmit E_b/N_0 is increased due to the increasing MPI from the common channels and thus, the average BER of 10^{-3} is not achieved for the MF-based Rake receiver even when the PC transmit diversity is applied when L is greater than three. However, the figure shows that the required average transmit E_b/N_0 is significantly reduced by applying PTA-MPIC to the common channels, which suppresses the severe MPI from the common channels.

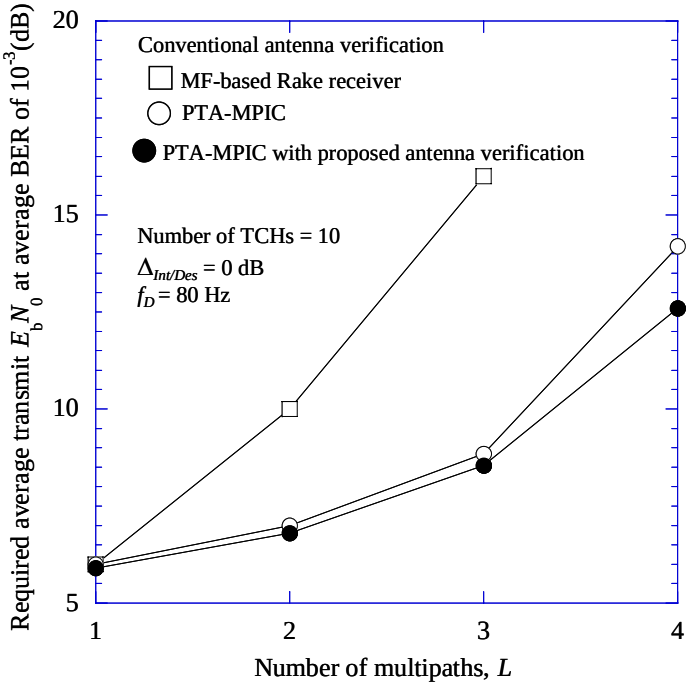

Fig. 4.10 Average transmit E_b/N_0 at the average BER of 10^{-3} employing PTA-MPIC for common channels as a function of L

Furthermore, the antenna verification using the pilot symbols after removing MPI exhibits further improvement in the required average transmit E_b/N_0 compared to the conventional antenna verification method in the PTA-MPIC thanks to the increasing transmit diversity effect derived from the improvements in the transmitted carrier phase verification: the required average transmit E_b/N_0 at the average BER of 10^{-3} is further reduced by approximately 0.3, 0.5, and 1.7 dB for L = 2, 3, and 4, respectively.

4.6.2 PTA-MPIC for common channels and DPCHs

In this section, I investigate the average BER performance using PTA-MPIC, which removes the MPI not only from the common channels, but also from the TCHs (hereafter called PTA-MPIC for all channels), associated with PC transmit diversity. The number of stages in the PTA-MPIC for common channels was set to be one. However, it is anticipated that by increasing the number of stages, the number of the data decision errors in the MPIC for the TCHs is decreased. Furthermore, the MPI replicas of all common channels including the PICH from the other paths were subtracted from the received signal in and after the second stage.

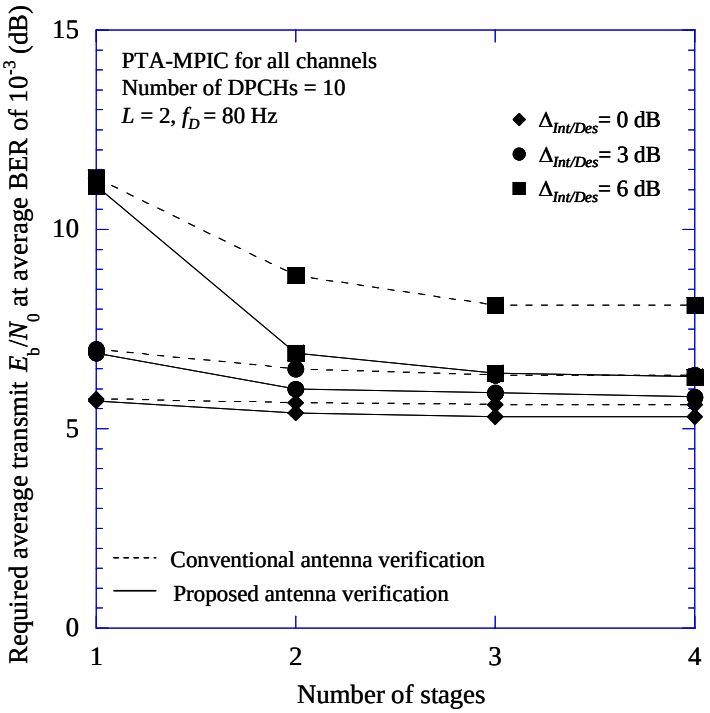

Fig. 4.11 Average transmit E_b/N_0 at the average BER of 10^{-3} employing PTA-MPIC for all channels as a function of number of stages.

Thus, the average transmit E_b/N_0 at the average BER of 10^{-3} employing PTA-MPIC is plotted in Fig. 4.11 as a function of the number of stages of the MPIC using the proposed antenna verification method along with the conventional antenna verification method. The IRW, which is a weighting factor for the generated MPI, was 1.0 (note that the optimum IRW value is to be investigated in Fig. 4.12). It is assumed that L = 2 and f_D = 80 Hz with the $\Delta_{Int/Des}$ value as a parameter. The dotted and solid lines indicate the BER performance using conventional antenna verification and that of the proposed antenna verification, respectively. Figure 4.11 shows that when the $\Delta_{Int/Des}$ value is 0 and 3 dB, the improvement in the required average transmit E_b/N_0 by increasing the number of stages beyond one is slight, because the influence of the data decision error for the TCHs is small. However, when the interfering power from other TCHs is large such as the $\Delta_{Int/Des}$ of 6 dB, it is appropriate to increase the number of stages to two. The required average transmit E_b/N_0 at the average BER of 10^{-3} is reduced by approximately 4.3 (2.4) dB by increasing the number of stages from one to two for the proposed (conventional) antenna verification method. This is because the number of the data decision errors for the TCHs is decreased by increasing the number of stages to two. Moreover, we find that in the case of $\Delta_{Int/Des}$ = 6 dB, the required average transmit E_b/N_0 using the proposed antenna verification is reduced by

approximately 2.0 dB compared to that with the conventional antenna verification method when the number of stages is two. This result indicates that the number of the estimation errors of the carrier modulation phase for the TCH is significantly reduced by using the pilot symbols within the TCH after MPI suppression in the proposed antenna verification method. Then, based on the results of Fig. 4.11, we set the number of stages in the PTA-MPIC for the TCH to be two in the subsequent evaluations.

Next, the average BER performance is plotted in Fig. 4.12 as a function of the IRW value in PTA-MPIC assuming that the average transmit E_b/N_0 of the TCH is 5 and 9 dB. Figures 4.12(a) and 4.12(b) show the average BER performance employing the conventional antenna verification method and the proposed antenna verification method using the pilot symbols of the TCH after MPI suppression. It is assumed that $L = 2$, $f_D = 80$ Hz, and that there are ten TCHs with the $\Delta_{Int/Des}$ value as a parameter. The dotted and solid lines indicate the BER performance using the conventional antenna verification and that of the antenna verification using the pilot symbols after removing MPI, respectively. Figure 4.12 shows that the optimum IRW in the PTA-MPIC for all channels associated with PC transmit diversity using the conventional antenna verification is 1.0 for $\Delta_{Int/Des} = 0$ dB and 0.9 for $\Delta_{Int/Des} = 3$ and 6 dB, respectively. Furthermore, the optimum IRW for the antenna verification using the pilot symbols after removing the MPIC becomes 1.0. This is because the improved accuracy of the antenna verification brings about improved accuracy of the generated MPI replica. Therefore, in the subsequent evaluations in PTA-MPIC for all channels, we use the IRW value of 1.0.

The average BER performance employing the combination of the PTA-MPIC for all channels and PC transmit diversity is plotted in Fig. 4.13 as a function of the average transmit E_b/N_0 for $L = 2$, $f_D = 80$ Hz, and ten TCHs with $\Delta_{Int/Des} = 0$ dB. The average BER performance using the PTA-MPIC for only the common channels is also given in the figure for comparison. The figure indicates that the average transmit E_b/N_0 at the average BER of 10^{-3} using PTA-MPIC for all channels is reduced by approximately 1.4 dB compared to that with PTA-MPIC for only the common channels assuming the use of the conventional antenna verification method. Furthermore, the required average transmit E_b/N_0 in the PTA-MPIC for all channels with the antenna verification using the pilot symbols after removing MPI is further decreased by approximately 0.3 dB compared to that with the conventional antenna verification.

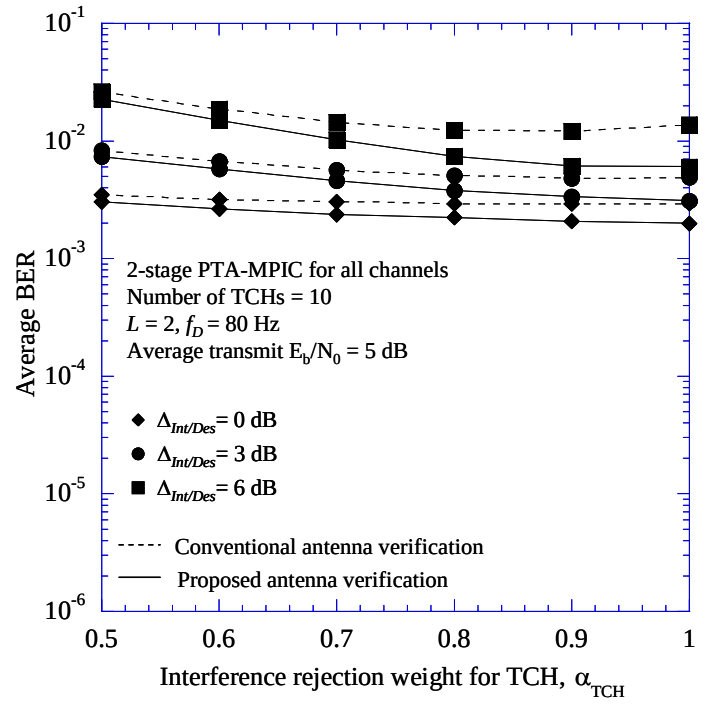

(a) Average transmit E_b/N_0 = 5 dB

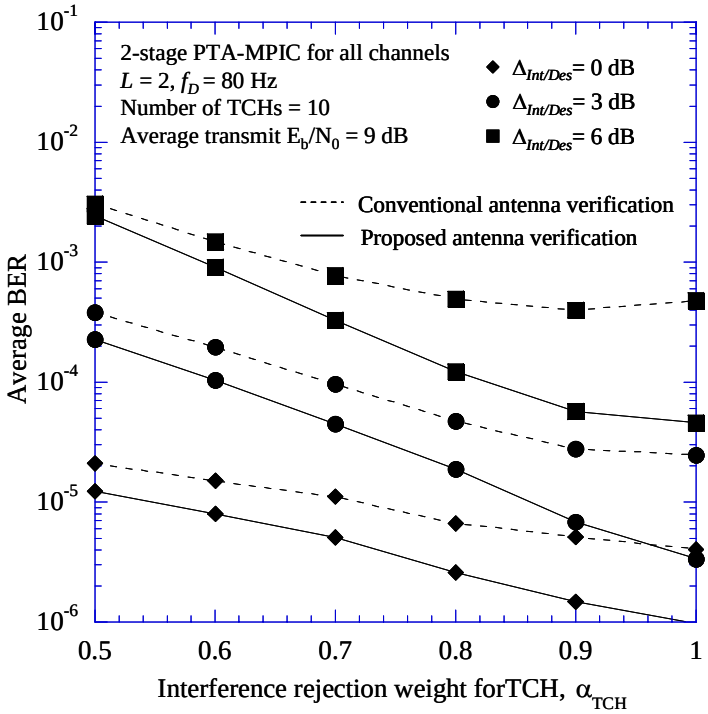

(b) Average transmit E_b/N_0 = 9 dB

Fig. 4.12 Influence of interference rejection weight in PTA-MPIC for TCHs

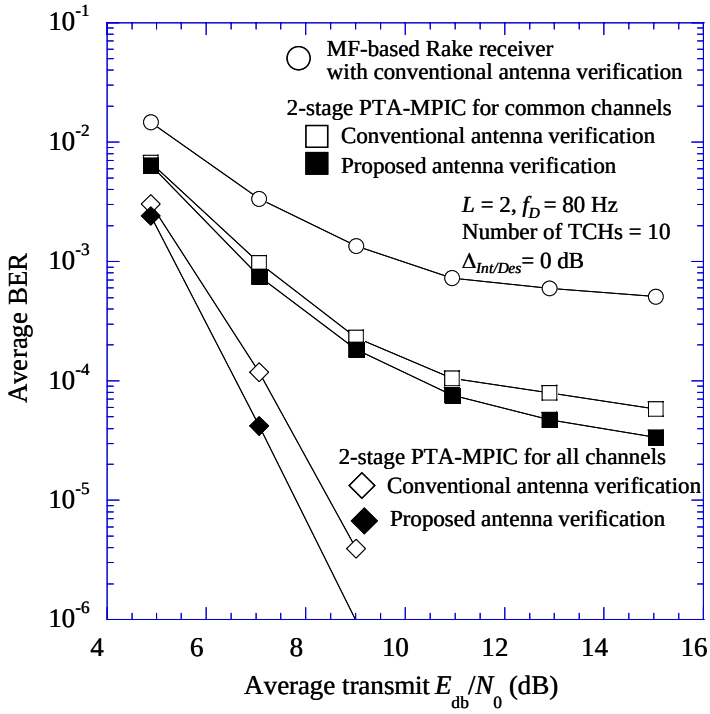

Fig. 4.13 Average BER performance employing PTA-MPIC for all channels as a function of the average transmit E_b/N_0.

The average BER performance with the combination of the PTA-MPIC for all channels and the PC transmit diversity with the $\Delta_{Int/Des}$ value as a parameter is plotted in Fig. 4.14 as a function of the average transmit E_b/N_0 for L = 2 and f_D = 80 Hz. The figure shows that according to the increase in the $\Delta_{Int/Des}$ value, the average BER performance using the MF-based Rake receiver associated with the PC transmit diversity is significantly degraded due to the severe MPI from the high-rate TCHs with high transmission powers.

However, it is also observed that the PTA-MPIC for all channels remarkably improves the BER performance, because the severe MPI from the TCHs as well as the common channels is sufficiently removed. Furthermore, in the PTA-MPIC for all channels associated with PC transmit diversity, the required average transmit E_b/N_0 employing the antenna verification using the signal after removing MPI can be reduced by approximately 0.3 dB, 0.5 dB, and 1.2 dB compared to that using the conventional antenna verification when the $\Delta_{Int/Des}$= 0 dB, 3 dB, and 6 dB. Thus, we see that the proposed antenna verification using the pilot symbols after removing MPI is very effective in mitigating the antenna verification error due to the severe MPI, because the number of detection errors of the transmitted carrier phase in the second antenna due to FBI-bit decoding error is reduced, thereby decreasing the required average transmit E_b/N_0.

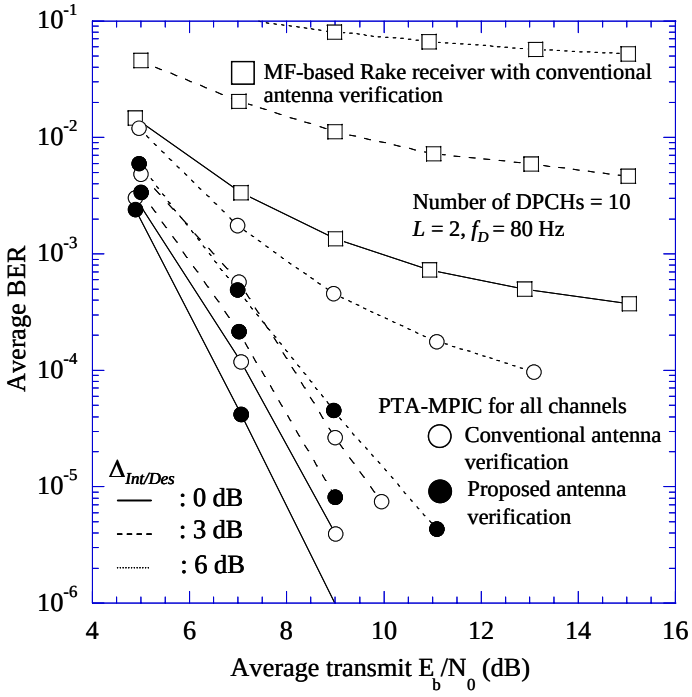

Fig. 4.14 Average BER performance employing PTA-MPIC for all channels with $R_{Int/Des}$ value as a parameter.

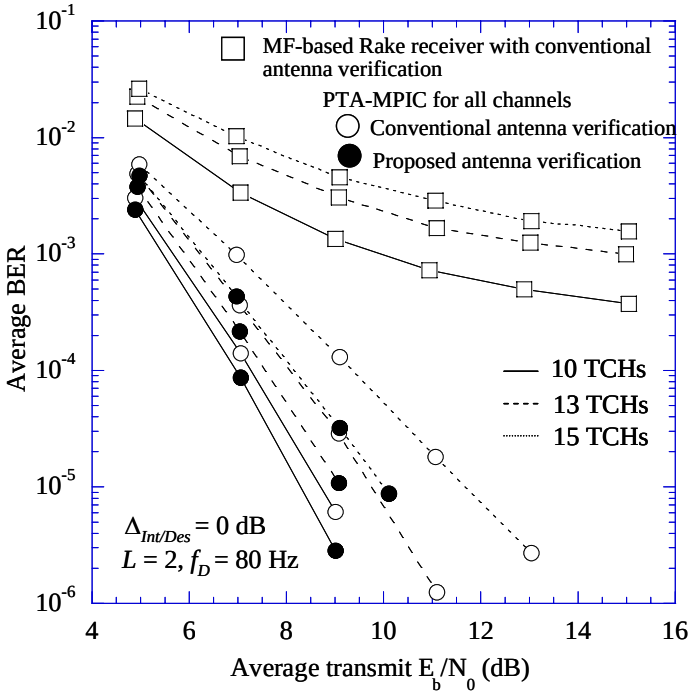

Fig. 4.15 Average BER performance employing PTA-MPIC for all channels with the number of DPCHs as a parameter.

The average BER performance with the combination of the PTA-MPIC and the PC transmit diversity with the number of TCHs as a parameter is plotted in Fig. 4.15 as a function of the average transmit E_b/N_0 for $\Delta_{Int/Des}$= 0 dB. The increase in the number of TCHs is equivalent to the increase in the rate in the interfering TCHs in Fig. 4.14. Similar to the tendency in Fig. 4.14, we see that as the number of TCHs is increased, the average BER performance using the MF-based Rake receiver with the PC transmit diversity is significantly degraded due to the severe MPI. However, the beneficial effect by removing MPI of PTA-MPIC can be revealed. Moreover, I find that the proposed antenna verification using the signal after removing the MPI is efficient in improving the PC transmit diversity effect especially for the number of TCHs is 15. The required average transmit E_b/N_0 at the average BER of 10^{-3} with the proposed antenna verification method is reduced by approximately 0.8 dB compared to that with the conventional antenna verification.

Finally, I compared the processing complexity of PTA-MPIC with the proposed antenna verification method to that of the MF-based Rake receiver with the conventional antenna verification method based on a number of complex-value multiplication operations (hereafter simply multiplications). The number of multiplications needed for each constituent process of the PTA-MPIC with the proposed antenna verification or the conventional antenna verification method and that of the MF-based Rake receiver is given in Table 4.2.

The MF-based Rake receiver has operations such as despreading, channel estimation, and compensation of the channel estimate. Furthermore, in each stage of the MPIC, operations such as multiplication of the estimated channel gain to the decision data symbols and the re-spreading to regenerate the MPI replica are added to the operations needed for the MF-based Rake receiver. In Table 2, the parameters N_s, SF, K, L, and P denote the number of symbols including pilot symbols within one-slot duration, the spreading factor, the number of simultaneous TCHs, the number of paths, and the number of stages, respectively.

Then, based on the number of complex multiplications given in Table 4.2, I calculated the total number of multiplications of MPIC with the proposed or conventional antenna verification method and that of the MF-based Rake receiver. In Table 4.2, we assumed that $N_s = N_p + N_d = 160$ symbols, $SF = 16$, $K = 10$ TCHs, and $L = 2$ paths. This table indicates that the complexity of the 1-stage MPIC with only common channels or that with MPI suppression for all channels is almost 5 or 20 times that of the MF-based Rake receiver. It was also found that the increase in the computation complexity of the proposed antenna verification method using the pilot symbols in the TCH after MPI suppression from the conventional antenna verification method is even smaller than that of the MF-based Rake receiver. Furthermore, allowing almost twice the computational complexity of the

PTA-MPIC by increasing the number of stages from one to two, the required average transmit E_b/N_0 at the average BER of 10^{-3} can be reduced by approximately 4.3 dB under heavy channel load conditions such as $\Delta_{Int/Des}$ = 6 dB as shown in Fig. 4.11.

Table 4.2 Number of Complex Multiplication Required for Conventional MF-based Rake Receiver and PTA-MPIC

		MF-based Rake	PTA-MPIC			
			Common channels only		All channels	
			With conventional antenna verification	With proposed antenna verification	With conventional antenna verification	With proposed antenna verification
Despreading		N_s x SF x 2 x L	P x N_s x SF x 3 x L		P x N_s x SF x (K + 2) x L	
Channel compensation		2 x N_s x L	P x 2 x N_s x 2 x L		P x 2 x N_s x (K + 1) x L	
Antenna verification		N_s x 2 x L + L	N_s x 2 x L + L	P x (N_s x 2 x L + L)	N_s x 2 x L + K x L	P x (N_s x 2 x L + K x L)
Multiplication of channel estimates		0	(P - 1) x 2 x N_s x 4 x L + 2 x N_s x 3 x L		(P - 1) x 2 x N_s x (K + 3) x L + 2 x N_s x (K + 2) x L	
Re-spreading		0	(P - 1) x 2 x N_s x SF x 4 x L + 2 x N_s x SF x 3 x L		(P - 1) x 2 x N_s x SF x (K + 3) x L + 2 x N_s x SF x (K + 2) x L	
Total		$2N_sL(SF+2)+L$	$PN_sL(11SF+12)$ $+L(-2N_sSF+1)$	$PN_sL(11SF+14)+$ $L(-2N_sSF-2N_s+P)$	$PN_sL(K(3SF+4)$ $+8SF+8)+L(N_s$ $(-2SF+6)+K-6)$	$PN_sL(K(3SF+4)$ $+8SF+10)+L(N_s$ $(-2SF+4)+PK-6)$
Example (N_s = 160, SF = 16, K = 10, L = 2)	1-stage (P = 1)	11522	49922	49922	201608	201608
	2-stage (P = 2)		110082	110724	411528	412178

4.7. Conclusion

This chapter presented a MPIC configuration based on MPI replica generation per transmit antenna (called PTA-MPIC) associated with STTD for CCH, which exploited tentative decision data after STTD decoding and with closed-loop type PC transmit diversity for the TCH employing tentative decision data after diversity combining, in the W-CDMA forward link. This chapter also proposed transmitter carrier phase verification, i.e., an antenna verification method used in PC transmit diversity, that utilizes the dedicated pilot symbols in a DPCH after the PTA-MPIC removes the MPI components.

The simulation results showed that the one-stage PTA-MPIC, which removes the MPI from the CICH, CCH, and SCH, reduces the required average transmit E_b/N_0 of the TCH at the average BER of 10^{-3} by approximately 3.0 dB compared to that using a MF-based Rake receiver (the transmit power ratio of each common channel to TCH is $\Delta_{PICH/TCH}$ = 3 dB, $\Delta_{CCH/TCH}$ = 5 dB, and $\Delta_{SCH/TCH}$ = 3 dB, with TPC and without antenna diversity reception at the user equipment). Furthermore, it was elucidated that in the two-stage PTA-MPIC with MPI suppression for all channels associated with PC transmit diversity, the required average transmit E_b/N_0 employing the proposed antenna verification

was reduced by approximately 0.3 dB, 0.5 dB, and 1.2 dB compared to that using the conventional antenna verification when the transmission power ratio of the interfering TCH to the desired TCH is $\Delta_{Int/Des}$ = 0 dB, 3 dB, and 6 dB for ten TCHs, because the number of detection errors of the transmitted carrier phase in the second antenna due to feedback information bit decoding error was reduced. In addition, with a large channel load such as $\Delta_{Int/Des}$ = 6 dB, the improvement by the proposed antenna verification method compared to the conventional one became larger by increasing the number of stages to two at the cost of computational complexity.

Chapter Five

Conclusions and Suggestions for Future Work

Commercial 3G services using W-CDMA air interface have been launched in Japan by NTT DoCoMo in 2001 and global scale introduction is underway. The system capacity of W-CDMA system is interference limited because all users share the same frequency bandwidth simultaneously. Further, high data-rate services such as high-speed data downloading and Internet broadcasting are to be introduced in the near future by which the amount of traffic in the forward link is expected to be much greater than that of the reverse link. Although the use of OVSF codes establishes orthogonality among channels within same propagation path, the interference from different paths, MPI, are large. Thus, this thesis proposed the application of MPIC to orthogonal code-multiplexed channels in the forward link.

Chapter 3 proposed an MPIC for orthogonal multiplexed channels in the W-CDMA forward link. Therein, common pilot channel was used for channel estimation for generating MPI replicas because it has large transmission power, thus yielding higher accuracy. In addition, WMSA channel estimation filter was applied to increase further the channel estimation accuracy. Because dedicated channel instantaneous amplitude is different from that of common pilot channel, especially when fast TPC is applied, the amplitude ratio of both channels is measured and the channel estimates obtained from common pilot channel scaled (note that to generate accurate MPI replicas phase and amplitude variations of the channel are required). To minimize the number of stages, serial type MPIC, i.e., MPI replica generation is performed in the order of received power, was considered although this costs longer processing delay. Finally, prioritization to channels with higher received power to be cancelled was proposed to abate the increase in processing complexity. Intensive computer simulation results confirmed the effectiveness of the proposed MPIC receiver.

Chapter 4 presented a PTA-MPIC configuration based on MPI associated with STTD for CCH, which exploited tentative decision data after STTD decoding and with closed-loop type PC transmit diversity for the TCH employing tentative decision data after diversity combining, in the W-CDMA forward link. This chapter also proposed transmitter carrier phase verification, i.e., an antenna verification method used in PC transmit diversity, that utilizes the dedicated pilot symbols in a TCH after the PTA-MPIC removed the MPI components. Computer simulation results showed that combination of MPIC at mobile station receiver and transmit diversity at base station transmitter is effective in improving

the forward link transmission performance both in noise limited and interference limited conditions. Further, it was also clarified that the proposed antenna verification method is beneficial in improving the MPIC performance and reducing the required number of stages hence the complexity.

Simulation results clarified the following:

1. A one-stage MPIC, which removes the MPI from the PICH, CCH, and SCH, achieves a sufficient MPI suppression effect, and that the required received E_b/N_0 of the TCH at the average BER of 10^{-3} with the MPIC applied to the common channels is decreased by approximately 6.5 dB compared to that with the MF-based Rake receiver (the transmit E_b/N_0 ratio of each common channel to TCH: $\Delta_{PICH/TCH}$ = 0 dB, $\Delta_{CCH/TCH}$ = 5 dB, $\Delta_{SCH/TCH}$ = 3 dB, without fast transmit power control and antenna diversity reception).
2. By using the MPIC, the required transmit E_b/N_0 at the average BER of 10^{-3}, when the ratio of the target E_b/N_0 of the desired user to 9-interfering users is $\Delta_{Int/Des}$ = 6 dB with fast TPC, is increased only by approximately 0.6 dB compared to that when $\Delta_{Int/Des}$ = 0 dB.
3. The MPIC is effective for removing MPI considering diversification of non-voice communication services, i.e. various services with different required BER. The MPIC for all channels decreased the required average received E_b/N_0 at average BER of 10^{-2} by about 5.3 dB when the value of $\Delta_{SCH/TCH}$ =3dB without fast TPC.
4. A one-stage PTA-MPIC, which removes the MPI from the PICH, CCH, and SCH, reduces the required average transmit E_b/N_0 of the DPCH at the average BER of 10^{-3} by approximately 3.0 dB compared to that using a MF-based Rake receiver (the transmit power ratio of each common channel to DPCH is $\Delta_{PICH/TCH}$ = 3 dB, $\Delta_{CCH/TCH}$ = 5 dB, and $\Delta_{SCH/TCH}$ = 3 dB, with TPC and without antenna diversity reception at the user equipment).
5. A two-stage PTA-MPIC with MPI suppression for all channels associated with PC transmit diversity, the required average transmit E_b/N_0 employing the proposed antenna verification was reduced by approximately 0.3 dB, 0.5 dB, and 1.2 dB compared to that using the conventional antenna verification when the transmission power ratio of the interfering TCH to the desired TCH is $\Delta_{Int/Des}$ = 0 dB, 3 dB, and 6 dB for ten DPCHs, because the number of detection errors of the transmitted carrier phase in the second antenna due to feedback information bit decoding error was reduced. In addition, with a large channel load such as $\Delta_{Int/Des}$ = 6 dB, the improvement by the proposed antenna verification method compared to the conventional one became larger by increasing the number of stages to two at the cost of increasing computational complexity.

The results presented here should be viewed as indicative results because single-cell environment was considered. The proposed MPIC is to be applied at mobile station receiver whose propagation environment varies significantly with geographic location and distance from neighboring base stations. Therefore, further investigation considering cellular environment or geometry parameter is required. In addition, strategies for interference cancellation during soft or softer handover need further investigation during which a mobile station is connected to more than two base stations.

In Chapter 4, zero received timing difference between Antenna 1 and Antenna 2 was assumed. However, non-zero received timing difference is possible due to the environment and system configuration. Further investigation on the effect of received timing difference is required to quantify the degradation that may result thereof. This is also important from complexity consideration. Since if we can justify that the effect of received timing difference is small enough than we can reduce the PTA-MPIC complexity, because MPI replica generation for received signal from both transmit antennas of TCH can be simplified. However, the above investigations may require special purpose hardware due to required computational power.

References

[1] K. Tachikawa ed. “W-CDMA Mobile Communications System,” John Wiley & Sons, 2002.

[2] Telecommunications Carrier Association, “The number of subscribers of mobile telephone, PHS Internet provider services and radio paging,” Available: http://www.tca.or.jp/

[3] UMTS Forum, “3G Offered Traffic Characteristics”, Available: http://www.umts-forum.org/servlet/dycon/ztumts/umts/Live/en/umts/Resources_Reports_index

[4] H. Holma and A. Toskala, “WCDMA for UMTS: Radio Access for Third Generation Mobile Communications,” John Wiley & Sons 2000.

[5] F. Adachi, M. Sawahashi and H. Suda, “Wideband DS-CDMA for Next-generation Mobile Communications Systems,” IEEE Commun. Mag., vol.36, no.9, pp 56-59, Sept. 1998.

[6] K. Okawa and F. Adachi, “Orthogonal Forward Link Using Orthogonal Multi-spreading Factor Codes for Coherent DS-CDMA Mobile Radio,” IEICE Trans. Commun., vol. E81-B, no. 4, pp. 777-784, April 1998.

[7] U. Madhow, “Blind Adaptive Interference Suppression for Direct-Sequence CDMA,” Proceedings of the IEEE, special issue on blind identification and equalization, vol. 86, no. 10, pp. 2049-2069, October 1998

[8] K. Li and H. Liu, “A New Blind Receiver for Downlink DS-CDMA Communications,” IEEE Commun. Lett., vol.3, no. 7, pp.193-195, July 1999

[9] A.Klein, “Data Detection Algorithms Specially Designed for the Downlink of CDMA Mobile Radio Systems,” in Proc. IEEEVTC’97, pp.203-207, Phoenix, AZ, May 1997.

[10] I. Ghauri and D.T.M. Slock, “Linear Receivers for the DS-CDMA Downlink Exploiting Orthogonality of Spreading Sequences,” in Proc. Asilomar Conf. Signals, Systems and Computers, Pacific Grove, pp. 650-654, CA, Nov.1998.

[11] F. Petre, G.. Leus, E. Engels, M. Moonen and H. De Man, “Semi-blind Space-Time Chip Equalizer Receives for WCDMA Forward Link with Code-Multiplexed Pilot”, in Proc. ICASSP 2001, pp.2245 – 2248, Salt Lake City, UT, May 2001.

[12] M. Latva-aho and M. Juntti, “Modified Adaptive LMMSE Receiver for DS-CDMA Systems in Fading Channels,” in Proc. 8th IEEE Intl. Symposium on Personal, Indoor and Mobile Radio Communications Helsinki, pp. 554-558, Finland, Sept. 1997.

[13] K. Higuchi, A. Fujiwara, and M. Sawahashi, "Throughput Performance of High-Speed Packet Transmission with Adaptive Modulation and Coding Scheme

Using Multipath Interference Canceller in W-CDMA Forward Link," in Proc. IEEE VTC2001, pp. 2297-2301, Greece, May 2001.

[14] K. Okawa, K. Higuchi and M. Sawahashi, “Parallel-Type Coherent Multistage Interference Canceller with Iterative Channel Estimation Using Both Pilot and Decision Feedback Data Symbols for W-CDMA Mobile Radio”, IEICE Trans. Commun., vol.E84-B, no.3, pp.446-456, March 2001.

[15] S. Sun, L. K. Rasmussen, T. J. Lim and H. Sugimoto, “A Hybrid Interference Canceller in CDMA”, in the Proceedings of the IEEE International Symposium on Spread Spectrum Techniques and Application, pp. 150-154, Sun City South Africa, Sept. 1998.

[16] ETSI/SMG2, “Feedback Mode Transmit Diversity” Tdoc SMG2 UMTS-L1 696/98, Dec. 1998.

[17] K. I. Kim, “Handbook of CDMA System Design, Engineering and Optimization,” Prentice Hall PTR, 1999.

[18] K. Higuchi, M. Sawahashi and F. Adachi, “Fast Cell Search Algorithm in DS-CDMA Mobile Radio Using Long Spreading Codes”, IEICE Trans. Commun., vol.E81-B, no.7, pp. 1527-1534, July 1998.

[19] S. Fukumoto, K. Higuchi, A. Morimoto, M. Sawahashi and F. Adachi, “Combined Effect of Site Diversity and Fast Transmit Power Control in W-CDMA Mobile Radio”, Proc. VTC’2000, pp.1527-1534, Tokyo, May 2000.

[20] 3GPP RAN, 3G TS 25.211 V3.2.0, March 2000.

[21] 3GPP RAN, 3G TS 25.214 V3.4.0, Sept 2000.

[22] S. Fukumoto, K. Higuchi, M. Sawahashi and F. Adachi, “Experiment on Space Time Block Coding Transmit Diversity (STTD) in W-CDMA Forward Link”, IEICE Trans. Fundamentals, vol. E-84A, no. 12, pp. 3045-3057, Dec. 2001.

[23] S. M. Alamouti, “A Simple Transmit Diversity Technique for Wireless Communications," IEEE J. Select. Areas Commun., vol. 16, no.8, pp. 1451-1458, Oct. 1998.

[24] A.J. Viterbi, “CDMA: Principles of Spread Spectrum Communication”, Addison-Wesley Wireless Communication Series, Addison-Wesley, Reading, MA, 1995.

[25] H. Andoh, M. Sawahashi and F. Adachi, “Channel Estimation Filter Using Time-Multiplexed Pilot Channel for Coherent Rake Combining in DS-CDMA Mobile Radio”, IEICE Trans. Commun., vol. E-81-B, no. 7, pp. 1517-1526, July, 1998.

[26] S. Abeta, M. Sawahashi and F. Adachi, “Adaptive Channel Estimation for Coherent DS-CDMA Mobile Radio Using Time-Multiplexed Pilot and Parallel Pilot Structures”, IEICE Trans. Commun., vol.E82-B, no.9, pp. 1505-1513, Sept. 1999.

[27] S. Fukumoto, K. Okawa, K. Higuchi, M. Sawahashi and F. Adachi, “Path Search Performance and Its Parameter Optimization of Pilot Symbol-Assisted Coherent Rake Receiver for W-CDMA Mobile Radio”, IEICE Trans. Fundamental, vol. E83-A, no. 11 pp.2110-2119, Nov. 2000.

[28] M. Sawahashi, H. Andoh and K. Higuchi, “Interference Replica Weight Control for Pilot Symbol-Assisted Coherent Multistage Interference Canceller Using Recursive Channel Estimation in DS-CDMA Mobile Radio”, IEICE Trans. Fundamentals vol. E81-A, no. 7, pp. 957-972, May 1998.

[29] S. Ariyavisitakul, “Signal and Interference Statistics of a CDMA System with Feedback Power Control –Part II”, IEEE Trans. Commun., vol.42, nos.2-4, pp.597-605, Feb./March/April 1994.

[30] S. Seo, T. Dohi and F. Adachi, “SIR-Based Transmit Power Control of Reverse Link for Coherent DS-CDMA Mobile Radio”, IEICE Trans. Commun., vol.E81-B, no.7, pp.1508-1516, July 1998.

[31] K. Higuchi, H. Andoh, K. Okawa, M. Sawahashi and F. Adachi, “Experimental Evaluation of Combined Effect of Coherent Rake Combining and SIR-Based Fast Transmit Power Control for Reverse Link of DS-CDMA Mobile Radio”, IEEE J. Sel. Areas Commun., vol.18, no.8, pp.1526-1535, Aug. 2000.

[32] ETSI/SMG2, UMTS-L1, “Space Time Block Coded Transmit Antenna Diversity for WCDMA”, Tdoc 662/98, Dec. 1998.

[33] ETSI/SMG2 UMTS-L1, “Proposal for Downlink Time Switched Transmission Diversity,” Tdoc 53/98, May 1998.

[34] S. Fukumoto, K. Higuchi, M. Sawahashi and F. Adachi, “Field Experiments on Closed Loop Mode Transmit Diversity in W-CDMA Forward Link”, in Proc. IEEE ISSSTA2000, pp.433-438, New Jersey, Sept. 2000.

[35] Wei Zha and Steven D. Blostein, “Soft-Decision Multistage Multiuser Interference Cancellation,” IEEE Transactions on Vehicular Technology, vol. 52, no. 2, pp. 380-389, March 2003

List of Publications

Journal

[1] Akhmad Unggul Priantoro*, Heiichi Yamamoto*, Kenichi Higuchi, and Mamoru Sawahashi, “Multipath Interference Canceller for Orthogonal Code-Multiplexed Channels and Its Performance in W-CDMA Forward Link”, IEICE Trans. Fundamentals, vol.E-85A, no.7, pp.1524-1535, July 2002.

[2] Akhmad Unggul Priantoro*, Heiichi Yamamoto*, Kenichi Higuchi, and Mamoru Sawahashi, “Antenna Verification Method for Multipath Interference Canceller Based on Replica Generation per Transmit Antenna with Phase Control Transmit Diversity in W-CDMA Forward Link”, accepted for publication in IEICE Trans. Commun.

International Conference

[1] Akhmad Unggul Priantoro*, Heiichi Yamamoto*, Kenichi Higuchi, and Mamoru Sawahashi, “Closed-Loop Type Transmit Diversity Employing Antenna Verification Associated with Multipath Interference Canceller in W-CDMA Forward Link”, Proceeding of Asia Pacific Conference on Communications 2002, pp.117-120 Sept. 2002.

Domestic Conference

[1] Akhmad Unggul Priantoro*, Heiichi Yamamoto*, Kenichi Higuchi, and Mamoru Sawahashi, “Multipath Interference Canceller for Orthogonal-Code Multiplexed W-CDMA Forward Link”, IEICE Technical Report, RCS Vol.100,No.558 ,pp.27-34,2001/01

[2] Akhmad Unggul Priantoro*, Heiichi Yamamoto*, Kenichi Higuchi, and Mamoru Sawahashi, “Performance of Multipath Interference Canceller Using Fast Transmit Power Control in W-CDMA Forward Link”, IEICE, General Conference B-5-4,pp.402, 2001/03